MACROSCALE MIXING AND DYNAMIC BEHAVIOR OF AGITATED PULP STOCK CHESTS

by

FARHAD EIN-MOZAFFARI

B.Sc., Amir Kabir University of Technology, Tehran, Iran, 1986
M.Sc., Amir Kabir University of Technology, Tehran, Iran, 1989

A THESIS SUBMITTED IN PARTIAL FULFILMENT OF
THE REQUIREMENTS FOR THE DEGREE OF

DOCTOR OF PHILOSOPHY

in

THE FACULTY OF GRADUATE STUDIES

DEPARTMENT OF CHEMICAL AND BIOLOGICAL ENGINEERING

We accept this thesis as conforming
to the required standard

THE UNIVERSITY OF BRITISH COLUMBIA
December 2002

In presenting this thesis in partial fulfilment of the requirements for an advanced degree at the University of British Columbia, I agree that the Library shall make it freely available for reference and study. I further agree that permission for extensive copying of this thesis for scholarly purposes may be granted by the head of my department or by his or her representatives. It is understood that copying or publication of this thesis for financial gain shall not be allowed without my written permission.

Department of Chemical and Biological Engineering

The University of British Columbia
Vancouver, Canada

Date December 16, 2002

ABSTRACT

Agitated pulp chests provide attenuation of high-frequency disturbances in fibre mass concentration, freeness and other quality factors. This contrasts with process control loops, which attenuate low-frequency variations. Dynamic tests made on industrial stock chests show the existence of non-ideal flows such as channeling, recirculation and dead zones. Since these non-ideal flows reduce the degree of disturbance attenuation from the chests, they have been considered in the dynamic modeling of the chest. This model allows for two parallel suspension flow paths: a mixing zone consisting of a first order plus delay transfer function with a positive feedback for recirculation, and a channeling zone consisting of a first order plus delay transfer function. A new identification method was developed for estimation of dynamic model parameters.

A scale-model stock chest was designed and built to study macroscale mixing and disturbance attenuation in a laboratory setting. Fully bleached kraft pulp (FBK) was used for preparation of the pulp suspensions. First preliminary batch studies were made on the scale-model chest to characterize its behavior and to develop test protocols for use in dynamic tests. Initial tests in batch-mode confirmed established trends for the power required for chest behavior, although existing literature correlations underpredict the power and momentum flux requirements need for complete motion inside the chest. Our visual observation with the aid of a digital video camera showed that the power recommended by existing design criteria is not sufficient to eliminate stagnant zones and even when the whole suspension is in motion, poor mixing regions, where pulp flows significantly slower than in the bulk motion zone, still exist inside the chest. Dynamic response of liquid and solid phase tracers showed that a liquid phase

tracer (saline solution) can be used to trace the fibre phase provided the fibre mass concentration is ≥ 2%. It was found that mixing-time for the laboratory chest is both a function of impeller momentum flux and fibre mass concentration.

The extent of non-ideal flow in the scale-model chest was evaluated by exciting the system. The process of model identification required two experiments. In the first experiment, the input signal was a rectangular pulse, which allowed the estimation of an approximate model for designing the excitation for the second experiment. The excitation energy for the second experiment was chosen at frequencies where the magnitude of the Bode plot is sensitive to parameter variations. A frequency-modulated random binary input signal was designed for this purpose.

Dynamic test results showed that the extent of non-ideal flow and the degree of disturbance attenuation are significantly affected by the location of the input and output in the chest, the fibre mass concentration, the impeller speed and diameter, and the pulp flow rate through the chest. At higher pulp flow rates and fibre mass concentration greater than 3% the system is prone to a high percentage of channeling and dead volume, and a low degree of upset attenuation even at impeller speeds above the criteria of complete motion used to size the chest. Under these circumstances, the degree of disturbance attenuation could be improved by reducing the pulp flow rate through the chest, increasing impeller speed, or decreasing fibre mass concentration.

It was found that the degree of upset attenuation is a function of the impeller momentum flux, rather than the power input. Dynamic tests made on scale-model and industrial chests showed that the power calculated based on smooth surface motion and even the onset of complete motion inside the chest does not completely eliminate dead volume and channeling. Additional power is required to have a desired dynamic response from the chest.

TABLE OF CONTENTS

List of Tables

List of Figures

Acknowledgements

I would like to express my profound appreciation to my research supervisors Dr. Chad P.J. Bennington and Dr. Guy A. Dumont for their guidance, encouragement, and support provided throughout this project.

I also gratefully acknowledge the advice and helpful suggestions of the members of my thesis committee, Dr. Richard M.R. Branion, Dr. Richard J. Kerekes, and Dr. Ezra Kwok.

I am deeply indebted to Dr. Leonardo C. Kammer of PAPRICAN for his innumerable assistance, especially in system identification.

I am grateful to Mr. Bill Bialkowski – EnTech Control Engineering Inc. – for providing industrial data. I also thank Chemineer Inc. for supplying the impellers.

I acknowledge the assistance of all the staff in Pulp and Paper center and Chemical and Biological Engineering Department at UBC. I am particularly grateful to Peter Taylor and Tim Patterson for their valuable help in the fabrication and installation of the experimental setup. Technical assistance from Ken Wong, computer support from Brian McMillan, and administrative assistance from Brenda Dutka, Lisa Brandly, Helsa Leong, and Lori Tanaka are highly appreciated.

Sincere thanks go to Dave L. Pouw of PAPRICAN for his help in the instrumentation of the experimental setup.

Financial support from the Mechanical Wood-Pulps Network and the Pulp and Paper Research Institute of Canada (PAPRICAN) is gratefully acknowledged.

To Laleh,

For her love, encouragement, and support.

CHAPTER 1

1 INTRODUCTION

Agitated pulp stock chests in pulp and paper mills perform a number of functions. Their chief purpose is to reduce high-frequency disturbances in pulp properties (mixture composition, fibre mass concentration, freeness, etc.) ahead of many pulping and papermaking unit operations. In essence, those chests behave as low-pass filters. This complements the action of control loops which can only attenuate low-frequency variability below the loop cut-off frequency (Bialkowski, 1992). It is important to ensure these chests are properly designed to achieve the desired overall degree of upset attenuation. Dynamic tests made on industrial stock chests show that non-ideal flows such as channeling, recirculation, and stagnant zones exist in agitated pulp stock chests. These non-ideal flows reduce the degree of upset attenuation at frequencies higher than the cut-off frequencies of paper machine control loops (Ein-Mozaffari et al., 2001). These disturbances are not fully attenuated, reducing paper quality and machine run-ability.

Little information is available on the effects of non-ideal flow on the dynamic behavior of stock chests, although studies have been made on ideal chests (Walker and Cholette, 1958; Reynolds et al., 1964; Brown, 1968). Since ignoring non-ideal flows can lead to errors in system design (Levenspiel, 1998), it is necessary to study the dynamic behavior of stock mixing under realistic mixing conditions. Current stock chest design is largely empirical and mostly proprietary. Therefore, the objectives of this study are: to enhance understanding of the dynamic behavior of stock chests, to improve upset attenuation by reducing the effects of non-ideal flows, and to incorporate process dynamics in the design criteria so that good mixing with a predictable dynamic response profile can be attained.

Chapter two reviews our current understanding of pulp suspension rheology, the mixing of Newtonian and non-Newtonian fluids, the existing design criteria of agitated pulp stock chests, and then dynamic behavior and the application of parametric and non-parametric methods in dynamic modeling.

In chapter three the specifications of the scale-model chest designed for this study, the experimental setup and procedures are described. In chapter four macroscale mixing characteristics are examined in terms of required power for complete motion, mixing time, and the resulting flow pattern observed in the scale-model chest. Existing correlations and design methods of agitated pulp stock chests are evaluated and the dynamic response of liquid and solid phase tracers are compared. Therefore, this chapter concentrates on preliminary batch studies made on the scale-model chest to characterize its behavior and to develop test protocols for use in later dynamic tests.

In chapter five the effect of non-ideal flow (channeling, recirculation and dead zone) on the performance of agitated pulp stock chests as low-pass filters is discussed and a dynamic model of an agitated pulp stock chest, incorporating these non-ideal flows, is developed. A numerical method for the estimation of dynamic model parameters from input-output data is presented.

To estimate the parameters of the dynamic model, the system must be excited by a proper input signal. Chapter six concentrates on excitation design and input-output data collection. The choice of input signals has a very substantial influence on the parameter estimation. In fact all modes of the system should be excited during the identification experiment. Therefore, in this chapter a frequency-modulated random binary input signal is designed for this purpose.

To improve the upset attenuation in the chest, the effect of non-ideal flows such as channeling and dead volumes must be reduced. In chapter seven the effect of impeller speed and diameter, fibre mass concentration, pulp flow rate through the chest, and pulp feed and exit locations on channeling, fully mixed volume, and disturbance attenuation is explored. In this chapter the effect of existing design methods using the criterion of complete surface motion (Yackel's method) or the onset of complete motion on dynamic response is investigated.

In chapter eight the performances of six industrial stock chests are evaluated based on dynamic tests made on these chests. Chapter nine summarizes the overall conclusions of this study and gives recommendations for future work.

CHAPTER 2

2 LITERATURE REVIEW

2.1 Introduction

Mixing is important in all the chemical process industries, and the pulp and paper industry is no exception. Mixing and agitation are an integral part of pulp and paper manufacturing process. For stock blending, consistency control, bleaching, chemical generation, and deinking, effective mixing is vital to successful process results. In pulp and paper industry –as in all other industries- mixing may be defined as an operation to reduce non-uniformities in composition and/or properties or to prevent the occurrence of the formation of non-uniformities. The agitated pulp stock chest is a subject of great importance as it impacts almost all facets of pulp and paper manufacture. Stock chests perform a number of functions. They act as a buffer between processes to permit continuous operation in the event of a breakdown, and reduce variability in fibre mass concentration, freeness and other quality factors. From the standpoint of variability reduction, stock chests provide a mean of reducing fast or high frequency variability. In essence those chests behave as a low-pass filters. This complements the action of control loops which can only control low-frequency variability below the loop cut-off frequency (Bialkowski, 1992). It is important to ensure that such chests are designed properly to achieve the desired degree of upset attenuation.

Although much work has been done on fundamental understanding of mixing (Uhl and Gray, 1966; Holland and Chapman, 1966; Brodkey, 1975; Nagata, 1975; Nauman and Buffman, 1983; Oldshue, 1983; Ulbrecht and Patterson, 1985; Harnby et al., 1985; McDonough, 1992; Zlokarnik, 2001), pulp suspension rheology (Gullichsen and Harkonen,

1981; Bennington, 1988; Bennington et al., 1990 and 1995) pulp suspension mixing (Oldshue and Gretton, 1956, 1958; Walker and Cholette, 1958; Attwood and Gibbon, 1963; Reynolds et al., 1964; Brown, 1968; Blasinski and Rzyski, 1972; Oldshue and Devries, 1985;Yackel, 1990; Bakker and Fasano, 1993; Bennington and Kerekes, 1996; Bennington, 1996; Wikstrom and Rasmuson, 1998), there still remains uncertainties in the interpretation of mixing in more complex hydrodynamic situations such as the one posed by pulp fibre suspension. This chapter reviews our current understanding of pulp suspension rheology, general equations for the mixing of Newtonian and non-Newtonian fluid, existing design criteria for agitated pulp stock chests, and then dynamic behavior and the application of parametric and non-parametric methods in the dynamic modeling.

2.2 Pulp suspension rheology

The pulp suspension, which is a suspension of wood fibres in water, exhibits a very complex rheology. Pulp suspensions are continuous fibre networks that possess structure and strength resulting from interaction between neighboring fibres. In suspensions having fibre mass concentration greater than 0.5%, cohesive strength occurs from mechanical forces caused by bending and hooking of fibres (Bennington, 1996). As the fibre mass concentration increases, the number of fibre/fibre interactions increases which in turn increases network strength. However, the distribution of fibres within the network is never uniform and local mass concentrations of fibres give rise to flocs within the suspension. Since network strength depends on the number of fibre contacts, flocs have a higher strength than the surrounding suspension. In a flowing pulp suspension, flocs may behave as independent entities.

In mixing it is important to create motion throughout the suspension. This requires the imposition of shear stresses greater than the strength of the pulp network. The initiation of

motion in pulp suspension first occurs at the weak zones of suspension, that is, between flocs. As the applied shear is increased, the relative motion between flocs increases and a reduction in floc size occurs (Kerekes, 1983). A further increase in shear causes more intense movement and leads eventually to turbulent flow.

Figure 2.1 shows torque vs. rotational speed for a bleached pine kraft pulp tested in the concentric cylinder device by Gullichsen and Harkonen (1981). These curves show a number of interesting features:

1- A yield stress must be exceeded before motion can be initiated in the suspension. This yield stress increased as the fibre mass concentration increased.

2- Once motion had been initiated, the shear stress increased or remained approximately constant as rotational speed increased.

3- The pulp suspension flow curves exhibited a discontinuity as they neared the flow curve for water. The points on the curves in Figure 2.1 mark the instant at which the vessel contents were observed to come into a complete turbulence.

4- The torque vs. rotational speed curves for the pulp suspensions approximately followed the water curve after attaining this turbulent state. In this figure the curve for water does not pass through the origin. However, water is a fluid without yield stress.

The creation of turbulence within a suspension is often referred to as fluidization. Fluidization implies relative motion among fibres, which leads to energy dissipation. Thus one potential method of quantifying fluidization is through power and energy expenditure. This concept was introduced by Wahren (1980) in his estimation of power dissipation per unit volume for the onset of fluidization (ε_f). He estimated values for the onset of fluidization from pulp suspension yield stress (τ_y) and obtained the following correlation:

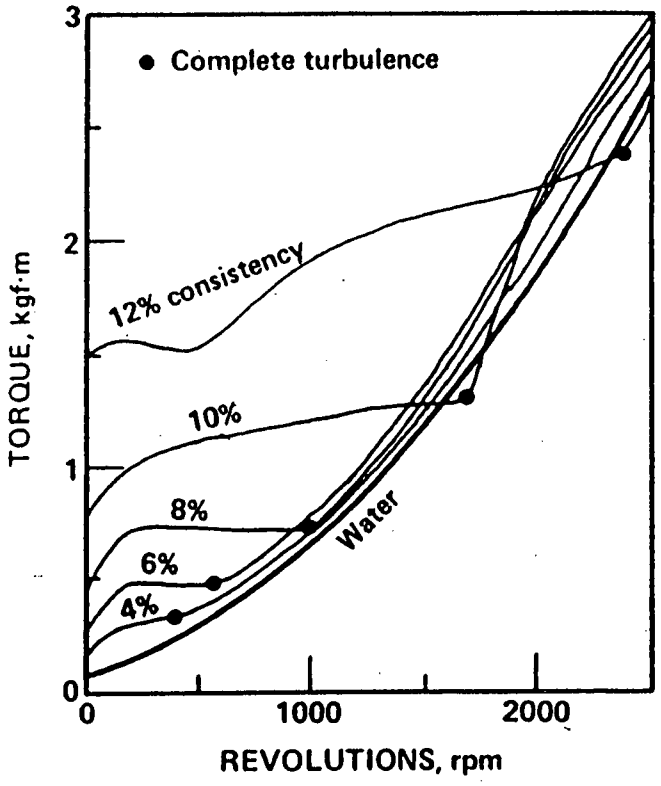

Figure 2.1: Torque vs. rotational speed response of pulp in dynamic shear test. Results are for a bleached pine kraft tested by Gullichsen and Harkonen (1981)

$$\varepsilon_f = \frac{\tau_y^{\,2}}{\mu} = 1.2\times10^4 C_m^{\,5.3} \tag{2.1}$$

where C_m is fibre mass concentration given as a percent and μ is the viscosity of water. Gullichsen and Harkonen (1981) visually determined the onset of fluidization in a rotary device. They defined fluidization as the onset of turbulent motion throughout the vessel. This point was also characterized by a sharp increase in the torque on the rotor (see Figure 2.1). An expression for the ε_f was obtained from their data by Bennington (1988) as:

$$\varepsilon_f = 3.4\times10^2 C_m^{3.4} \tag{2.2}$$

It can be noted that, for any given fibre mass concentration, the dependence of power dissipation for fluidization on fibre mass concentration measured by Gullichsen and Harkonen is approximately two orders of magnitude less than that estimated by Wahren. This may be due to differing definitions of fluidization (Bennington et al., 1991). However, a more likely explanation lies in Wahren's use of the viscosity of water in Equation 2.1. If a pulp suspension behaves as a fluid, the suspension has an apparent viscosity, which is most certainly larger than that of water (Bennington and Kerekes, 1996). Therefore the use of the viscosity of water to estimate the power required to fluidize a pulp suspension is inappropriate. Bennington and Kerekes (1996) used the criterion chosen by Gullichsen and Harkonen (1981) for the onset of fluidization to develop an expression to estimate the energy dissipation necessary for fluidization:

$$\begin{aligned} &\varepsilon_f = 4.5\times10^4 C_m^{2.5}(D_T/D)^{-2.3}; \\ &1.3 \le D_T/D \le 3.1; 1.0 \le C_m \le 12.6 \end{aligned} \tag{2.3}$$

where D_T is the diameter of the housing, D is the diameter of the rotor, and C_m is the fibre mass concentration, in percent. This equation can be extrapolated to a zero gap size ($D \rightarrow D_T$), to obtain:

$$\varepsilon_f = 4.5\times10^4 C_m^{2.5} \tag{2.4}$$

Since the power dissipation depends on the geometrical parameters of the mixer, the values given by Equation 2.2 and Equation 2.4 are different. For the Gullichsen and Harkonen tests,

the smaller number of impeller lugs and housing baffles may account for the lower power measured at any fibre mass concentration (Bennington and Kerekes, 1996).

Bennington (1996) measured the yield stress of a number of pulp suspensions over the wide range of fibre mass concentration (0.4-50%) and void fraction (0-90%) encountered in pulp processes. Using a cylindrical shear-tester with profiled rotors to impose shear within the network rather than at the network-solid interface, it was found that:

$$\tau_y = 7.7 \times 10^6 C_m^{3.2} (1 - X_g)^{3.4} A^{0.6} \tag{2.5}$$

where τ_y is the yield stress of the network in Pascal, C_m is the fibre mass concentration and X_g the gas content of the suspension both expressed as fractions, and A is the fibre aspect ratio.

As a result of this rheological behavior fibre suspensions are extremely difficult to agitate. To provide motion through the whole tank the shear stress has to exceed the yield stress everywhere in the suspension. Since gradients in shear stress can be expected, there will be regions in the fluid around the impeller where the fibre network structure is disrupted and the flow will be turbulent. At the same time the flow may be laminar or even be stagnant in other parts of the tank.

2.3 Mixing scales

Mixing may be defined as an operation to reduce non-uniformities in composition and/or properties. To achieve a well-mixed state, non-uniformities must be eliminated. Non-uniformities scales may span a wide spectrum of sizes. One useful basis to define scales of non-uniformities is the distance of relative motion required to even out variations (Bennington,

1996). The main concept in this approach is that of the division of mixing into two sub-processes namely, macroscale mixing and microscale mixing.

Macroscale mixing refers to large-scale flow characteristics (e.g. convection, turbulent dispersion) that are responsible for large-scale distributions in the system (e.g. residence time distribution, age distribution, etc.). These features are characterized by flow pattern, power input and circulation time.

Microscale mixing is concerned with all features of mixing that cause attainment of homogeneity at the small scale and molecular level. Small-scale variations can be removed by shear –local relative fluid movement induced by velocity gradients or turbulence, and by diffusion –molecular movement induced by concentration gradients.

2.4 General equation

2.4.1 Power consumption for Newtonian fluids

The general dimensionless equation for agitator power was derived by the early investigators using dimensional analysis. They considered that impeller power should be a function of the geometry of the impeller and the tank, the properties of the fluid (viscosity and density), the impeller speed, and the gravitational force. The Buckingham pi theorem gives the following general dimensionless equation for the relationship of variables (Rushton et al., 1950; Uhl and Gray, 1966):

$$f\left[\left(\frac{\rho D^2 N}{\mu}\right),\left(\frac{DN^2}{g}\right),\left(\frac{P}{\rho D^5 N^3}\right),\left(\frac{D}{T}\right),\left(\frac{D}{Z}\right),\left(\frac{D}{c}\right),\left(\frac{D}{p}\right),\left(\frac{D}{w}\right),\left(\frac{D}{l}\right),\left(\frac{n_2}{n_1}\right)\right]=0 \qquad (2.6)$$

where D, T, Z, c, w, p, n, l, ρ, μ, P, N, and g are impeller diameter, tank diameter, liquid depth, clearance of impeller off vessel bottom, blade width, pitch of blades, number of blades, blade

length, fluid density, fluid viscosity, power, impeller rotational speed, and gravitational acceleration, respectively.

Confining the discussion to a geometrically similar system, equation (2.6) may be stated as:

$$f\left[\left(\frac{\rho D^2 N}{\mu}\right),\left(\frac{DN^2}{g}\right),\left(\frac{P}{\rho D^5 N^3}\right)\right]=0 \tag{2.7}$$

where: $N_{Re} = \rho D^2 N/\mu$, $N_{Fr} = DN^2/g$, and $N_P = P/\rho D^5 N^3$ are Reynolds number, Froude number, and power number, respectively.

Equation (2.7) may be written in the following form:

$$N_P = K\left(N_{\mathrm{Re}}\right)^a \left(N_{Fr}\right)^b \tag{2.8}$$

where K, a, and b are equation constants. For a fully baffled tank, where surface waves and vortices are absent, the exponent b on the Froude number generally equals 0 and the power number is only a function of the Reynolds number, i.e.:

$$N_P = K\left(N_{\mathrm{Re}}\right)^a \tag{2.9}$$

At high Reynolds numbers, ($N_{Re} > 1000$), when the vessel is adequately baffled, the power number becomes independent of Reynolds number, so that

$$P = N_{P,turb} D^5 N^3 \rho \tag{2.10}$$

where $N_{P,turb}$ is a constant that depends only on the impeller and vessel geometry.

2.4.2 Power consumption for non-Newtonian fluids

When the fluid in the vessel is non-Newtonian, however, the variations in shear rate with distance from the impeller give rise to corresponding variations in fluid consistency. To allow for this, Metzner and Otto (1957) identified an average shear rate (γ_{avg}) in the vessel. The apparent viscosity (μ_a) corresponding to γ_{avg} equals the viscosity of that Newtonian fluid that would show exactly the same power consumption for agitation under identical conditions, at least in laminar flow. Metzner and Otto (1957) found an empirical relationship between the average shear rate (γ_{avg}) and the impeller rotation speed (N) as:

$$\gamma_{avg} = kN \tag{2.11}$$

where k is a constant of proportionality specific to a given geometry. For the disk flat-blade turbine used in their study, a value of 13 was proposed for the proportionality constant k and their approach was found to be a workable one for pseudoplastic fluids.

Calderbank and Moo-Young (1959) studied a wide variety of sizes and types of impellers in Bingham, pseudoplastic, and dilatant fluids and confirmed the conclusion of Metzner and Otto (1957) that the shear rate at an impeller is directly proportional to the impeller speed. However, they found the constant k to be 10 for pseudoplastic rather than 13.

2.4.3 Power consumption for pulp suspension

Oldshue and Gretton (1956) investigated the effect of impeller type, impeller position, impeller to chest diameter ratio, stock type, and fibre mass concentration on power in agitated pulp stock chests. They assumed that the "complete motion" in a chest was achieved when complete stock movement occurred across the surface of the chest.

Gibbon and Attwood (1962) and Blasinski and Rzyski (1972) showed that in the mixing of pulp suspension the power number is a function of Reynolds number and Reynolds number is a function of ND/m where N and D are impeller speed and impeller diameter, respectively. m is a parameter introduced by Head and Durst (1957) and defines the resistance of the fibre suspension to shear as:

$$m = \sqrt{\frac{\tau_y}{\rho}} \tag{2.12}$$

where ρ and τ_y are density and yield stress, respectively. Blasinski and Rzyski (1972) assumed that pulp suspension behaved as a Bingham fluid:

$$\tau = \tau_y + \eta_p \gamma \tag{2.13}$$

where τ, τ_y, η_p, and γ are shear stress, yield stress, plastic viscosity, and shear rate, respectively. The apparent viscosity (μ_a) is then given as

$$\mu_a = \frac{\tau}{\gamma} = \frac{\tau_y + \eta_p \gamma}{\gamma} \tag{2.14}$$

Applying the Metzner-Otto relationship ($\gamma = 10N$), we get:

$$\mu_a = \frac{\tau_y + 10N\eta_p}{10N} \tag{2.15}$$

Head and Durst (1957) showed that the slope of the flow curve for pulp suspension is small. Consequently, $\tau_y >> 10N\eta_p$ and

$$\mu_a = \frac{\tau_y}{10N} \tag{2.16}$$

Substituting this in the Reynolds number gives:

$$N_{\mathrm{Re}} = \frac{10N^2D^2\rho}{\tau_y} = 10\left(\frac{N^2D^2}{\frac{\tau_y}{\rho}}\right) = 10\left(\frac{ND}{m}\right)^2 \tag{2.17}$$

Both Gibbon et al. (1962) and Blasinski et al. (1972) used the above approach to show that for agitation of pulp suspensions inside cylindrical chests equipped with top entering impellers, power number is a function of the Reynolds number and the Reynolds number is a function of *ND/m*. In their study, they assumed that pulp suspension behaved as a Bingham fluid, and that Metzner and Otto's correlation was valid.

In a further study Attwood and Gibbon (1963) showed that

$$P = C_0 D^{2.6} m^{2.9} \tag{2.18}$$

where P is required power for complete motion in the agitated pulp stock chest, D is impeller diameter, and m is defined by Equation 2.12. C_0 is a constant dependent only on the geometry of the mixer. Therefore, by a single experiment in a model at one fibre mass concentration only, it is possible to determine C_0. Based on Equation 2.18 Attwood and Gibbon (1963) developed a scale-up relationship for estimating the power required to give complete motion of the pulp suspension

$$\frac{power\ for\ prototype}{power\ for\ \mathrm{model}} = \left(\frac{impeller\ diameter\ of\ prototype}{impeller\ diameter\ of\ \mathrm{model}}\right)^{2.60} \tag{2.19}$$

Wikstrom and Rasmuson (1998) studied the agitation of pulp suspensions in a 24 m^3 cylindrical tank equipped with a jet nozzle mixer. They assumed that the pulp suspension

behaved as a Bingham fluid and that laminar flow existed inside the chest. They showed that flow field obtained from CFD-calculations deviated increasingly from the velocities measured using sonar doppler velocimetry as the distance from the impeller increased and suggested that a Bingham fluid did not fully describe the rheology of the pulp suspension and a more sophisticated rheology model must be used to predict the entire flow field correctly.

2.4.4 Yackel's method

For any impeller operating freely in a vessel, we understand that the volumetric discharge is at its minimum at the impeller while the fluid velocity is at its maximum at the same point. However, as the fluid stream begins to move away from the impeller, the boundary layer between the fast moving fluid and the stagnant fluid in the vessel begins to entrain additional flow. At the same time, the velocity of the stream begins to decay. The realization that, as the flow increases, velocity decreases in the same ratio led investigators to the concept of "conservation of momentum" and how to use it to describe the capacity of a specific impeller. Fox and Gex (1956) found that the mixing quality is a function of the momentum flux generated by the impeller, rather than the power input. In fact, the same mixing results can be achieved with various power inputs by changing the impeller speed and diameter. A large, low speed impeller can produce equivalent mixing results with less power than is required with a smaller, higher speed impeller.

One of the methods used for designing agitated pulp stock chests is Yackel's method (Yackel and Mahony,1976; Yackel, 1983; Yackel, 1990 and Reed, 1995) based on the impeller momentum number (*Mo*) which is defined by:

$$Mo = Q_{impeller} v \tag{2.20}$$

where $Q_{impeller}$ and v are impeller pumping rate and fluid velocity leaving the impeller, respectively (see figure 2.2). Since $Q_{impeller}$ is proportional to ND^3 and v is proportional to ND, Mo can be rewritten as:

$$Mo = CN^2D^4 \tag{2.21}$$

where C is a constant that depends on the impeller type and impeller geometry. Yackel (1990) presented the effect of chest configuration, fibre mass concentration, stock type, temperature, and retention time on momentum number and showed that the relationship between momentum number and required power for complete motion (P) is as follows:

$$Mo = Q_{impeller}v = \frac{CP^{0.8}}{N_P^{0.8}N^{0.4}\left(\frac{\rho}{g}\right)^{0.8}} \tag{2.22}$$

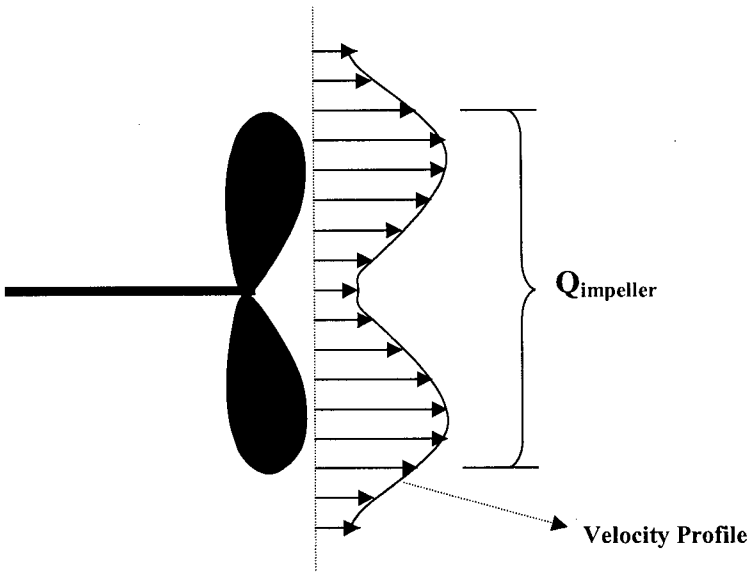

Figure 2.2: Velocity profile for an axial flow impeller (Nienow, 1997)

A scale-up criterion called level momentum was introduced by Yackel (1990) for agitated pulp stock chests. Level momentum (*LMo*) is defined as:

$$LMo = \frac{Mo}{(fluid\ volume)^{\frac{2}{3}}} \tag{2.23}$$

Based on this criterion, level momentum must be equal for model and prototype. McDonough (1992) showed that the average or bulk velocity (v_{bulk}) in an agitated tank is directly proportional to the square root of level momentum of the fluid developed by the impeller:

$$v_{bulk} \propto \sqrt{LMo} \tag{2.24}$$

Equal momentum levels at various scales will yield equal bulk velocities and equal velocities of fluid at corresponding points in different size vessels. Equal velocities in two different scales will produce similar mixing results for macroscale controlled applications such as agitated pulp stock chest.

2.5 Chest shape

In pulp and paper mills both cylindrical and rectangular chests are being used. Yackel (1990) suggested that to achieve complete motion of a pulp suspension with minimum power in a cylindrical chest, the ratio of stock height (Z) to the chest diameter (T) should be 0.8 (Z/T = 0.8). The penalty in increased power above this ratio greatly exceeded the increased volume attained.

Rectangular chests are widely used in pulp and paper industry. It may be asked, why even consider rectangular chests? The answer is quite simple: economics (Reed, 1994).

Cylindrical chests will generally have thinner walls than rectangular chests of the same height because cylindrical chests take advantage of hoop stress design (tension). Rectangular chests, when grouped together using common walls, save space and are equal in cost to equivalent individual cylindrical chests. Also, the optimum shape for a rectangular chest containing a pulp suspension to achieve complete motion is a cube ($L/W = 1.0$ and $Z/W = 1.0$ where L and W are chest length and chest width, respectively.). It is also interesting to note that a cubical chest requires less power than a cylindrical chest ($Z/T = 0.8$) with equivalent volume (Yackel, 1990).

All chests cannot be perfect cubes. Sometimes the L/W ratio must be greater than 1.0. In this case, a general rule of thumb is that the L/W ratio should not exceed 1.5. If it is necessary to have a chest in which the L/W ratio exceeds 1.5 to 2.0, then two agitators will be required (see Figure 2.3). The two units would be sized as though each were in a separate chest. $L/2$ would be used as the L for each unit and the chest would be designed for an $L/W = 1.0$ and $Z/W = 1.0$ (Reed, 1994).

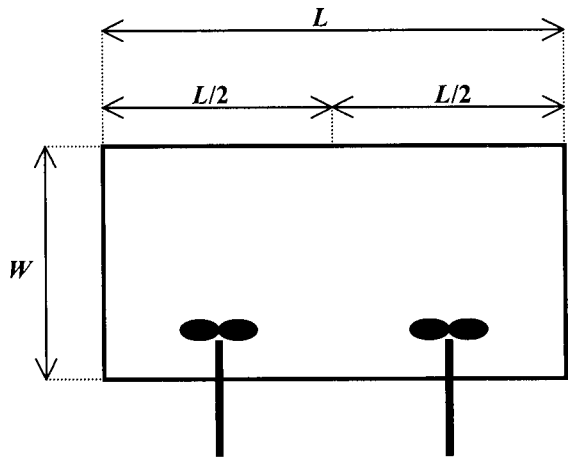

Figure 2.3: Plan view of a chest with $L/W > 1.5$ equipped with two impellers.

Also a controlled zone agitation system is being used in industry as shown in Figure 2.4 (Oldshue, 1983). The agitator is selected based on the requirement of agitating completely across the length or diameter of the tank and to a height that will provide the desired amount of mixing. The upper part of the chest is not agitated but is designed so that continuous plug flow occurs, preventing any stagnant zones. By using such a system, the entire contents of the tank are always in motion.

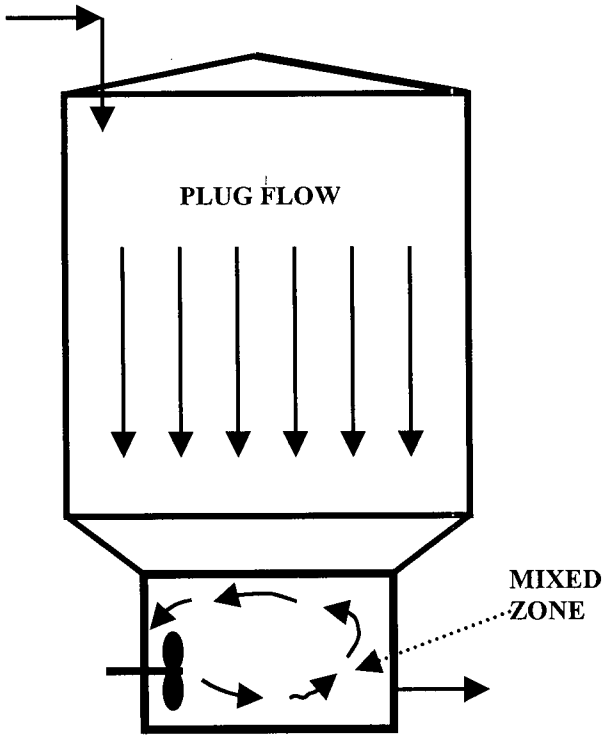

Figure 2.4: Schematic of side-entering impeller in a controlled zone agitation system.

2.6 Impeller types

We can classify impellers as two general types: radial-flow impellers and axial-flow impellers (Zlokarnik, 2001). A radial-flow impeller (flat-blade turbine, bar turbine, anchor, etc.) discharges flow along the impeller radius (see Figure 2.5). These impellers are generally not used in the agitation of pulp suspension but would have applications where high shear and high turbulence are required.

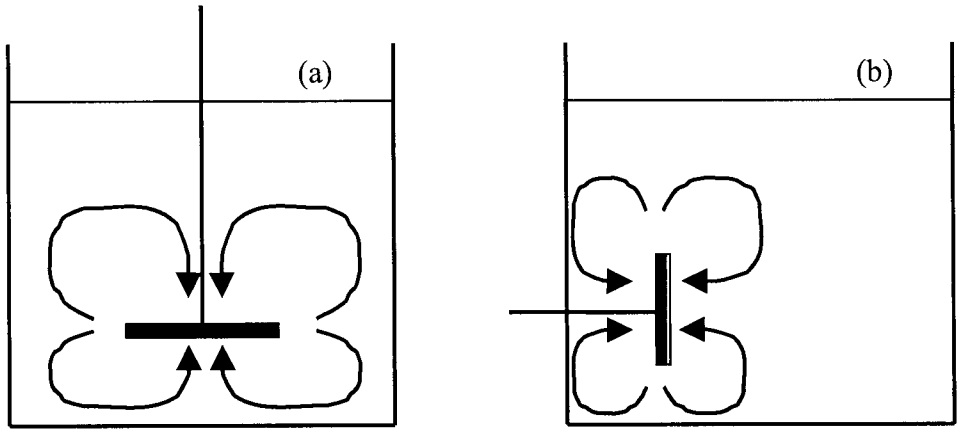

Figure 2.5: Flow pattern for a radial-flow impeller: (a) top-entry (b) side-entry

The second type of impeller is an axial-flow impeller. An axial-flow impeller (marine-type impeller, pitched-blade turbine, Maxflo, etc) is one in which the principal locus of flow occurs along the axis of the impeller (parallel to the impeller shaft, see Figure 2.6). These impellers have been designed to produce high flow with low turbulence. They produce more flow per unit power than do radial impellers and are more cost effective in flow controlled operations (i.e. solid suspension and blending). Therefore, they are widely used for the agitation of pulp suspensions.

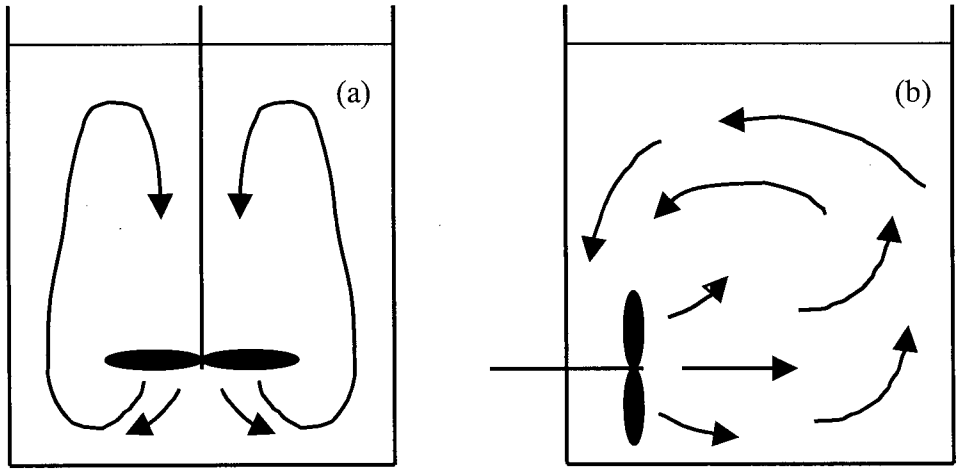

Figure 2.6: Flow pattern for an axial-flow impeller: (a) top-entry (b) side-entry.

Oldshue (1971) compared the performance of side-entering agitators with the performance of top-entering agitators. He concluded that at *Z/T* greater than 0.4, side-entering agitators are more economical than top-entering agitators for the same total volume. Between *Z/T* ratios of 0.4 and 0.25, top-entering agitators come very close to the performance of side-entering agitators, although these chest shapes are not optimum in terms of required power for complete motion.

2.7 Dynamic behavior of agitated pulp stock chest

Agitated pulp chests provide attenuation of high-frequency disturbances in pulp properties (mixture composition, mass concentration, freeness, etc.) ahead of many pulping and papermaking unit operations. Broadly speaking, a chest is expected to reduce the fluctuations of a variable input to a level acceptable for the next stage of processing. This is accomplished

by mixing current production with that produced previously so that random short-term deviations are averaged out and sudden changes turned into tolerable long-term trends (Walker and Cholette, 1958). In essence, those chests act as low-pass filters. This filtering complements the action of control loops, which can only control low-frequency variability.

Perfect mixing is often used to describe a situation where the feed stream is dispersed instantaneously. The composition of the outlet stream is equal to the composition in the tank (Oldshue, 1983). Figure 2.7 shows a perfectly mixed chest. It is assumed that the flows into and out of the chest are equal. $C_{m,in}$ and $C_{m,out}$ are input and output fibre mass concentrations. For an ideally mixed system the fibre mass concentration at any point in the mixed volume is the same and the mixed volume equals the volume of suspension in the chest. Under these conditions the fibre mass concentration in the outlet stream equals the fibre mass concentration in the chest. Therefore, the mass balance for fibres gives:

$$\rho Q C_{m,in} - \rho Q C_{m,out} = \rho V \frac{dC_{m,out}}{dt}$$

$$C_{m,in} - C_{m,out} = \tau \frac{dC_{m,out}}{dt} \qquad (2.25)$$

where t, ρ, Q, V, and $\tau = V/Q$ are time, suspension density, pulp flow rate, suspension volume in the chest, and chest time constant, respectively. Since at steady state $C_{m,in,s} = C_{m,out,s}$, Equation 2.25 can be rewritten as:

$$(C_{m,in} - C_{m.in,s}) - (C_{m,out} - C_{m,out,s}) = \tau \frac{d(C_{m,out} - C_{m,out,s})}{dt}$$

$$C'_{m,in} - C'_{m,out} = \tau \frac{dC'_{m,out}}{dt} \qquad (2.26)$$

where $C'_{m,in} = C_{m,in} - C_{m,in,s}$ and $C'_{m,out} = C_{m,out} - C_{m,out,s}$ are deviation variables (Seborg, et al., 1989). Take the Laplace transforms of both sides of Equation 2.26:

$$\tau s C'_{m,out}(s) = C'_{m,in}(s) - C'_{m,out}(s)$$
$$G(s) = \frac{C'_{m,out}(s)}{C'_{m,in}(s)} = \frac{1}{\tau s + 1} \qquad (2.27)$$

It can be seen that the dynamic behavior of a perfectly mixed chest is represented by a first order transfer function (*G(s)*). However, due to the complex rheology of pulp suspension, deviation from ideality can be considerable in agitated pulp chests. This deviation can be caused by channeling of fluid, by recycling of fluid, or by creation of stagnant regions in the chest (Ein-Mozaffari et al., 2001). Since ignoring the non-ideal flow can lead to errors in system design (Levenspiel, 1998), it is necessary to study dynamic behavior of stock mixing under realistic (less-than-ideal) mixing conditions.

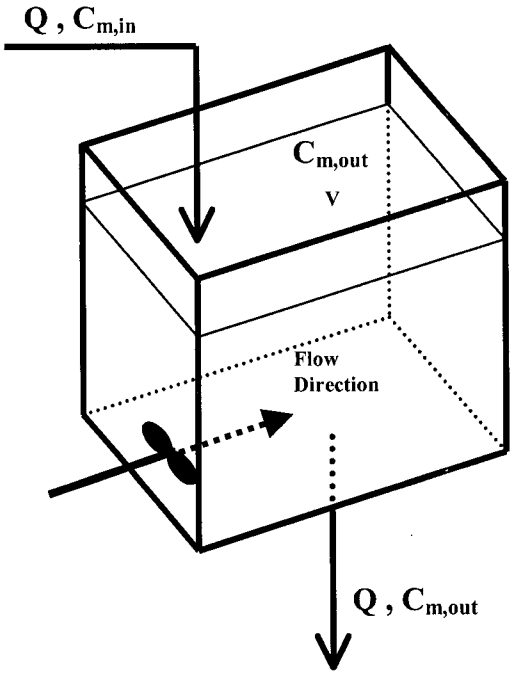

Figure 2.7: A perfectly mixed chest.

Little information is available on the effects of non-ideal flow on the dynamic behavior of stock chests, although studies have been made on ideal chests. For example, Walker and Cholette (1958) calculated the damping factors (the ratio of the amplitudes of the output to the input waves) for an ideal stock chest with a single feed for various disturbances including continuous sine, continuous square wave, and single square wave inputs. They made no comparison between their numerical results and the experimental data. Reynolds et al. (1964) studied the degree of upset attenuation for a stock chest. They suggested that additional smoothing could be achieved by either externally recirculating part of the output or by splitting the feed to the top and bottom of the chest. Brown (1968) studied the dynamic behavior of a paper mill stock chest, assuming ideal mixing, and described the dynamic response with a first order transfer function. In the above studies, effects of non-ideal flow on the dynamic response of stock chests were not considered.

2.8 System identification

System identification is the field of modeling dynamic systems from experimental data (Soderstrom and Stoica, 1989, Ljung, 1992, Ljung, 1999). In general terms, an identification experiment is performed by exciting the system (using some sort of input signal such as a step, a sinusoidal or a random signal) and observing its input and output over a time interval. These signals are normally recorded in a computer for subsequent information. Then we try to fit a parametric model of the process to the recorded input and output sequences. The first step is to determine an appropriate form of the model. As a second step some statistically based method is used to estimate the unknown parameters of the model. In practice, the estimations of structure and parameters are often done iteratively. This means that a tentative structure is

chosen and the corresponding parameters are estimated. The model obtained is then tested to see whether it is an appropriate representation of the system.

2.8.1 Non-parametric methods

Non-parametric methods are characterized by the property that the resulting models are curves or functions, which are not necessarily parameterized by a finite-dimensional parameter vector. Transient analysis is a non-parametric method. In this method the input is taken as a step or an impulse and the recorded output constitutes the model. Transient analysis is an excellent method to get a quick and easy insight into cause and effect relationships, time delays, time constants, and static gains. However, practical limits in the amplitude of the input, together with disturbances and measurement errors may make it difficult to determine quantitative models with a reasonable degree of accuracy. Therefore, transient analysis is a convenient way of deriving crude models. Levenspiel (1998) showed how input-output results, using either step or pulse inputs could give the residence time distribution (RTD) in the mixing tank. He described how the resulting RTD curves could be used for quantification of non-ideal flow in the continuous mixing processes.

Frequency analysis is another non-parametric method. The frequency response of a linear dynamic model describes how the model reacts to sinusoidal inputs. If we let the input be a sinusoid of a certain frequency, then the output will also be a sinusoid of this frequency. However, the amplitude and the phase (relative to the input) will be different. This frequency response is most often depicted by two plots; one that shows the amplitude change as a function of the sinusoid's frequency and one that shows the phase shift as a function of frequency. This is known as a Bode plot.

Frequency analysis is easy to use and requires no complicated data processing. It requires no structural assumptions about the system, other than it being linear. But the basic result is a table or a graph that can not be used directly for simulation. Many systems, especially in a process industry, can not be experimented with freely. Frequency analysis may need long periods of experimentation if the response has to be determined at many frequencies.

2.8.2 Parametric methods

There are two different kinds of parameterized models that can be used in the dynamic modeling (Ljung, 1994):

- Tailor-made models: These models are constructed from conservation laws (mass balance, energy balance, etc.) and constitutive relationships (the relationship between level and output flow of a tank, the relationship between pressure drop and flow for a valve, etc.). The system parameters in this kind of the dynamic model have a physical interpretation.
- Ready-made models: Sometimes we are faced with systems or subsystems that can not be modeled based on physical insights. The reason may be that the function of the system or its construction is unknown or that it would be too complicated to sort out the physical relationships. It is then possible to use standard models, which by experience are known to be able to handle a wide range of different system dynamics. The most common ready-made models are (Ljung, 1999, Soderstrom and Stoica, 1989): ARX (autoregressive with external input), ARMAX (autoregressive moving average with external input), OE (output error model structure), and BJ (Box-Jenkins model structure). The parameters in such models have no direct physical interpretation, but are only used as vehicles to describe the properties of the input-output relationships of the system.

To estimate correctly the unknown parameters in parametric models, it is important that the input signal is persistently exciting. Roughly speaking, this implies that all modes of the system should be excited during the identification experiment (Soderstrom and Stoica, 1989). The most common input signals in system identification are filtered Gaussian white noise, frequency-modulated random binary signal, and pseudo-random binary signal (Ljung, 1999).

2.9 Research objectives

It is clear from the above review of the available literature that the information and our understanding of the macroscale mixing and dynamic behavior of agitated pulp stock chests are still limited. The present study will try to answer some of the remaining questions regarding the design criteria linked to the process dynamics to ensure good mixing with a predictable dynamic response profile. Therefore, the research objectives are:

- To enhance understanding of macroscale mixing and the design criteria for stock chests,
- To study the effects of chest dimensions, impeller speed and diameter, suspension mass concentration, pulp feed and exit location, and pulp flow rate through the chest on dynamic behavior of the stock chests,
- To develop a dynamic model to enable prediction of stock chest response,
- To improve disturbance attenuation by reducing the effects of non-ideal flow such as channeling, recirculation, and stagnant regions in the chest.

Applying the finding of this study will reduce the effects of non-ideal flow, improve suspension mass concentration control in stock chests, and increase paper quality and machine run-ability.

CHAPTER 3

3 EXPERIMENTAL

3.1 Experimental setup

To study the macroscale mixing and dynamic behavior of agitated pulp stock chest, a scale-model stock chest was designed and built. A schematic diagram of the experimental setup is shown in Figure 3.1. Pulp suspension was pumped from the feed tank (1 m^3) to the plexiglas stock chest (0.2 m^3) and back to the discharge tank (1 m^3). Both the feed and discharge pumps are progressive cavity pumps (Moyno Industrial Products, Springfield, OH) equipped with variable frequency drives. Pulp suspension inside the feed tank was agitated using a 63.5 cm (25") top-entering Chemineer (Dayton, OH) A310 impeller driven with a 5-hp variable speed drive. The stock chest is rectangular with dimensions: width, W=40cm, height, Z=70cm, and length, L=70cm (see Figure 3.2). The length of the chest could be changed (to 40 cm, 53 cm or 70cm) to change the L/W ratio. A 3-hp variable speed motor was used to drive three test impellers. These were scaled versions of Maxflo impellers (Chemineer Inc.) having diameters of 10.2 cm (4"), 14.0 cm (5.5") and 16.5 cm (6.5") identical to those used in industry for stock agitation. Impeller torque and speed were measured using an inductive-rotary torque transducer with an encoder disk (model 0411IE50, Staiger Mohilo, Germany). The input and output flow rates were measured using two magnetic flow meters (RoseMount Analytical, Irvine, CA).

To study the dynamic response of the stock chest, a saline solution was injected through a computer controlled solenoid valve (8300D9u, Pacific Controls Ltd. Vancouver, BC) into the pulp stream using a metering pump (C121-362SI, LMI Milton Roy, Acton, MA). To remove pulsating flow from the injection pump, a pulsation dampener (ACCU-PULSE, APIF-PVC-V-

1, Burlington, ON) was mounted close to the injection pump discharge. Conductivity variations in the input and output streams were measured using flow-through conductivity sensors (2220254, RoseMount Analytical, Irvine, CA). For batch tests, the mixing time was measured using a conductivity probe (1921302-31-010T, Phoenix Electrode Company, Houston, TX). The pipe diameter was 5.1 cm (2") for pulp suspension handling and 1 cm (3/8") for tracer injection. Data acquisition was made using a 16-channel data acquisition card (PCI-6024E, National Instruments, Austin, TX) and LabVIEW software. Figure 3.3 shows a photo of our experimental setup.

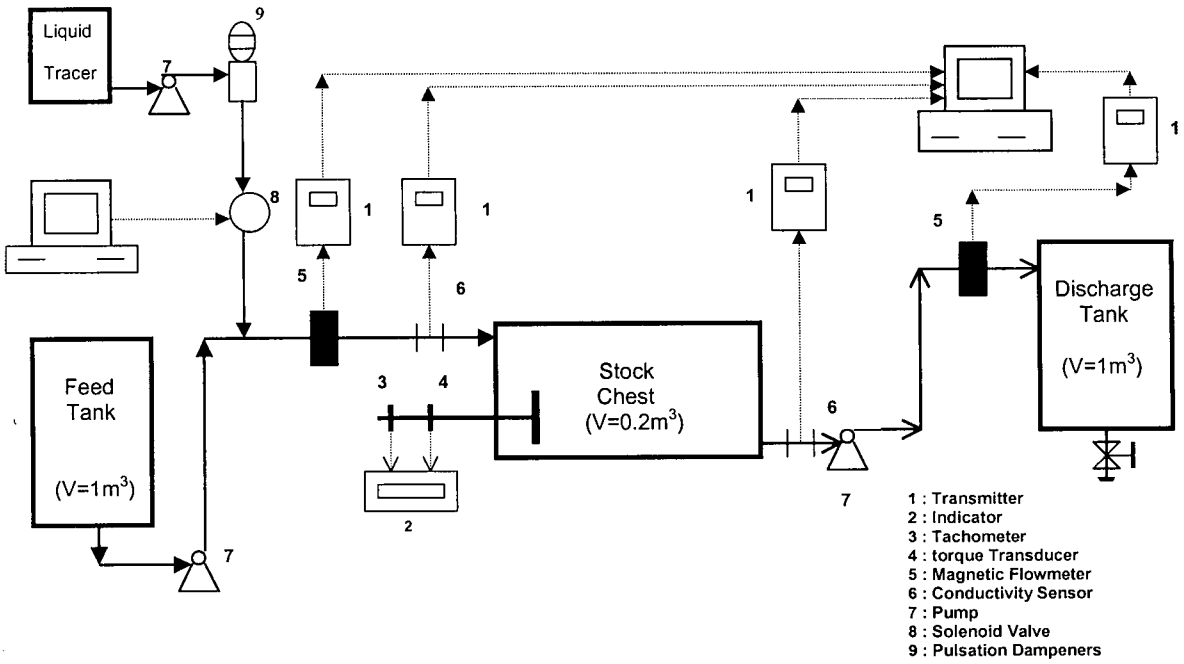

Figure 3.1: Schematic of experimental setup.

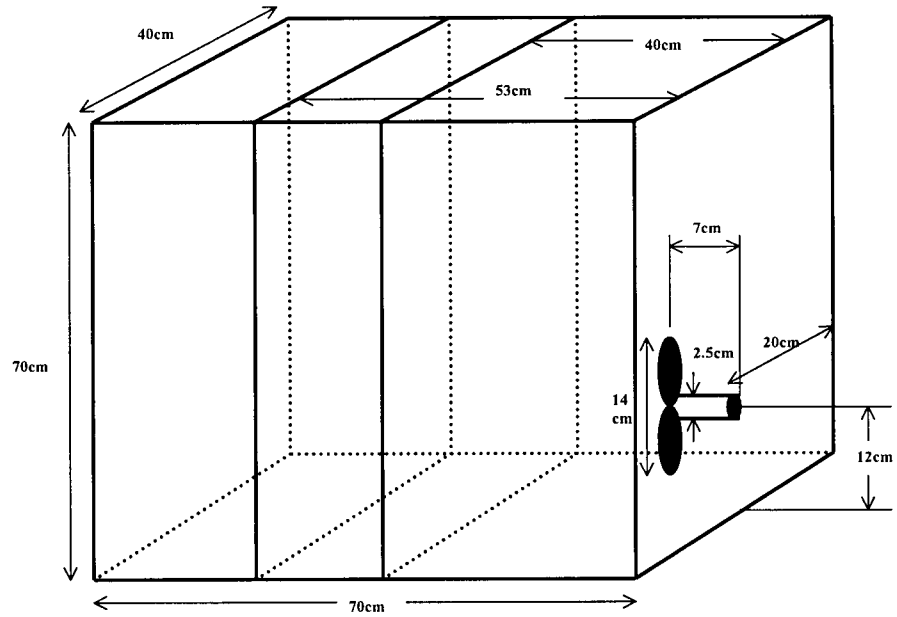

Figure 3.2: Scale-model stock chest dimensions

3.2 Impeller specifications

For this study three Maxflo Mark II impellers having different diameters (10.2 cm, 14.0 cm and 16.5 cm) were used. These axial-flow impellers are geometrically identical to those supplied by Chemineer to industry for stock agitation purposes. Figure 3.4 shows a photo of one of these impellers. The nominal pitch and C factor (see chapter 2) are 0.44 and 0.41, respectively. The power number for fully turbulent flow ($N_{P,turb}$) of the Maxflo impellers is:

$$N_{P,turb} = \frac{P}{\rho N^3 D^5} = 0.276 \qquad (3.1)$$

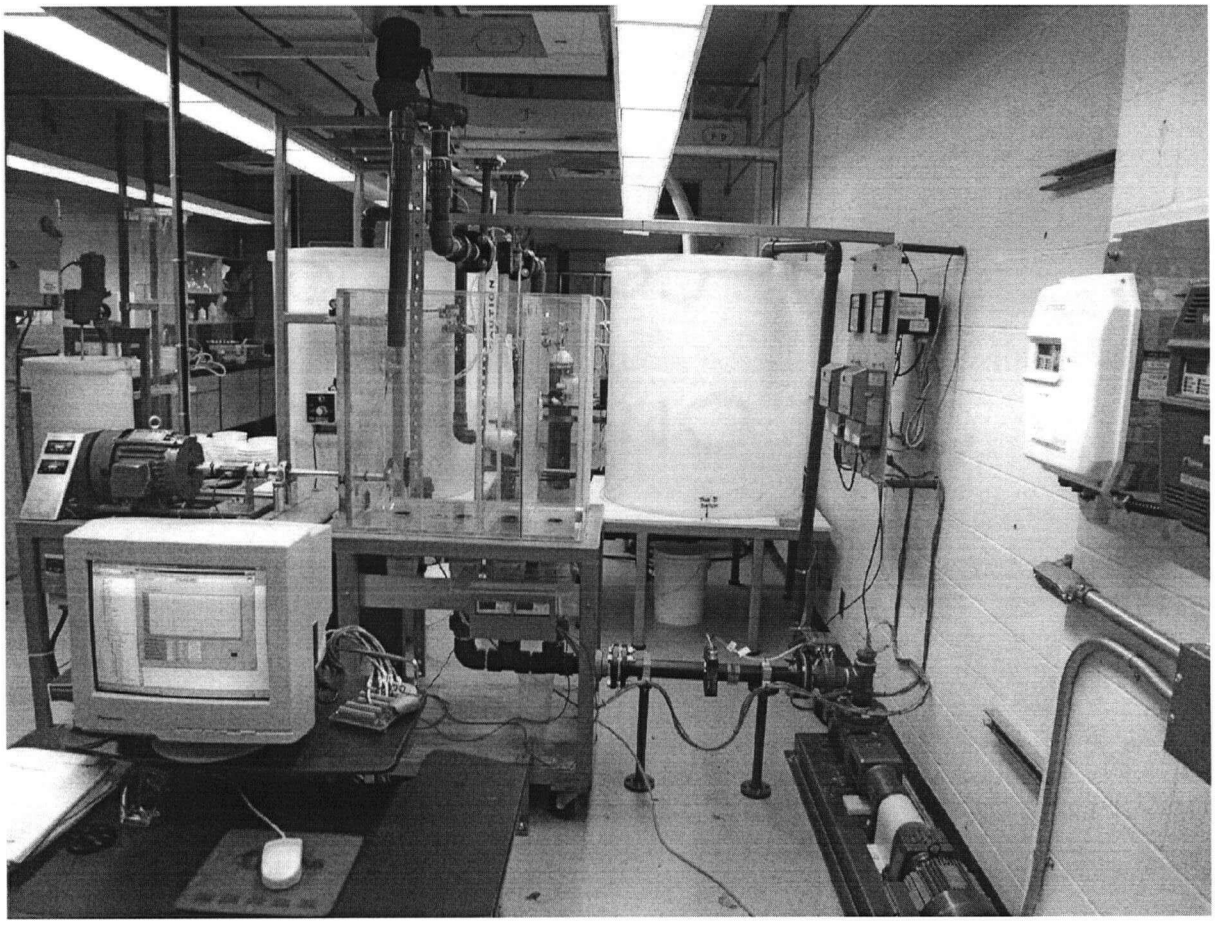

Figure 3.3: Experimental setup

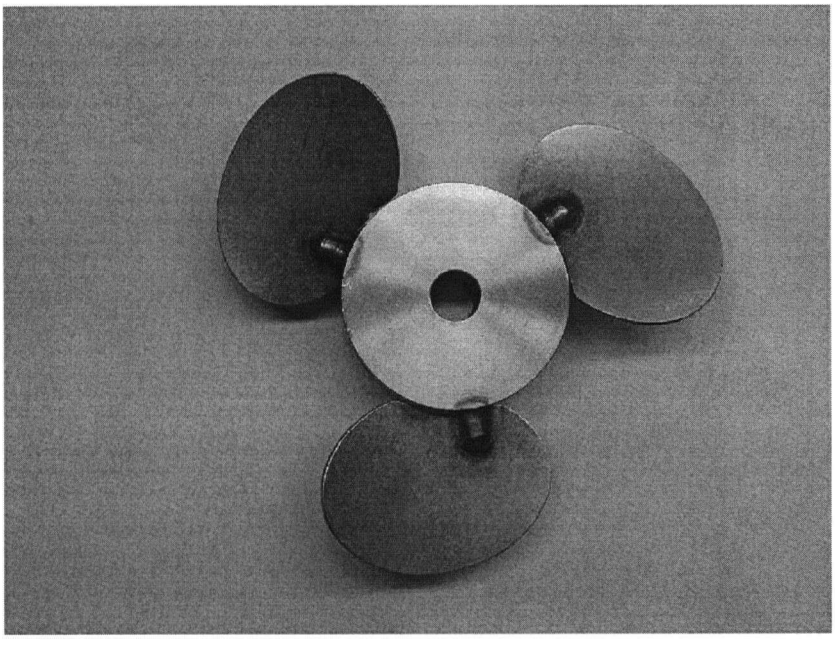

Figure 3.4: Maxflo impeller.

where P, ρ, N and D are power, fluid density, impeller speed, and impeller diameter, respectively. This value is in the range of the typical values of $N_{P,turb}$ (0.1 - 0.5) for the axial flow impellers (AIChE Equipment Testing Procedure, 2001).

The dimensionless flow number (N_Q) for the Maxflo impeller is:

$$N_Q = \frac{Q_{impeller}}{ND^3} = 0.643 \tag{3.2}$$

where $Q_{impeller}$ is the impeller pumping rate (Uhl and Gray, 1966). This value is in the range of the typical values (0.4 – 0.8) for the axial flow impellers (AIChE Equipment Testing Procedure, 2001). The impeller specifications are summarized in Table 3.1.

3.3 Power measurement

The power input to the impeller (P) is obtained from torque (M) and impeller speed (N) measurements using:

$$P = 2\pi NM \tag{3.3}$$

Table 3.1: Maxflo impeller specifications

Diameter	10.2 cm (4") , 14 cm (5.5") , 16.5 cm (6.5")
Pitch	0.44
C factor	0.41
Power number	0.276
Flow number	0.643

Impeller torque and speed were measured using an inductive-rotary torque transducer with an encoder disk (model 0411IE50, Staiger Mohilo, Germany) mounted on the rotor shaft with two flexible couplings at each end to accommodate radial, angular, and axial misalignment. The bearing friction was measured by operating the system with the chest empty. This friction torque was subtracted from all measured torques.

The power consumption per unit mass (also called specific power consumption) can then be obtained:

$$\varepsilon_{avg} = \frac{P}{\rho V} \tag{3.4}$$

where V and ρ are suspension volume and density, respectively.

3.4 Materials

In this study, fully bleached kraft pulp (FBK) was used for preparation of the pulp suspensions. A fully bleached kraft pulp was obtained from a western Canadian mill (Pacifica Paper, BC). The pulp, which was in wet sheet form (about 50% water), was soaked in water and defibred in a disintegrator. Since fibre length is an important property that influences the flocculation and formation of entaglements in fibre suspensions, the average fibre length was determined using LDA96072 Fibre Quality Analyzer. The Fibre Quality Analyzer results for FBK fibres are given in Table 3.2. In this table the length weighted average length (L_l) is defined by Equation 3.5 and the weight weighted average length (L_w) is defined by Equation 3.6:

$$L_l = \frac{\sum_{i=1}^{n} l_i^2}{\sum_{i=1}^{n} l_i} \tag{3.5}$$

$$L_w = \frac{\sum_{i=1}^{n} l_i^3}{\sum_{i=1}^{n} l_i^2} \tag{3.6}$$

Table salt was used for preparation of saline solution. It was obtained from Galloway's Wholesale (Richmond, BC).

Table 3.2: Fibre Quality Analyzer results for FBK fibre

Total number of fibres counted	10459
Arithmetic average length	1.25 mm
Length weighted average length	2.47 mm
Weight weighted average length	3.05 mm
Coarseness	0.143 mg/m

3.5 Test procedure

3.5.1 Dynamic response of liquid and solid phase tracers

To compare the dynamic response of both liquid and solid phases of a pulp suspension, both solid (blue dyed fibre) and liquid (NaCl solution) tracers were injected simultaneously. At $t = 0$, a pulse of tracers was added to the surface of the pulp suspension immediately above the impeller. Samples (about 300 cm^3) were withdrawn from the top of the suspension on a centre-line from the impeller 10cm from the opposite wall. The conductivity of aqueous phase of each sample (proportional to saline concentration in the liquid phase) was measured using a conductivity probe (1921302-31-010T, Phoenix Electrode Company, Housten, TX). A standard

hand sheet was made from the fibre according to standard C.5 of the CPPA Standard Testing Methods. The hand sheets were than optically tested for brightness using the Elrepho 2000 Spectrophotometer. More precisely, the values measured were the $L - a - b$ coordinates, which quantify color and brightness using a tree dimensional scale. For the application at hand, only the "L" brightness scale was used; "a" and "b" quantify color and did not vary much. The "L" brightness scale has a maximum of 100 corresponding to bright white and a minimum of 0 corresponding to black.

In order to correlate the conductivity of the aqueous phase with the percentage of salt and the brightness of the hand sheets with the percentage of blue pulp, two calibration curves were made. Figure 3.5 shows the relationship between conductivity and the salt concentration in aqueous phase and Figure 3.6 shows the relationship between brightness and the blue kraft pulp concentration in the hand sheets.

3.5.2 Mixing time

To study the mixing time in the laboratory stock chest, saline solution was added to the chest and then the suspension conductivity measured by a conductivity probe (1921302-31-010T, Phoenix Electrode Company, Houston, TX) located in front of the impeller (about 20 cm from the impeller centre) and the conductivity signal was recorded in a computer for the mixing time estimation. Figure 3.7 shows the transient response of the scale-model chest to the injection of saline solution. The mixing time was defined as the required time for the conductivity to reach 97% of the steady state value.

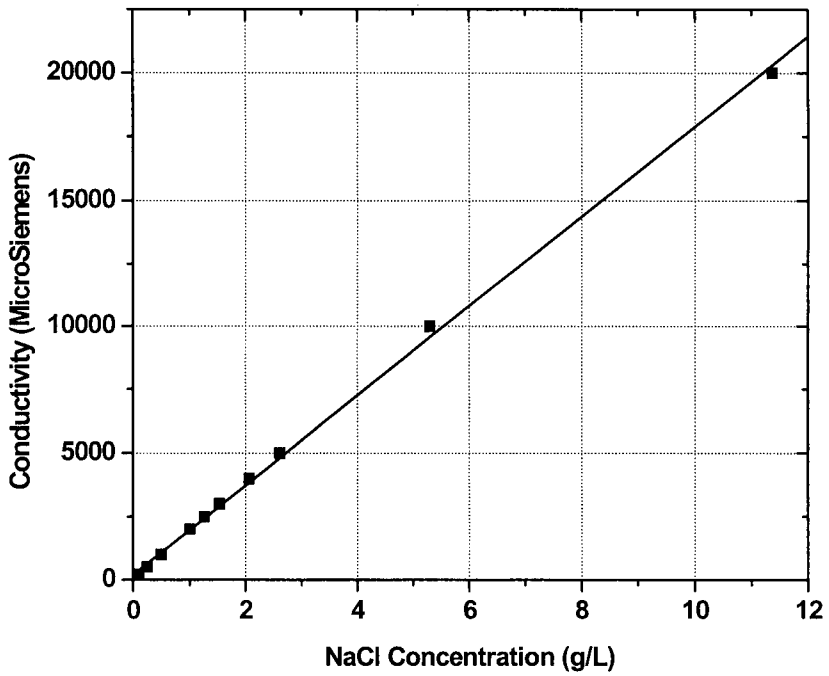

Figure 3.5: Relationship between conductivity and salt concentration in aqueous phase.

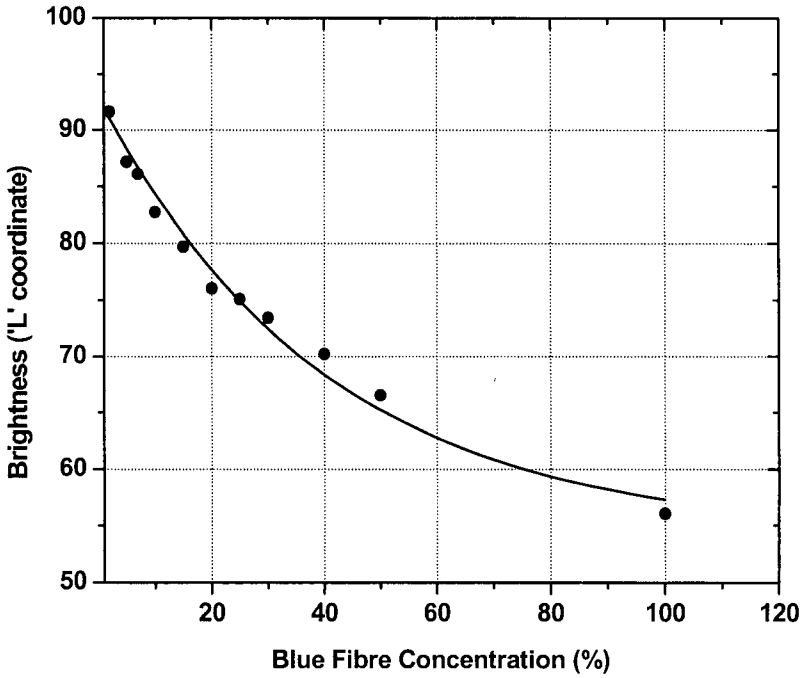

Figure 3.6: Relationship between brightness and blue fibre concentration in hand sheets.

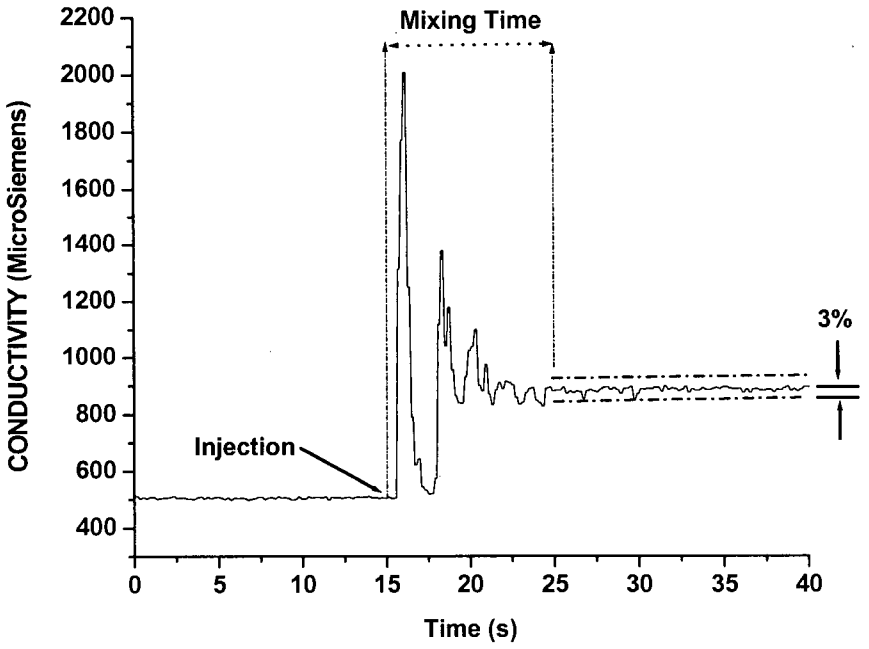

Figure 3.7: Method of determining mixing time.

3.5.3 Dynamic testing procedure

The identification experiment was performed by exciting the system and observing its input and output over a time interval. To study the dynamic response of the stock chest, a saline solution was injected through a computer controlled solenoid valve into the pulp feed stream and the conductivity variations in input and output streams were measured using flow-through conductivity sensors. The input and output signals were recorded in a computer for the estimation of dynamic model parameters. The excitation provided in the dynamic experiments was limited to binary sequences as the input signal was controlled by an on-off solenoid valve. The process of model identification required two experiments. In the first experiment, the input signal was a rectangular pulse, which allowed the estimation of an approximate model for

designing the excitation for the second experiment. The excitation energy for the second experiment was chosen at frequencies where the Bode plot is sensitive to parameter variations (Ljung, 1999). A frequency-modulated random binary input signal was designed for the second experiment. The details are discussed in chapter six.

The control of solenoid valve and data acquisition including conductivity variations and pulp flow rates in input and output streams was accomplished using LabVIEW software.

3.6 Experimental conditions

The effect of operating conditions and design criteria on the dynamic behavior of the stock chest was studied by varying the impeller speed (700 – 1750 rpm), fibre mass concentration (2.1% - 3.3%), pulp flow rate through the chest (7.9 – 37.1 L/min) and impeller diameter (10.2 – 16.5 cm). The effect of pulp feed and exit locations was tested for the two configurations shown in Figure 3.8.

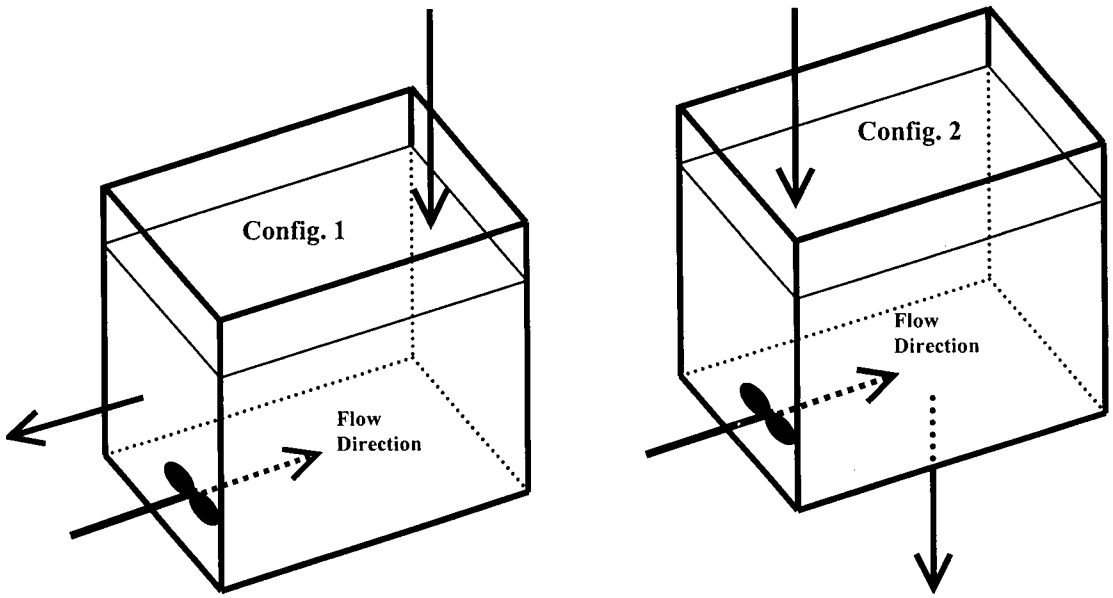

Figure 3.8: Input-output configurations studied.

CHAPTER 4

4 MACROSCALE MIXING IN AGITATED PULP STOCK CHESTS

4.1 Introduction

Macroscale mixing refers to large-scale flow characteristics that are responsible for large-scale distribution in the system. In this chapter macroscale mixing characteristics will be examined in terms of required power for complete motion, mixing time, and the resulting flow pattern observed in the scale-model chest. Existing correlation and design methods of agitated pulp stock chests are evaluated and dynamic response of liquid and solid phase tracers are compared. This chapter concentrates on preliminary batch studies made on the scale-model chest to characterize its behavior and to develop test protocols for use in later dynamic tests.

4.2 Power number

For this study three Maxflo Mark II impellers having different diameters (10.2 cm, 14.0cm and 16.5 cm) were received from Chemineer Inc. These impellers are geometrically scaled versions of those supplied by Chemineer Inc. to industry for stock agitation purposes.

One of the parameters widely used to characterize impeller performance is the power number for fully turbulent flow ($N_{P,turb}$) which is constant for a given impeller:

$$N_{P,turb} = \frac{P}{\rho N^3 D^5} \tag{4.1}$$

where P, ρ, N and D are power input, suspension density, impeller speed and diameter, respectively. The power input per unit mass (ε_{avg}) can be obtained:

$$\varepsilon_{avg} = \frac{P}{\rho V} \tag{4.2}$$

where V is the suspension volume. If we combine Equations 4.1 and 4.2 we obtain an expression for power input per unit mass:

$$\varepsilon_{avg} = N_{P,turb} \frac{D^5 N^3}{V} \tag{4.3}$$

The power number can be obtained by taking a least square regression of the power input per unit mass against the cube of impeller speed when operating under turbulent conditions (Mmbaga and Bennington, 1997 and Bubicco et al., 1997). Figure 4.1 uses this method and gives the power number of the Maxflo impeller as 0.276, identical to the value obtained from the manufacturer. This value is in the range of the typical values of $N_{P,turb}$ (0.1-0.5) for the axial flow impellers (AIChE Equipment Testing Procedure, 2001).

4.3 Required power for complete motion

Oldshue and Gretton (1956) assumed that "complete motion" in a chest was achieved when complete stock movement occurred across the surface of the chest. Industrial design is based on achieving this state. However, observations made in the laboratory chest showed that significant stagnation zones could persist in the chest corners even upon achieving complete surface motion. This would explain the existence of stagnant volumes in industrial chests designed using conventional methods. In this study, "complete motion" is defined to exist when there are no stagnant zones in the chest.

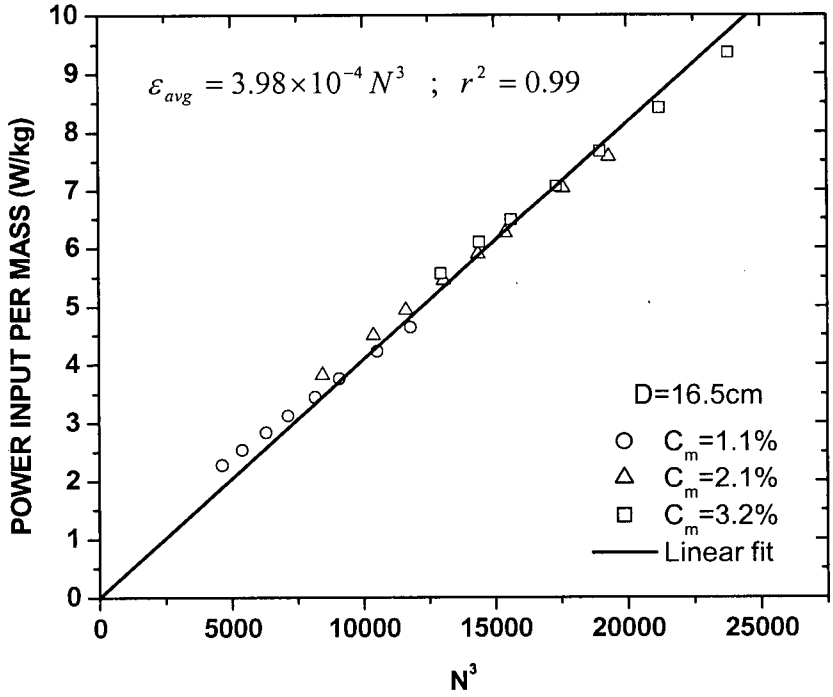

Figure 4.1: Power versus the cube of impeller speed for Maxflo impeller.

A number of factors affect the power required for complete motion in the stock chest. The variables studied include chest dimensions, impeller diameter and fibre mass concentration. Fibre mass concentration is the most critical parameter, as shown in Figure 4.2 with power varying as the square of fibre mass concentration (C_m) over the range of 1.1 - 4.7%. Oldshue (1983) reported that power increased with the cube of suspension mass concentration over C_m = 2 - 6%.

Figure 4.3 shows the effect of the suspension height to chest width ratio (Z/W) on the power. This data show that power decreases as Z/W increases from 0.63, reaching a minimum

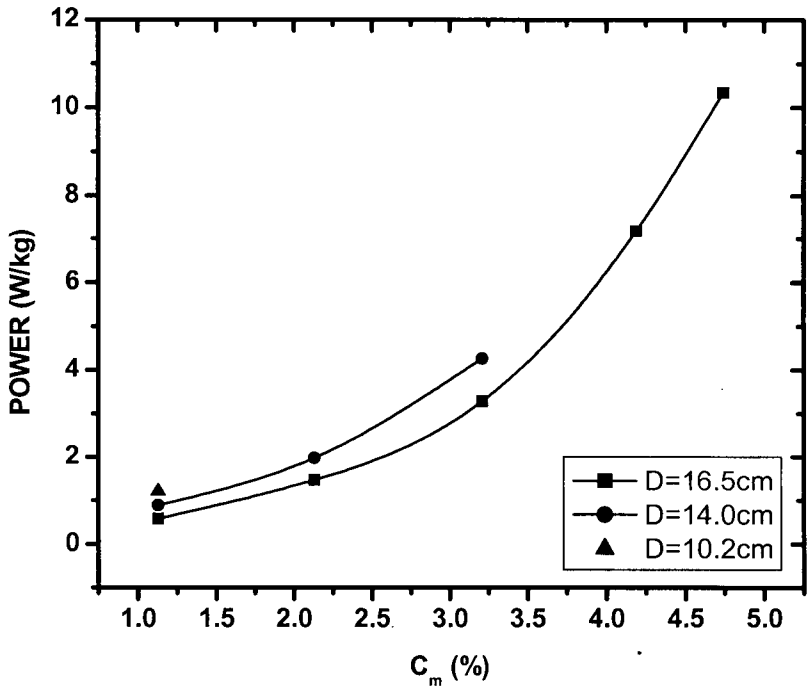

Figure 4.2: Power required for complete stock motion versus the fibre mass concentration. Impeller diameter is given as a parameter.

at Z/W = 1.13. Further increases in Z/W increase the required power. The optimum Z/W ratio for the laboratory chest is close to the optimum ratio of Z/W=1 suggested by Yackel (1990).

Figure 4.4 shows the effect of chest length to chest width ratio (L/W) on power. It can be seen that the optimum L/W ratio for laboratory chest is approximately 1.3 which is in the range 1.0-1.5 suggested by Yackel (1990).

From Figures 4.2 and 4.3 it can be seen that the required power decreases with an increase in impeller diameter. The results show that the impeller having D = 16.5 cm gives the best performance for the agitation of pulp suspension in the laboratory chest. The impeller diameter to chest width ratio (D/W) for D = 16.5 cm is 0.41 again in the range (0.20-0.45)

suggested by Yackel (1990). Therefore, the optimum *Z/W*, *L/W*, and *D/W* ratios for the scale-model chest are in the range suggested in literature.

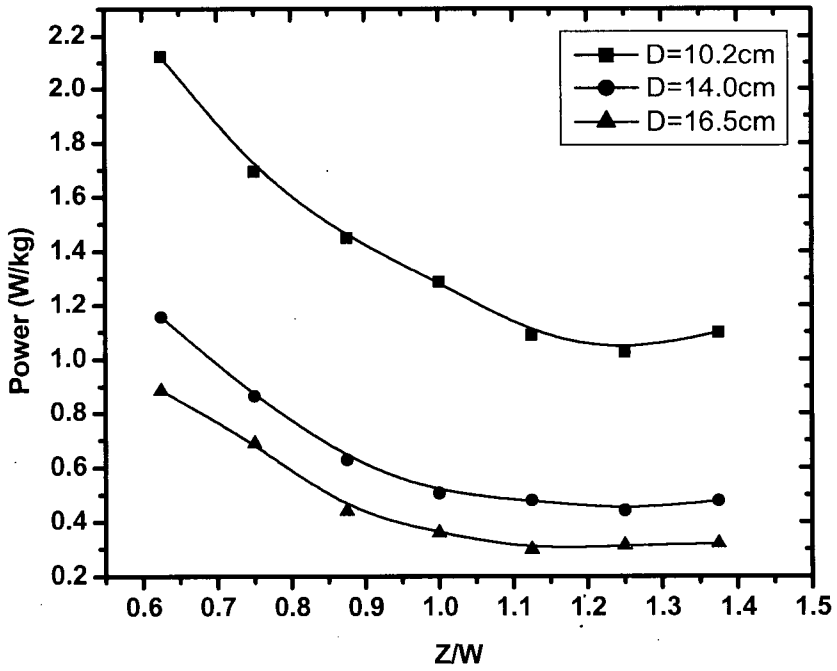

Figure 4.3: Power required for complete motion versus stock height to width ratio (*Z/W*).

4.4 Evaluation of existing correlation and design methods

Gibbon and Attwood (1962) and Blasinski and Rzyski (1972) showed that for agitation of pulp suspensions inside cylindrical chests equipped with top entering impellers, power number ($P/\rho N^3 D^5$) was a function of ND/m, where P is the power, N the impeller speed and D the impeller diameter (see chapter 2). m is equal to:

$$m = \left(\frac{\tau_y}{\rho} \right)^{\frac{1}{2}} \tag{4.4}$$

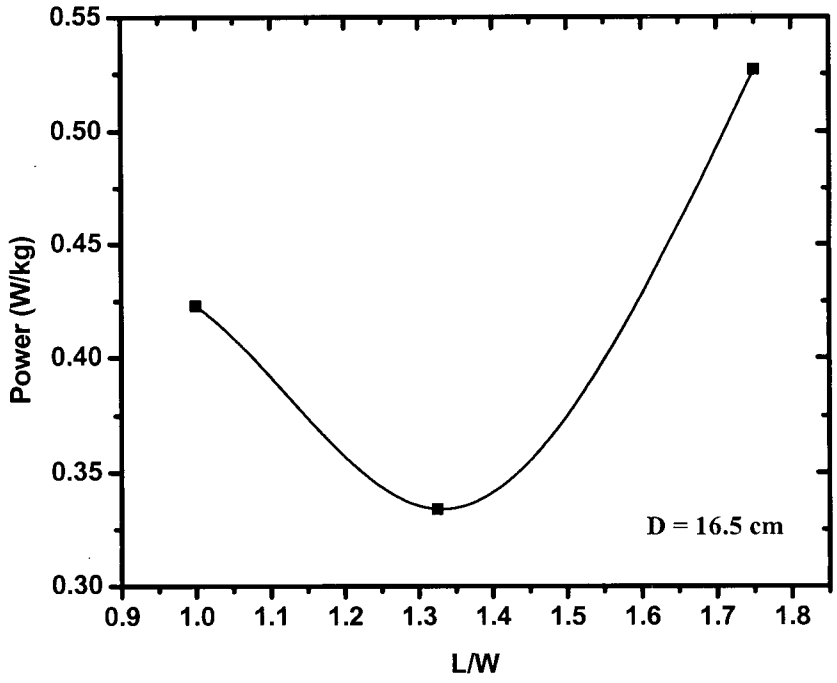

Figure 4.4: Power required for complete motion versus chest length to width ratio (*L/W*).

where τ_y is suspension yield stress and ρ the suspension density. In their study, Gibbon and Attwood assumed that pulp suspension behaved as a Bingham fluid, and that Metzner and Otto's (1957) correlation ($\gamma_{avg} = KN$, where γ_{avg} is average shear rate, N is impeller speed, and K is a constant $\cong$ 10) was valid.

In this study the yield stress for the FBK pulp suspension was calculated using the correlation developed by Bennington et al. (1990) for a fully bleached kraft pulp similar to the one used in this work:

$$\tau_y = 3.12 \times 10^6 C_m^{2.79} \tag{4.5}$$

where C_m is the fibre mass concentration (in Equation 4.5 given as a fraction). The power number versus *ND/m* is plotted for data obtained from laboratory chest in Figure 4.5. It can be seen that the power number changes with fibre mass concentration. Thus, for rectangular chest geometry power number is not only a function of *ND/m* but also of the fibre mass concentration. Therefore, the rheology of a pulp suspension can not be solely described by the *m* factor. Wikstrom and Rasmuson (1998) studied the agitation of pulp suspensions assuming that the pulp suspension behaved as a Bingham fluid and that laminar flow existed inside the chest. They showed that flow field obtained from CFD-calculations deviated increasingly from the velocities measured using sonar doppler velocimetry as the distance from the impeller increased and suggested that a Bingham fluid did not fully describe the rheology of the pulp

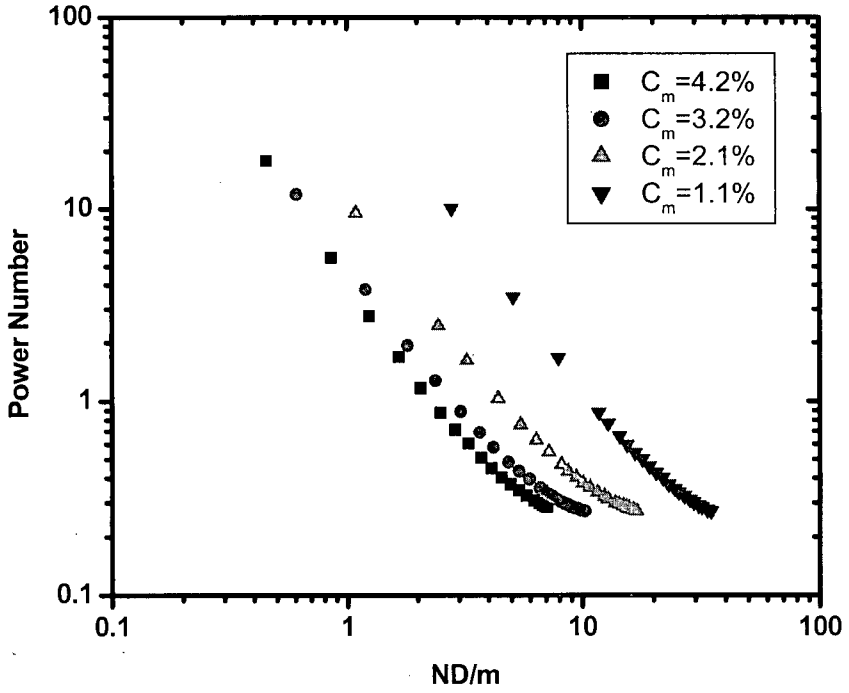

Figure 4.5: Power number versus *ND/m* for tests conducted in the scale-model chest.

suspension. Figure 4.5 supports the results found by Wikstrom and Rasmuson that the rheology of pulp suspension is more complex than a Bingham fluid.

One of the methods used for designing agitated pulp stock chests is Yackel's method (1990) based on the momentum flux generated by the impeller. The impeller momentum number (*Mo*) is defined by: $Mo = Q_{impeller}v$ where $Q_{impeller}$ is impeller pumping rate and v is fluid velocity leaving the impeller. Since $Q_{impeller}$ is proportional to ND^3 and v is proportional to ND, Mo can be rewritten as: $Mo = CN^2 D^4$ where C is a constant that depends on the impeller geometry and impeller type. In Figures 4.6 and 4.7 the power and momentum number needed for complete motion in the laboratory chest are compared with those calculated using Yackel's method. It can be seen that the values calculated from Yackel's method are less than the values

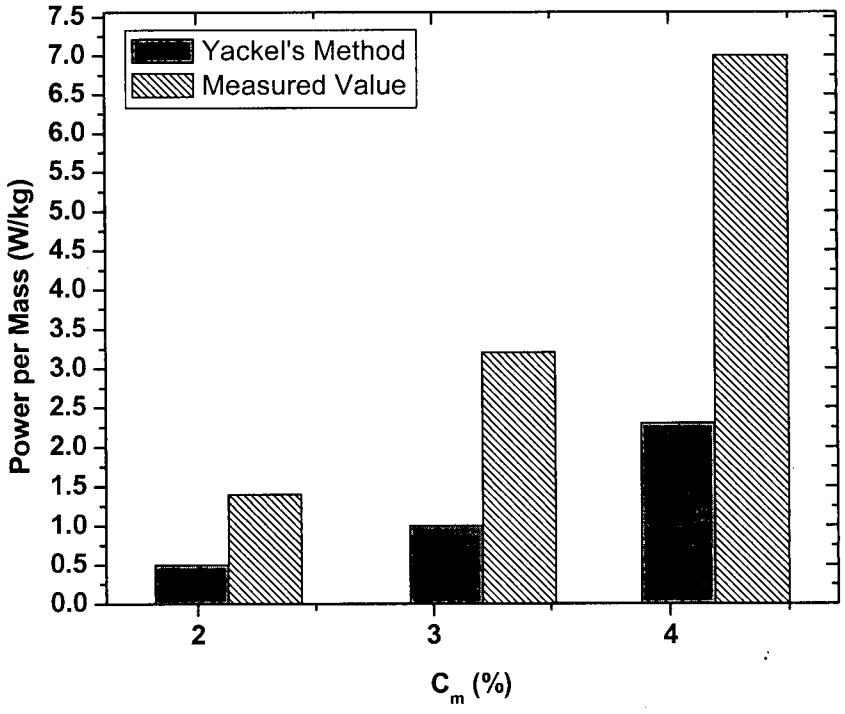

Figure 4.6: Comparison between power needed for complete motion in the scale-model chest and that calculated using Yackel's method.

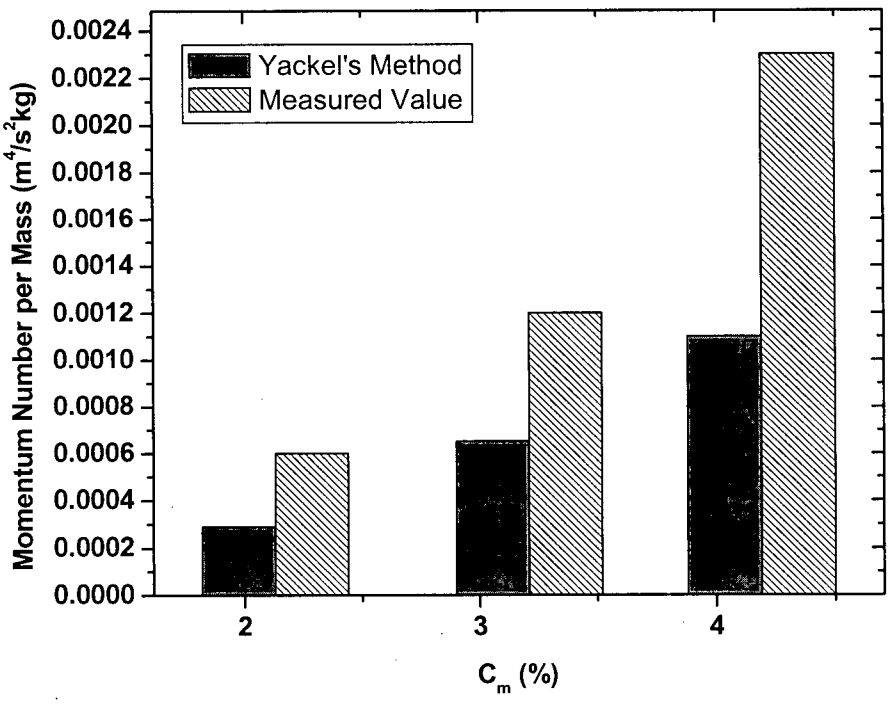

Figure 4.7: Comparison between impeller momentum number needed for complete motion in the scale-model chest and that calculated using Yackel's method.

we found.

The likely reason for this is that in the existing design methods assume that complete motion inside the chest can be achieved when smooth surface motion is observed. However, tests made with the laboratory chest showed that even with smooth surface motion considerable stagnant zones could exist in the corners of the chest, especially at the bottom of the chest along the impeller opposite wall. Since in this study we define "complete motion" when there is no stagnant zones in the chest, additional power was required.

4.5 Dynamic response of liquid and solid phase tracers

Different types of tracers have been used to study the dynamic response of stock chests. Radioactive tagged fibres, sodium chloride solution, and radioactive lithium were used by Attwood and Gibbon (1963), Brown (1968), and Ljung and Glad (1994), respectively. But nothing has been reported regarding the comparison of dynamic response of liquid and solid phase tracers.

To compare the dynamic response of both liquid and solid phases of a pulp suspension, both solid (dyed fibre) and liquid (NaCl solution) tracers were injected simultaneously. At t = 0, a pulse of tracers was added to the surface of the pulp suspension immediately above the impeller. Samples were withdrawn from the top of the suspension on a centre-line from the impeller 10cm from the opposite wall. The solid and liquid phases were separated by filtration. The conductivity of aqueous phase of each sample (proportional to saline concentration in the liquid phase) was measured. A standard hand sheet was made according to standard C.5 of the CPPA Standard Testing Methods from the fibre and its brightness (proportional to the concentration of dyed fibers) determined.

The response curves for both solid and liquid phase for three different fibre mass concentrations are shown in Figures 4.8 to 4.10. These results show that at suspension mass concentrations greater than 2%, the solid and liquid phase mixing response curves are very similar.

Pulp suspensions are continuous fibre network and possess structure and strength resulting from interactions between neighboring fibres. As the mass concentration of the suspension increases, the number of fibre/fibre interactions increases which increases network strength (Bennington, 1996). Therefore, solid/liquid phase tracer behavior become closer as fibre mass concentration increases. A possible explanation can be offered. The zone of active

suspension motion around the impeller, where flocs are disrupted, is reduced (at a given N) as C_m increases. Reflocculation occurs rapidly in the decaying turbulence as flow moves away from the impeller. At higher C_m and lower N, the volume of this active zone is smaller. Consequently, the dynamic responses of both liquid and solid tracers are more similar. Therefore, using saline solution as a tracer in the study of mixing time and dynamic behavior of agitated pulp stock chest will be acceptable for fibre mass concentrations greater than 2%.

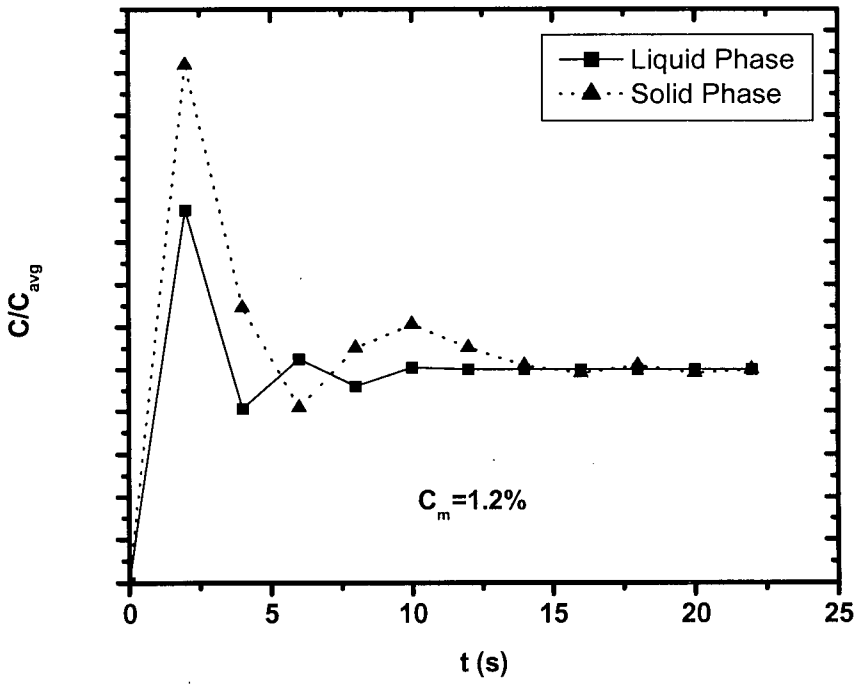

Figure 4.8: Dynamic response of liquid and solid tracers at C_m = 1.2% and N = 549 rpm.

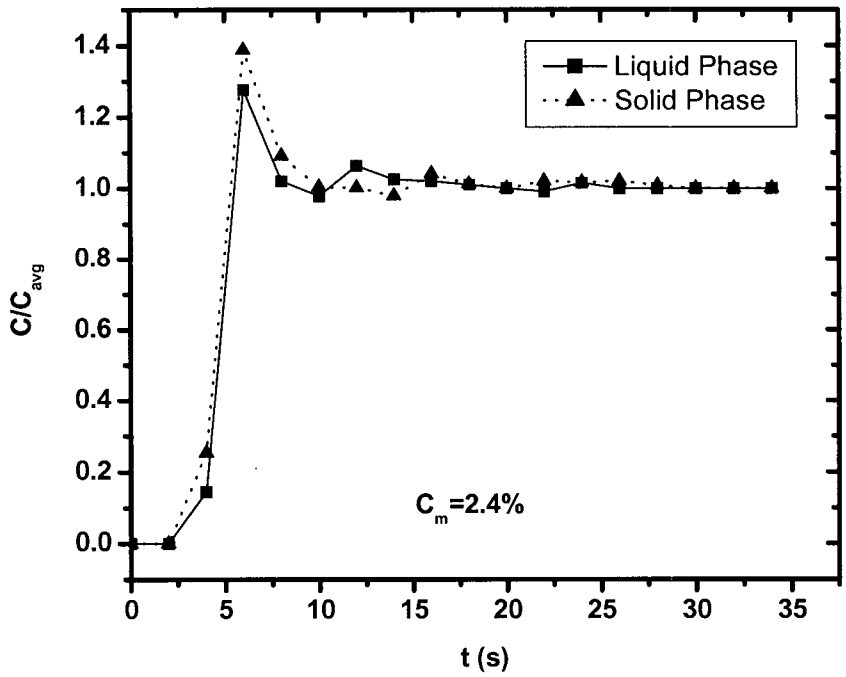

Figure 4.9: Dynamic response of liquid and solid tracers at $C_m = 2.4\%$ and $N = 948$ rpm.

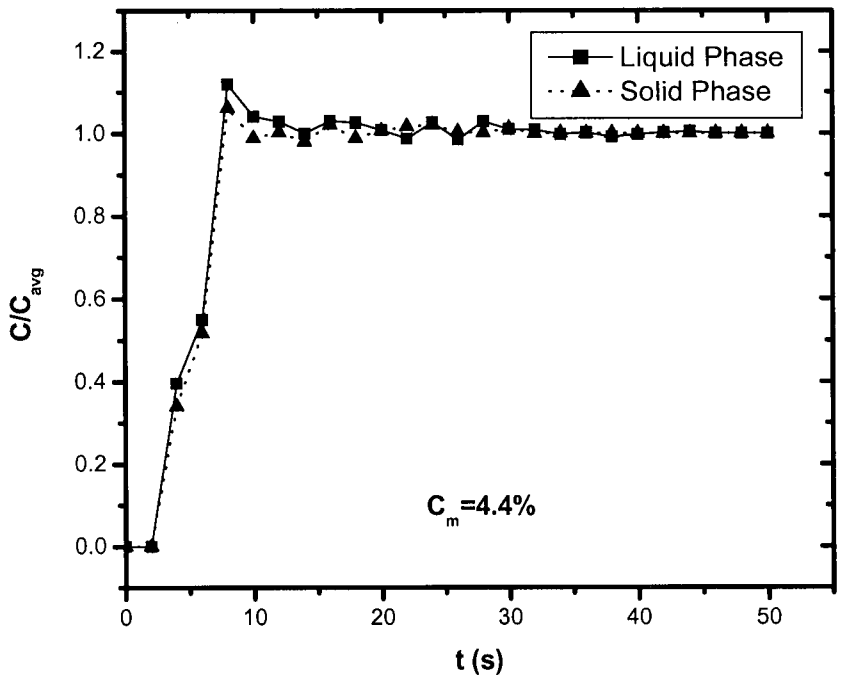

Figure 4.10: Dynamic response of liquid and solid tracers at $C_m = 4.4\%$ and $N = 1531$ rpm.

4.6 Mixing time

Mixing time (θ_m) is the time required to achieve to a predetermined state of mixedness or mixture quality by a mixer. θ_m is widely used to quantify the effect of geometry (mixer and impeller) and operating conditions on mixing quality. Since different experimental methods and different methods of calculating mixing time have been used it is not possible to directly compare data from different sources. Most reported work is on cylindrical vessels. Nienow (1997) used bulk flow concepts to obtain the mixing time. He found that the circulation time is equal to the ratio of mixer volume to the impeller pumping rate for a vessel with an aspect ratio (fluid height to vessel diameter ratio) of about 1 and reported that the system was homogenized after about 5 circulations. Ruszkowski (1994) reported that for water mixed in a cylindrical tank equipped with a top entering impeller, the mixing time was a function of $1/N$, $P/\rho V$, and D/T, where V is fluid volume, and T the tank diameter. Fox and Gex (1956) found that mixing time for water in a cylindrical tank equipped with a top entering impeller was a function of the momentum flux from the impeller, rather than the power input. In fact, the same mixing result in a given mixing operation could be achieved with various power inputs by changing the diameter and speed of the impeller. A large, low speed impeller could produce an equivalent mixing result with less power than a smaller, higher speed impeller. Wesselingh (1975) studied the effect of the "off-centre" angle of the impeller shaft, liquid height, and Reynolds number on the mixing time of water mixed in cylindrical storage tanks with side entering impellers. Uhl and Gray (1966) reported the effect of fluid density, power, and ratio of impeller diameter to tank diameter on mixing time of liquids of different density in cylindrical tanks agitated by a side entering impeller.

To study the mixing time in the laboratory chest, a saline solution was added to the chest and then the suspension conductivity measured by a conductivity probe located in front of

the impeller (about 20 cm from the impeller center). The mixing time was defined as the required time for the conductivity to reach 97% of the steady state value. The effects of impeller speed (N) and power consumption per unit mass ($P/\rho V$) on mixing time (θ_m) are shown in Figures 4.11 and 4.12, respectively. Mixing time decreased with increasing impeller speed and power per unit mass, but remained almost constant at high values of impeller speed and power consumption per unit mass. This result shows that mixing time increases rapidly with an increase in suspension mass concentration.

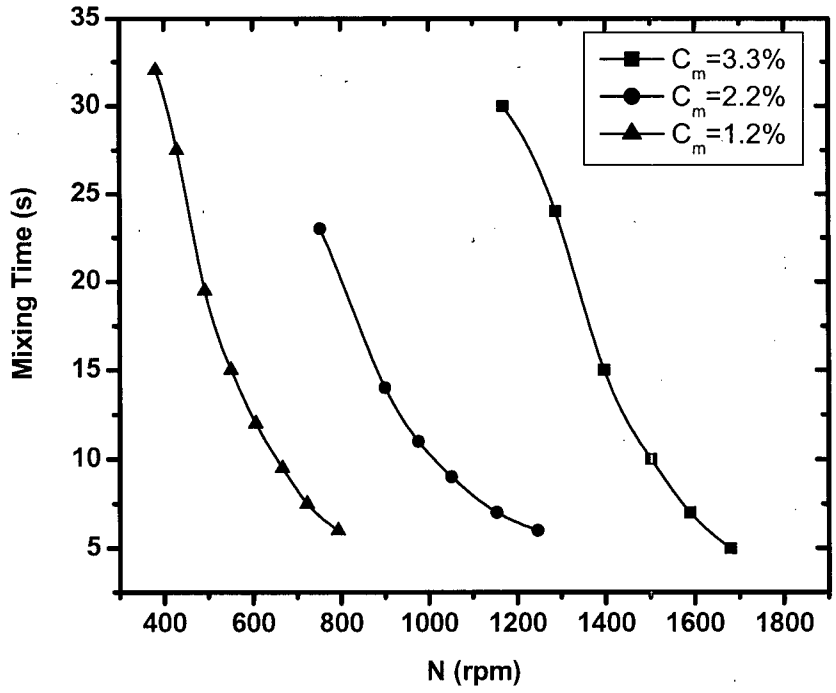

Figure 4.11: Mixing time versus impeller speed ($L/W = 1.3$, $Z/W = 1.1$).

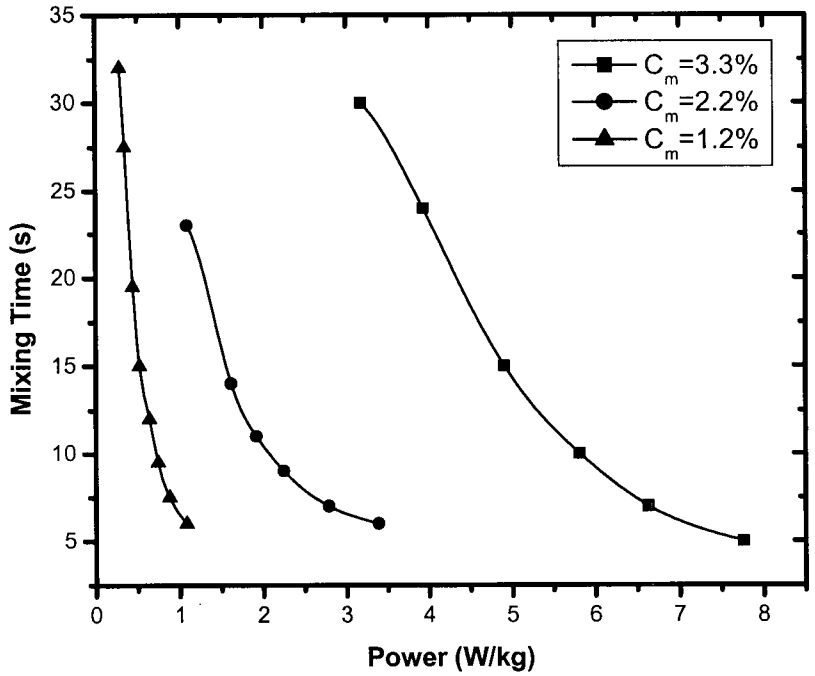

Figure 4.12: Mixing time versus power ($L/W = 1.3$, $Z/W = 1.1$).

Since the impeller momentum flux, which is proportional to N^2D^4 (see chapter 2), was introduced by Fox and Gex (1956) for mixing time correlation and used by Yackel (1990) for designing agitated pulp stock chests, this parameter was correlated with the mixing time measured in our tests. The data was correlated using:

$$\theta_m = A(N^2D^4)^n \tag{4.6}$$

where, θ_m is mixing time, and A and n are functions of C_m. Therefore, mixing time for pulp suspension is both a function of impeller momentum flux and fibre mass concentration. Table 4.1 shows the values of A and n at different fibre mass concentrations. Using these data (shown in Table 4.1), two expressions for A and n were obtained:

Table 4.1: The effect of fibre mass concentration on A and n.

C_m (%)	A	n
1.2	0.5629	-1.1760
2.2	1.1498	-1.4088
3.3	1.3583	-2.5581
4.2	1.4532	-3.1689

$$\begin{aligned} A &= 0.7185\ln(C_m) + 0.4787 \quad ; \quad r^2 = 0.97 \\ n &= -0.7053\,C_m - 0.1419 \quad ; \quad r^2 = 0.95 \\ 1.2\% &\le C_m \le 4.2\% \end{aligned} \tag{4.7}$$

where, C_m is the fibre mass concentration (%). Figure 4.13 shows the experimental data and the results of the correlation.

4.7 Flow pattern

The flow pattern is one way to characterize the mixing achieved on macroscale level. The flow pattern in the scale-model chest was observed with the aid of a digital video camera. Figure 4.14 shows the flow patterns obtained from different perspectives: side view, top view, impeller wall view, and opposite impeller wall view. These photos were taken when using the 16.5cm diameter Maxflo impeller running at 1320 rpm in 3.3% fibre mass concentration. Under these circumstances the whole suspension inside the chest was in motion and no stagnant zones were observed. Our observations showed that even when the whole suspension is in motion, poor mixing regions still exist at the bottom of the chest along the impeller opposite wall and on the surface of the chest along the impeller wall and impeller opposite wall (Figure 4.14) where pulp

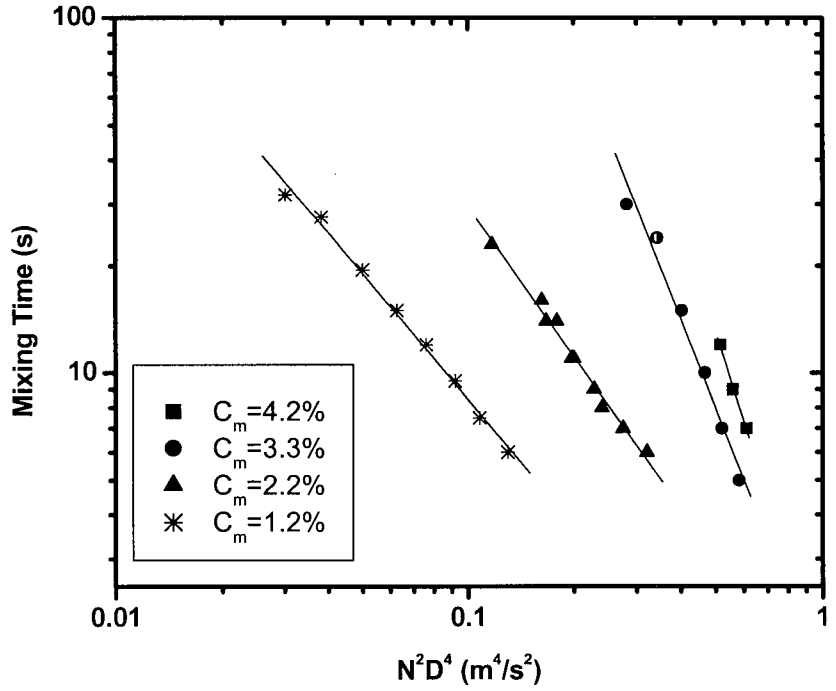

Figure 4.13: Mixing time versus N^2D^4. Lines are given by the correlation, Equation 4.6.

flows significantly slower than in the bulk motion zone. In these regions pulp remains for a longer time, which decreases the percentage of fully mixed volume within the chest. Figure 4.14(a) shows that pulp suspension is pushed by impeller toward the impeller opposite wall. Pulp moves from the bottom of the chest toward the surface of the chest along the impeller opposite wall (Figure 4.14(d)). Due to the impeller pumping action (Figure 4.14(c)) on the surface of the chest pulp moves from the opposite wall toward the impeller wall (Figure 4.14(b)). This flow pattern shows that in Config.1 (Figure 3.8), where the pulp feed enters on the surface of the chest close to the opposite wall, a percentage of the pulp feed can easily channel when it moves on the surface toward the exit location at the impeller wall without

being forced to the mixing zone by the impeller. However, based on this flow pattern, Config.2 (Figure 3.8) will force flow into the mixing zone before leaving the chest.

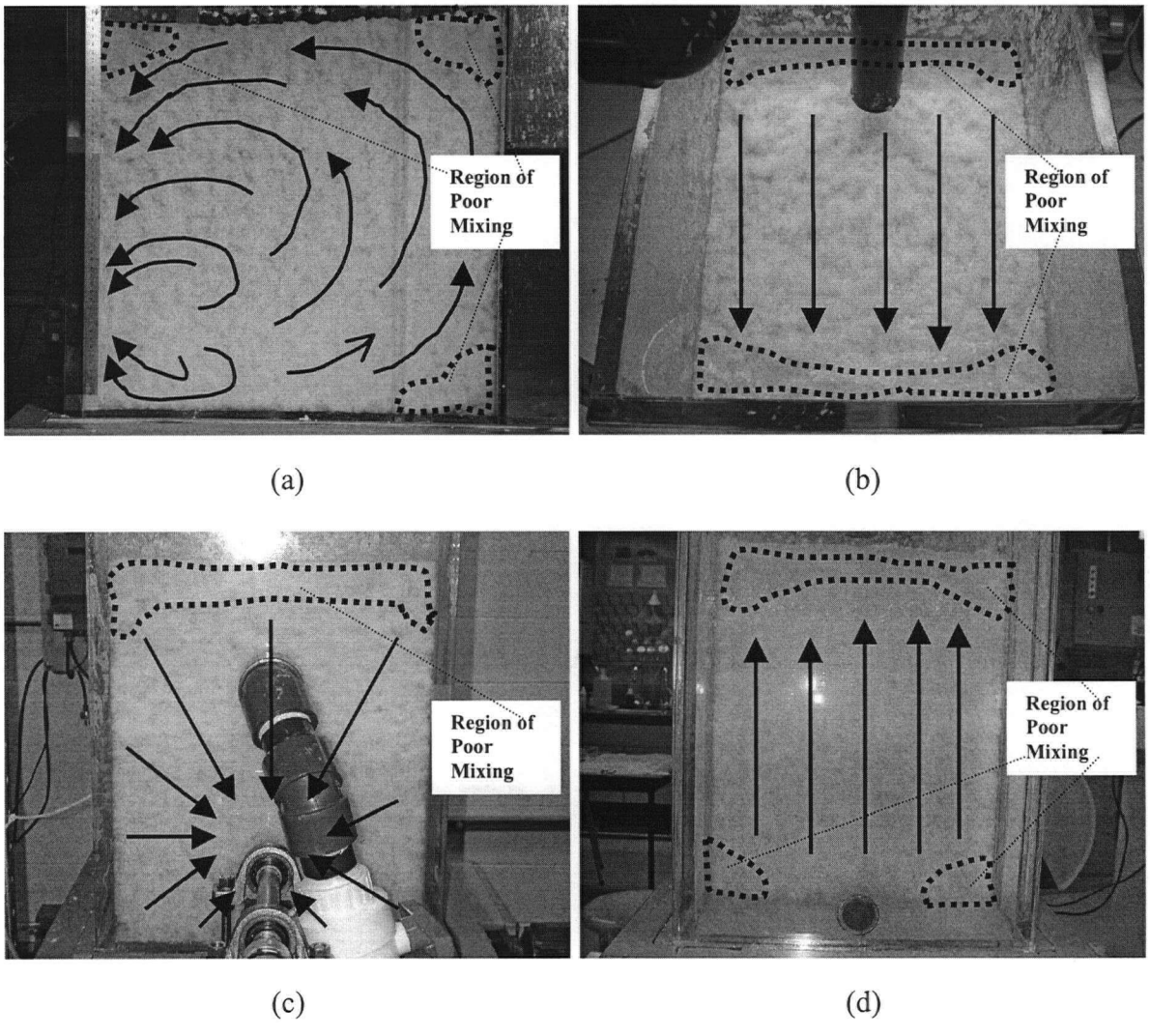

Figure 4.14: Flow pattern obtained in scale-model chest for N = 1320 rpm, D = 16.5 cm and C_m = 3.3% views from (a) side, (b) top, (c) impeller wall and (d) opposite impeller wall.

4.8 Summary

1. Observations made in the scale-model chest showed that significant stagnation zones could persist in the chest corners even upon achieving complete surface motion. In this study, "complete motion" is defined to exist when there are no stagnant zones in the chest.
2. Batch results confirm established trends for the power input needed to create complete motion in a chest versus fibre mass concentration, impeller diameter and chest dimensions. Power varying as the square of fibre mass concentration over the range of 1.1 – 4.7%. The optimum *Z/W* ratio for the scale-model chest is close to the optimum ratio of *Z/W* = 1 suggested by Yackel (1990). The optimum *L/W* ratio for the scale-model chest is approximately 1.3 which is in the range 1.0 – 1.5 suggested by Yackel (1990). The *D/W* ratio for the *D* = 16.5 cm is 0.41 again in the range 0.20 – 0.45 suggested by Yackel (1990).
3. Since evaluation of surface motion alone may not be sufficient to eliminate stagnant zones in remote regions of the chest, the power calculated from existing design criteria did not completely eliminate stagnant regions below the chest surface. Therefore, a chest which shows very good surface motion may produce a process result which is not ideal.
4. The experimental data obtained with the scale-model chest showed that the power number is not only a function of *ND/m* but also of the fibre mass concentration. Therefore, the rheology of a pulp suspension can not be solely described by the $m = (\tau_y/\rho)^{1/2}$ and Bingham fluid did not fully describe the rheology of the pulp suspension.
5. Dynamic response of liquid and solid phase tracers showed that at fibre mass concentrations >2% and impeller speed which is 5-10% greater than that required for "complete motion", the mixing responses of solid and liquid phases are very similar. Therefore, a liquid phase tracer can be used to study the mixing time and dynamic response of stock chests.

6. Mixing time for the scale-model chest is both a function of impeller momentum flux (N^2D^4) and fibre mass concentration: $\theta_m = A\ (N^2D^4)^{\ n}$ where A and n are a function of fibre mass concentration.
7. Experimental data obtained with the scale-model chest under turbulent conditions gave the power number of the Maxflo impeller as 0.276 ± 0.001, identical to the value obtained from the manufacturer. This value is in the range of the typical values of power number (0.1 – 0.5) for the axial flow impellers.
8. Our visual observation with the aid of a digital video camera showed that even when the whole suspension is in the motion, poor mixing regions still exist at the bottom of the chest along the impeller opposite wall and on the surface of the chest along the impeller wall and impeller opposite wall where pulp flows significantly slower than in the bulk motion zone. In these regions pulp remains for a longer time, which decreases the percentages of fully mixed volume within the chest.

CHAPTER 5

5 DYNAMIC MODELING OF AGITATED PULP STOCK CHESTS

5.1 Introduction

The chief purpose of agitated pulp stock chests is to reduce high-frequency variability in fibre mass concentration, freeness and other quality factors. These chests behave as a low-pass filters to complement the action of control loops, which only control low-frequency variability (Bialkowski, 1992). Each control loop has a cut-off frequency, which is a function of process dynamics (time constant, dead time), the type of algorithm used, and the closed-loop time constant. The faster the tuning, the higher the cut-off frequency. Unfortunately, as the loop tuning becomes more aggressive, it is more likely to oscillate or resonate near its cut-off frequency and degrade product uniformity (Sell, 1995; Herrold, 1998). From Figure 5.1 it can be seen that a control loop can only impact disturbances with frequencies lower than the loop cut-off frequency. However a control loop is not able to attenuate disturbances with frequencies higher than the loop cut-off frequency. Therefore, low-frequency variability has to be attenuated by the control loops and high-frequency variability has to be attenuated by the agitated pulp stock chests. It is thus important to ensure these chests are properly designed to achieve the desired overall degree of upset attenuation.

Industrial data show that non-ideal flows such as channeling, recirculation and stagnant zones exist in agitated pulp stock chests (Ein-Mozaffari et al., 2001). These non-ideal flows should be avoided since they decrease the performance of the chest. No information is available on the effects of non-ideal flow on the dynamic behavior of stock chests, although studies have been made on ideal chests (Walker and Cholette, 1958; Reynolds et al., 1964; Brown, 1968).

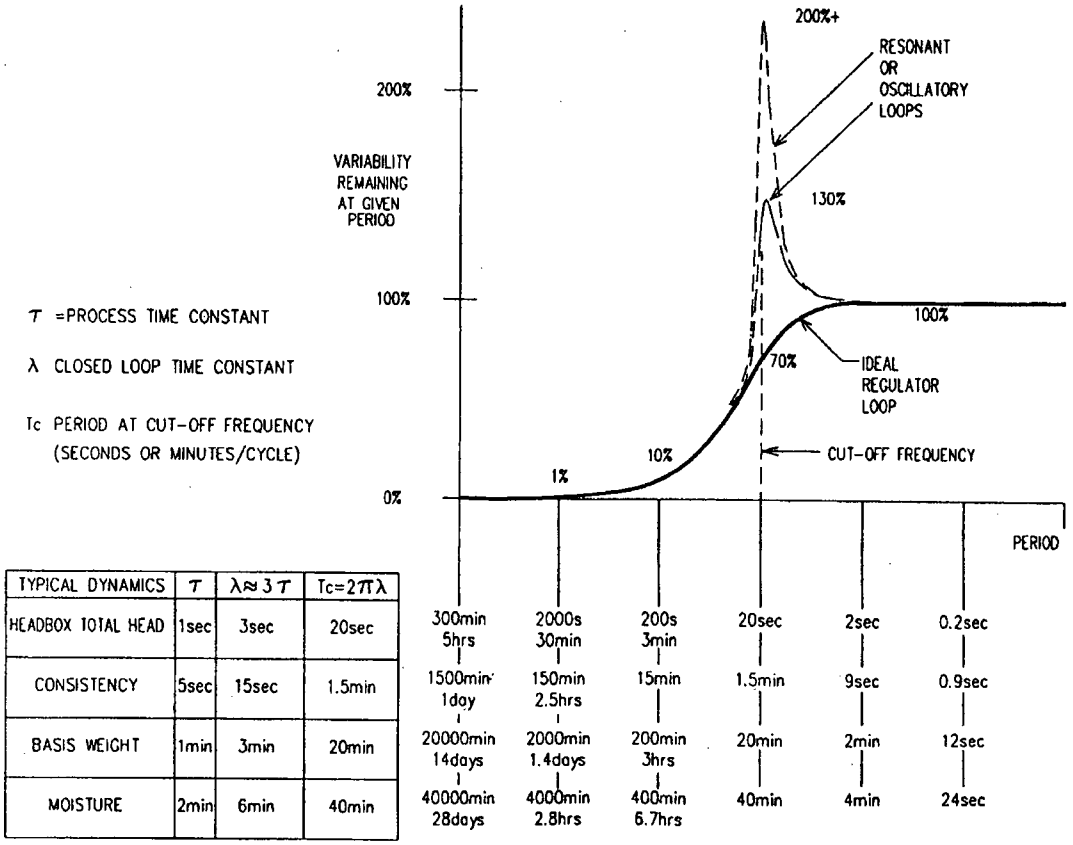

TYPICAL DYNAMICS	τ	$\lambda \approx 3\tau$	$Tc=2\pi\lambda$
HEADBOX TOTAL HEAD	1sec	3sec	20sec
CONSISTENCY	5sec	15sec	1.5min
BASIS WEIGHT	1min	3min	20min
MOISTURE	2min	6min	40min

Figure 5.1: Typical control loop frequency response (Bialkowski, 1992).

Since ignoring non-ideal flows can lead to errors in system design (Levenspiel, 1998), it is necessary to study the dynamic behavior of stock mixing under realistic (less-than-ideal) mixing conditions. In this chapter a dynamic model of agitated pulp stock chests, incorporating these non-ideal flows has been developed and a numerical method for the estimation of dynamic model parameters is presented.

5.2 An example of step response for an industrial stock chest

Figure 5.2 shows the measured response of an industrial stock chest (shown in Figure 5.3) to a step input change at t = 200 s (private communication, Bill Bialkowski, 2001). The upper curve is the input signal and the lower curve is the output response. In this figure the output signal was shifted by –0.2 so as not to overlap with the input signal. The chest response is clearly not ideal. The output shows an initial bump (at about t = 300 s) which is due to short-circuiting within the chest and which was not stabilized until t = 450s. The response also shows a series of first order exponential responses, each one getting progressively smaller. From this it can be concluded that a portion of stock is recirculated within the chest. The theoretical time constant for this chest is $\tau = V/Q$ = 14 minutes where V and Q are suspension volume in the chest and pulp flow rate through the chest, respectively. To estimate the real time constant for this chest,

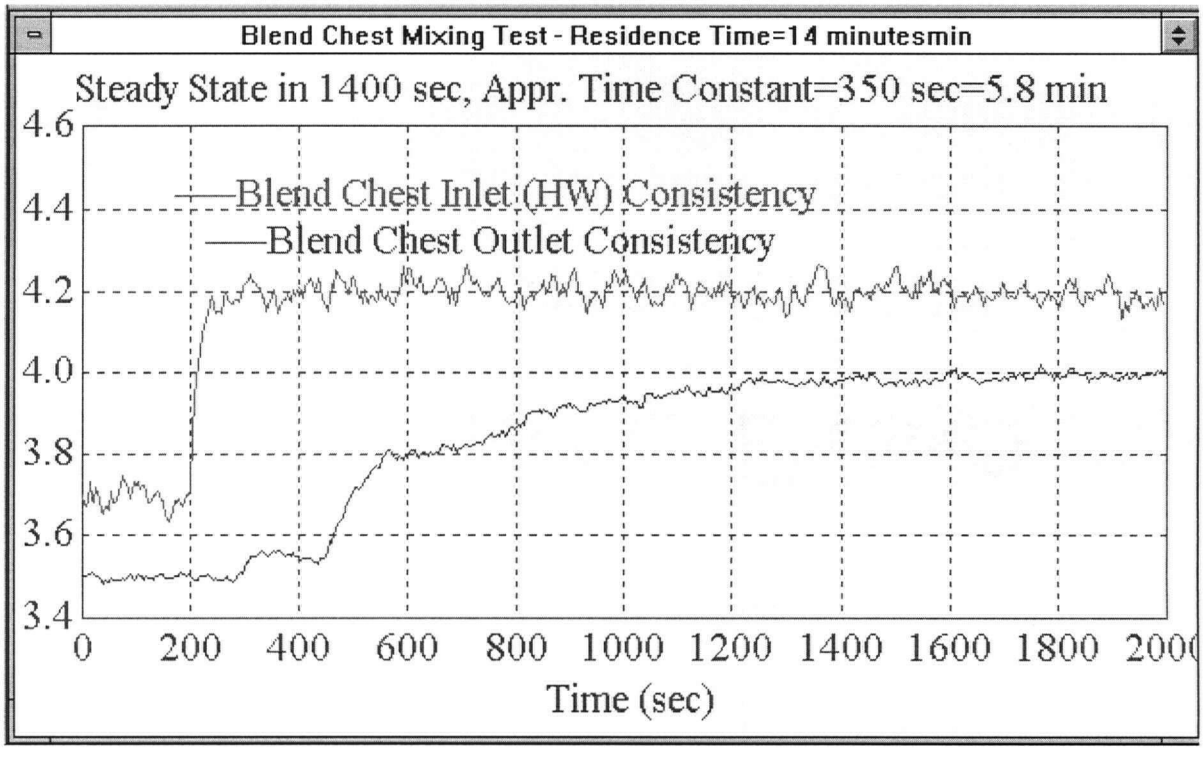

Figure 5.2: Step response of the industrial stock chest shown in Figure 5.3

the series of first order exponential responses was approximated by only one first order exponential response and then the time constant for this first order response was calculated (Seborg et al., 1989). Since the real time constant for this chest is 5.8 minutes, it can be concluded that stagnant and/or dead zones exist inside the chest. The dead zones, where pulp remains for a longer time, represent effectively unused volume inside the chest. Such zones can arise from the interaction between the circulation patterns produced by the impeller and the flow generated by a comparable throughput rate. The flow within a dead zone need not be stagnant; lack of access to the outlet is the only criterion (Silvester, 1985).

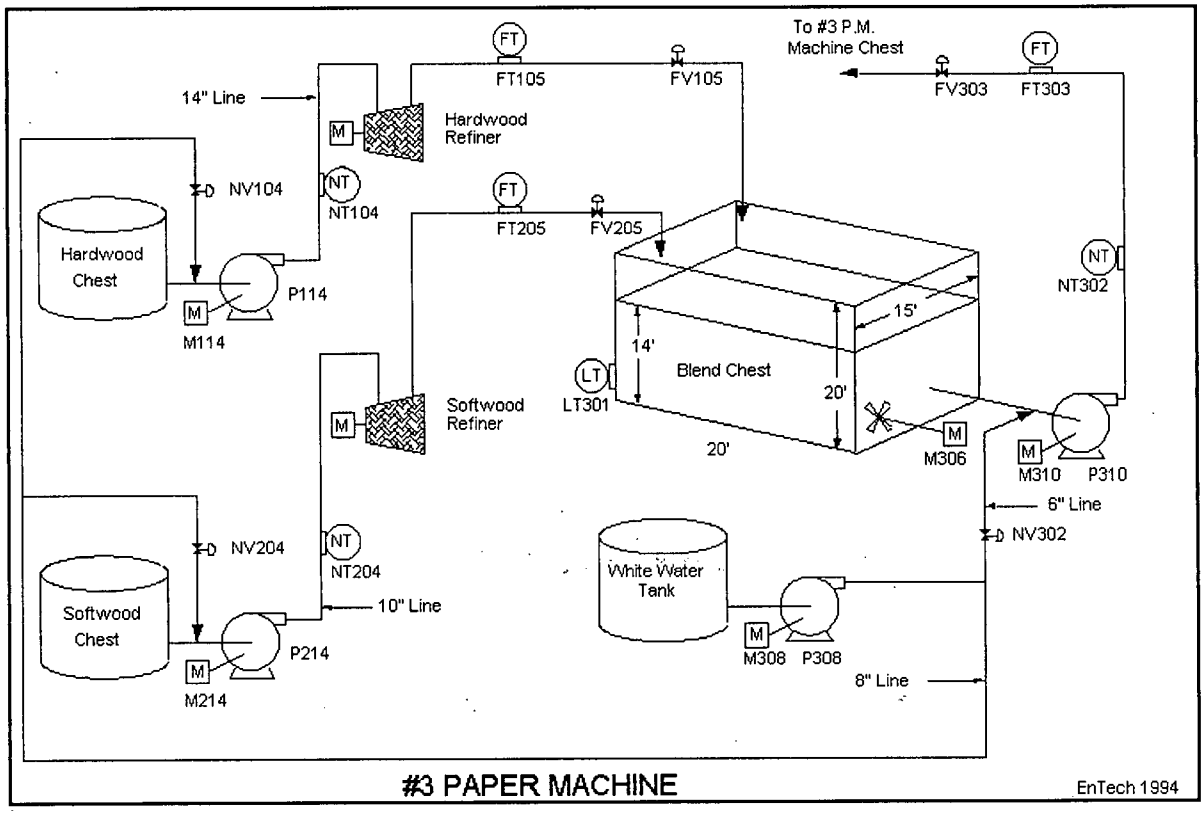

Figure 5.3: Industrial stock chest (Provided by EnTech Control Engineering Inc.).

Frequency responses calculated for this industrial stock chest and for a perfectly mixed chest having the same volume and flow rate are plotted in Figure 5.4. The degree of upset

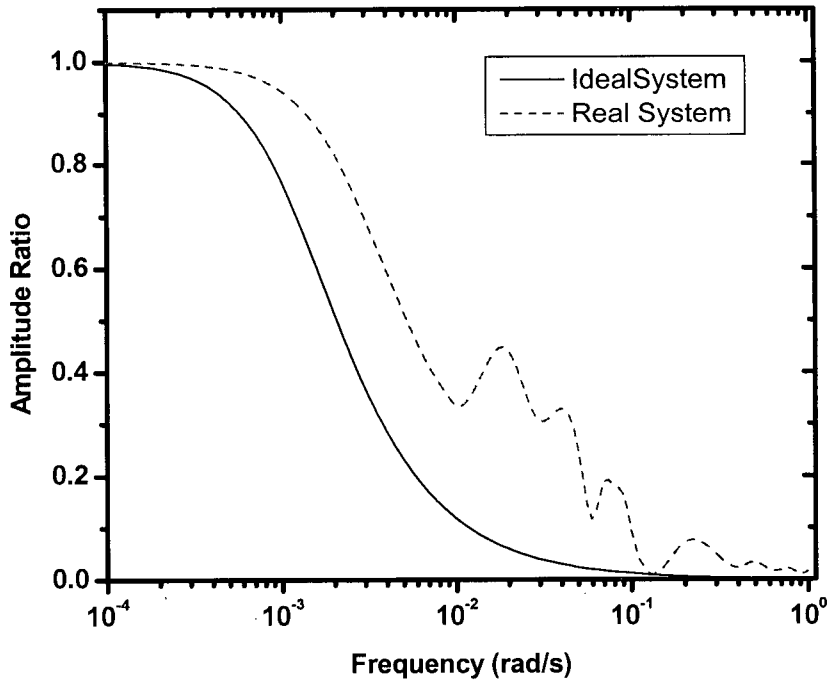

Figure 5.4: The frequency response measured for the industrial chest compared with its ideal response.

attenuation for the industrial stock chest is considerably worse than that of the equivalent perfectly mixed chest, especially for frequencies from 0.01 to 0.1 rad/s. These frequencies are higher than the cut-off frequencies of paper machine control loops which are from 0.002 to 0.005 rad/s (Bialkowski, 1992). Therefore, disturbances at these frequencies would not be attenuated sufficiently and would affect paper quality and machine run-ability. Since the existence of non-ideal flows such as channeling, recirculation and dead zones decrease the performance of the chest as a low-pass filter, the effect of these non-ideal flows should be considered in dynamic modeling of agitated pulp chests. Better understanding of these non-

ideal flows would also lead to the design of the chests with mixing characteristics closer to the ideal case.

5.3 Dynamic model

A simple continuous-time dynamic model that represents the observed behavior of the industrial chest is shown in Figure 5.5. This model was constructed from basic principles where the system parameters have a physical interpretation. In this figure, f is the portion of stock bypassed in the mixing zone and R is the portion of the stock recirculated within the mixing zone. G_2 is the first order transfer function for the agitated zone (Ogunnaike and Ray, 1994; Stephanopoulos, 1984). Since a limited amount of mixing occurs in the short circuit flow, it also has a first order transfer function (G_1). τ_1 and τ_2 are the time constants for the channeling and agitated zones and are such that $\tau_1 < \tau_2$. The step response signal also shows the possibility of transport delays in both paths, and these were incorporated as well. T_1 and T_2 are the time delays for the channeling and agitated zone and typically $T_1 < T_2$.

To estimate the dynamic model parameters, the system has to be excited. Then the model parameters can be estimated from the input-output data (Soderstrom and Stoica, 1989; Ljung, 1999). Identification of continuous-time models has long been a topic of research interest (Whitfield and Messali, 1987; Johansson, 1994; Soderstrom et al., 1997; Johansson et al., 1999), but time delays add considerable difficulties to the identification mechanism. Some recent developments accomplish the identification of continuous-time models with time delay (Wang et al., 2001; Sung and Lee, 2001). Nevertheless, those schemes are not generic enough to handle the model structure shown in Figure 5.5.

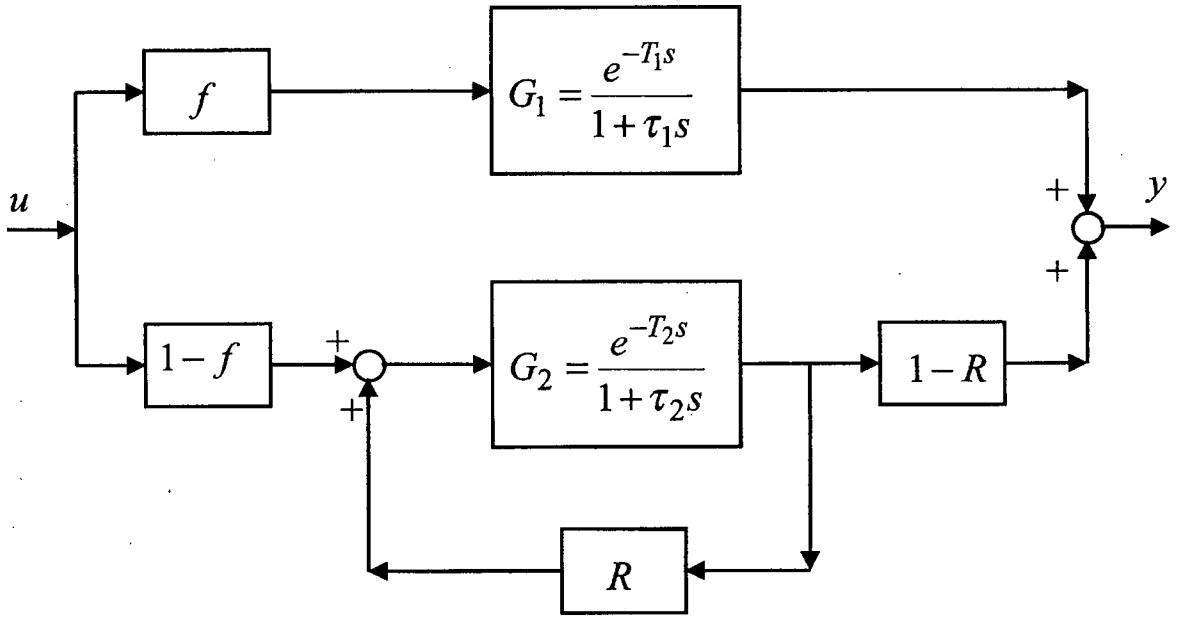

Figure 5.5: Continuous-time dynamic model of the stock chest.

5.4 Estimation of dynamic model parameters from input-output data

Since the data are measured at fixed time intervals, the continuous model is initially transformed into a simple discrete-time model (Kammer et al., 2001). It is assumed that each time delay can only be a multiple value of the sampling time, t_s. Therefore, the zero order hold (ZOH_{ts}) equivalent to each of the transfer functions becomes (Seborg et al., 1989):

$$ZOH_{t_s}\left\{\frac{e^{-Ts}}{1+\tau s}\right\} = \frac{1-e^{-t_s/\tau}}{1-e^{-t_s/\tau}q^{-1}} q^{-(1+T/t_s)} \tag{5.1}$$

Note that the discretization of the system in Figure 5.5 involves the zero-order hold of the term $G_2/(1-RG_2)$. Because of the delay term in G_2, this transfer function is not rational and in order to discretize it one would need to replace the delay term in its denominator by a Pade

approximant. The resulting discrete transfer function would be quite complex. A simpler approximation that is valid for small sampling time t_s or small R consists in approximating $ZOH\{G_2/(1-RG_2)\}$ by $G_2(z)/(1-RG_2(z))$.

As long as the indicated constraints are enforced, there is a one-to-one transformation between the following discrete-time and continuous-time parameters:

$$a = e^{-t_s/\tau} \leftrightarrow \tau = -\frac{t_s}{\ln a} \qquad a \in [0,1] \tag{5.2}$$

$$d = 1 + T/t_s \leftrightarrow T = t_s(d-1) \qquad d \in N \tag{5.3}$$

The discrete-time transfer function of the system shown in Figure 5.5 becomes:

$$\hat{G}(q) = \frac{\rho_1 q^{-d_1} + \rho_2 q^{-(d_1+1)} + \rho_3 q^{-d_2} + \rho_4 q^{-(d_2+1)} + \rho_5 q^{-(d_1+d_2)}}{1 + \rho_6 q^{-1} + \rho_7 q^{-2} + \rho_8 q^{-d_2} + \rho_9 q^{-(d_2+1)}} \tag{5.4}$$

where

$$\begin{aligned}
&d_1 \le d_2 && \rho_5 = -fR(1-a_1)(1-a_2)\\
&\rho_1 = f(1-a_1) && \rho_6 = -a_1 - a_2\\
&\rho_2 = -f(1-a_1)a_2 && \rho_7 = a_1 a_2\\
&\rho_3 = (1-f)(1-R)(1-a_2) && \rho_8 = -R(1-a_2)\\
&\rho_4 = -(1-f)(1-R)a_1(1-a_2) && \rho_9 = Ra_1(1-a_2)
\end{aligned} \tag{5.5}$$

and q^{-1} is backward shift operator: $q^{-1}f(k) = f(k-1)$.

The continuous-time model can also be transformed to its discrete-time counterpart when T_1 and T_2 are discretized to fractional time delays using a modified Z-transform (Seborg et al., 1989). This would add more terms to the discrete-time model (Equation 5-4). Since the

sampling time (t_s) is small enough to describe time delays with significant accuracy, the consideration of fractional time delays is not necessary.

The cost function (J_N) to be minimized by the identification algorithm is (Kammer et al., 2001):

$$J_N = \frac{1}{N}\sum_{t=1}^{N}\left[y_t - \hat{G}(q)u_t \right]^2 \tag{5.6}$$

where N, y_t, and u_t are the length of the data set, measured output, and measured input, respectively. There are several challenges to be tackled towards the solution of this problem:

- The initial conditions must be estimated from data.
- The estimation of d_1 and d_2 is quite problematic as these variables can only assume integer values.
- Given d_1 and d_2, the estimation of $\rho_1,\ldots,\rho_2$ can be performed via least squares, but the estimation of f, R, a_1 and a_2 has to be performed iteratively due to the nonlinear relationship among these parameters.

Each set of experimental data made on the scale-model chest has a maximum length that is determined by the capacity of the feed tank and the flow rate of the pulp suspension. The maximum duration of the experiment typically contains about two complete step responses. This limitation strongly emphasizes the need for estimating the initial conditions of the plant, instead of waiting for the process to reach steady state before the experiment is started.

The number of states in the process can be very high, depending on the values of d_1 and d_2. This can render the estimation of the initial conditions a useless exercise. Instead, the initial conditions for the input and output signals are each represented by a constant value, which is

actually what physically happens inside the process when the experiment begins. In mathematical terms, the initial conditions complement Equation 5.6 with:

$$u_k = u_1 \ , \ y_k = \hat{y}_0 \quad k = -\infty, \cdots, -1, 0 \tag{5.7}$$

Due to its special characteristic, the estimation of the time delays is performed independently from the estimation of the remaining parameters of the dynamic model. Since, d_1 and d_2 can assume a large range of values, we have to limit the search for the optimal delays to the most promising region. Therefore, there are two distinct stages in the identification mechanism: one efficient but less accurate search for the optimal delays followed by an accurate search for the whole set of parameters $\{d_1, d_2, f, R, a_1, a_2, \hat{y}_0\}$.

5.4.1 First stage

Given a pair $\{d_1, d_2\}$, according to the algorithm below, the parameters $\rho_1, \ldots, \rho_9$ are estimated via least squares:

1. Create a grid of 5 by 5 points linearly spaced by any power of 2; this grid is used for mapping a significant part of the feasible range of d_1 and d_2 (see Figure 5.6).
2. Compute the cost function associated with the points $\{d_1, d_2\}$ in the grid for only $d_1 < d_2$. While $d_1 > d_2$, the program returns infinity for the cost function (see "function V" in Appendix A).
3. While the minimum cost function is not at the centre of the grid, re-centre it at the pair $\{d_1, d_2\}$ with the minimum cost and evaluate the new points.
4. If the grid spacing is larger than one, zoom into the centre of the grid, forming a new 5 by 5 grid with half of the previous spacing, and go back to 3 (see Figure 5.7).
5. The first-stage estimated time delays, $\{d_1^*, d_2^*\}$, are at the centre of the grid.

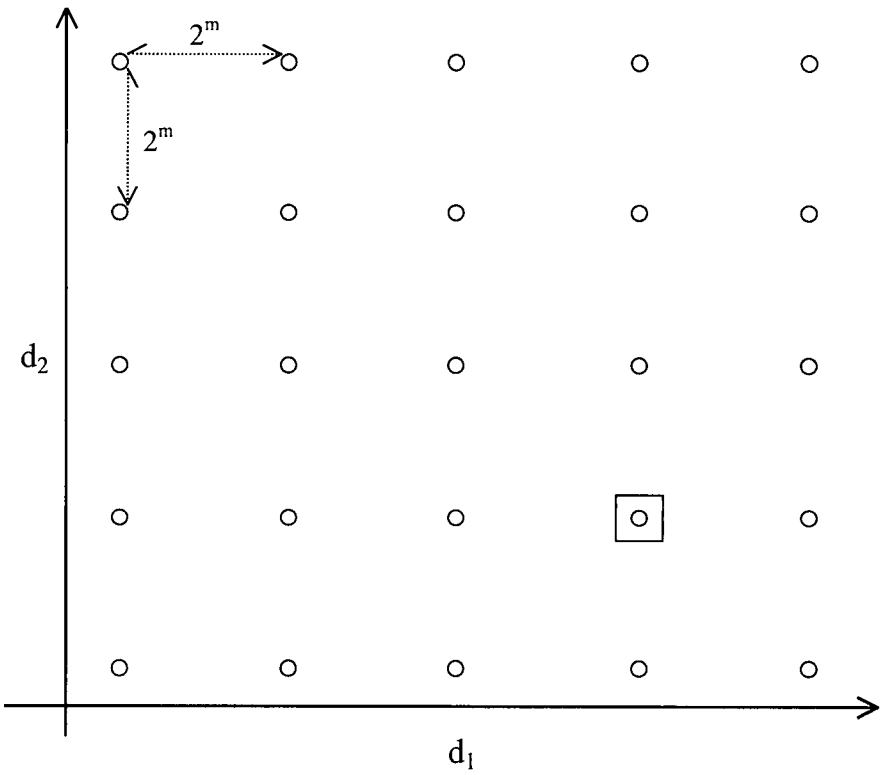

Figure 5.6: A grid of 5 by 5 points linearly spaced by any power of 2. Square shows the point with the minimum cost function.

5.4.2 Second stage

Given a pair $\{d_1, d_2\}$, according to the algorithm below, the parameters f, R, a_1, and a_2, as well as the initial condition $\hat{y}_0$ are estimated via a Sequential Quadratic Programming (SQP) method (Fletcher, 1987; Edgar et al., 2001). This is an iterative method designed to solve constrained nonlinear optimization problems. The parameters f, R, a_1, and a_2 are all constrained into the range [0,1].

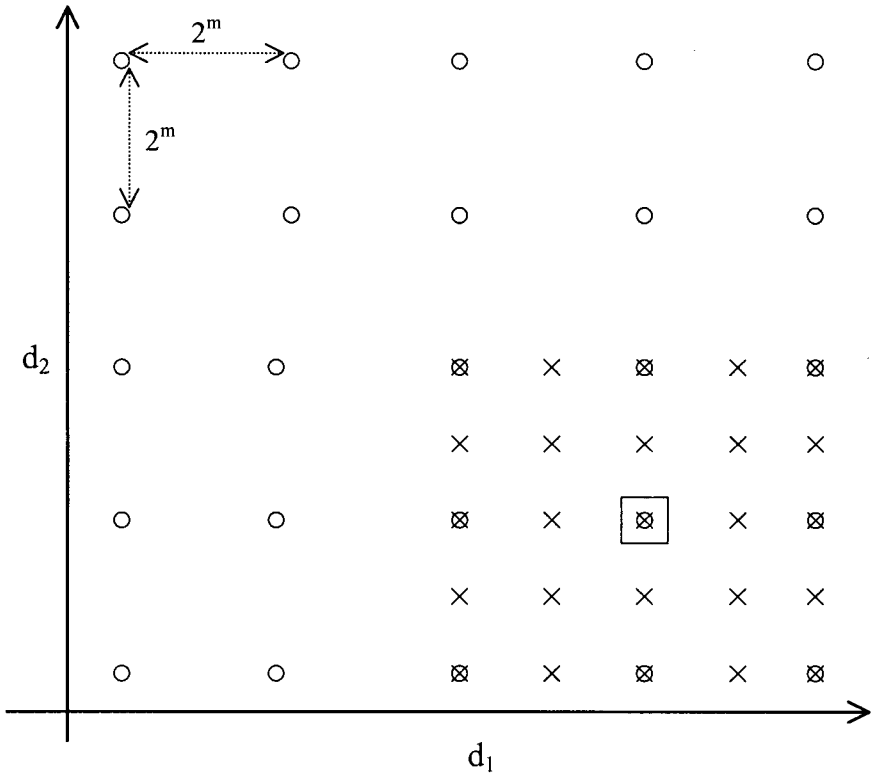

Figure 5.7: A new grid with half of the previous spacing is re-centred at the point (square) with the minimum cost function.

Since this iterative method requires the definition of initial conditions, the first pair, $\{d_1^*, d_2^*\}$, is associated with the following arbitrary initial conditions: $f = 0.5$, $R = 0.5$, $a_1 = 0.8$, $a_2 = 0.8$ and $\hat{y}_0 = y_1$. Any subsequent pair $\{d_1, d_2\}$ uses the previous result as initial conditions:

1. Evaluate the cost function at $\{d_1^*, d_2^*\}$ and at its eight immediate neighbors, forming a 3 by 3 grid of unitary spacing.
2. If the minimum cost is not at $\{d_1^*, d_2^*\}$, perform a line search in the direction of steepest descent (minimum cost function), establish the new $\{d_1^*, d_2^*\}$ as the point of minimum cost along that line and go back to 1 (see Figure 5.8).
3. The optimal estimates for f, R, a_1 and a_2 are the values obtained at $\{d_1^*, d_2^*\}$.

Although this mechanism is not guaranteed to converge to the global minimum, the optimal d_1 and d_2 are expected to be surrounded by a large region of near optimal performance. Therefore, the grid system used in the first stage of the identification is very likely to converge to the region near the global minimum.

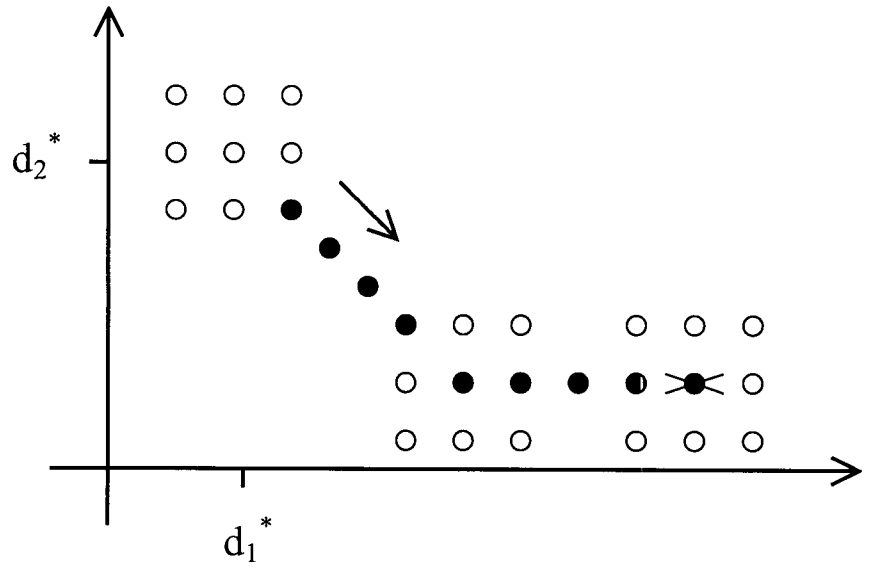

Figure 5.8: A line search in the direction of minimum cost function (black circles). Cross is the final point.

A computer program written in MATLAB to estimate the model parameters from input-output data based on numerical method described in this chapter is given in Appendix A.

5.5 Summary

1. A continuous–time dynamic model of agitated pulp stock chests, incorporating the non-ideal flows was developed. This model allows for two parallel suspension flow paths: a mixing zone consisting of a first order plus delay transfer function with a positive feedback

for recirculation, and a channeling zone consisting of a first order plus delay transfer function.

2. Since the input-output data are measured at fixed time intervals, the continuous-time model, which contains physically relevant parameters, was transformed into a simple discrete-time model. This transformation introduces some challenging identification problems, as the discrete-time parameters become a non-linear combination of the original continuous-time parameters.
3. The estimation of the model parameters from input-output data includes two stages: the estimation of discrete-time model parameters is performed via least squares, but the estimation of continuous-time model parameters has to be performed iteratively due to the nonlinear relationship among these parameters.

CHAPTER 6

6 EXCITATION PROCEDURE AND INPUT SIGNAL DESIGN

6.1 Introduction

System identification is the field of modeling dynamic systems from experimental data. The system identification procedure has a natural logic flow:

- Excite the system and collect input-output data,
- Choose a dynamic model structure,
- Choose a numerical criterion to estimate the unknown parameters of the dynamic model from input-output data,
- Validate the model by using a new set of input-output data.

This procedure is illustrated in Figure 6.1. In chapter 5 a dynamic model for agitated pulp stock chests was developed and a numerical method for estimation of model parameters from input-output data was presented. This chapter concentrates on excitation design and input-output data collection. To estimate model parameters, the system must be excited by a proper input signal. The choice of input signals has a very substantial influence on the observed data. In fact all modes of the system should be excited during the identification experiment (Soderstrom and Stoica, 1989). For instance, one single pure sinusoid with the frequency ω only gives information of the value of the frequency function at ω. There are infinitely many systems that give the same output with this input. It is thus important that the input signal contains enough frequencies. In this chapter a frequency-modulated random binary input signal is designed for this purpose.

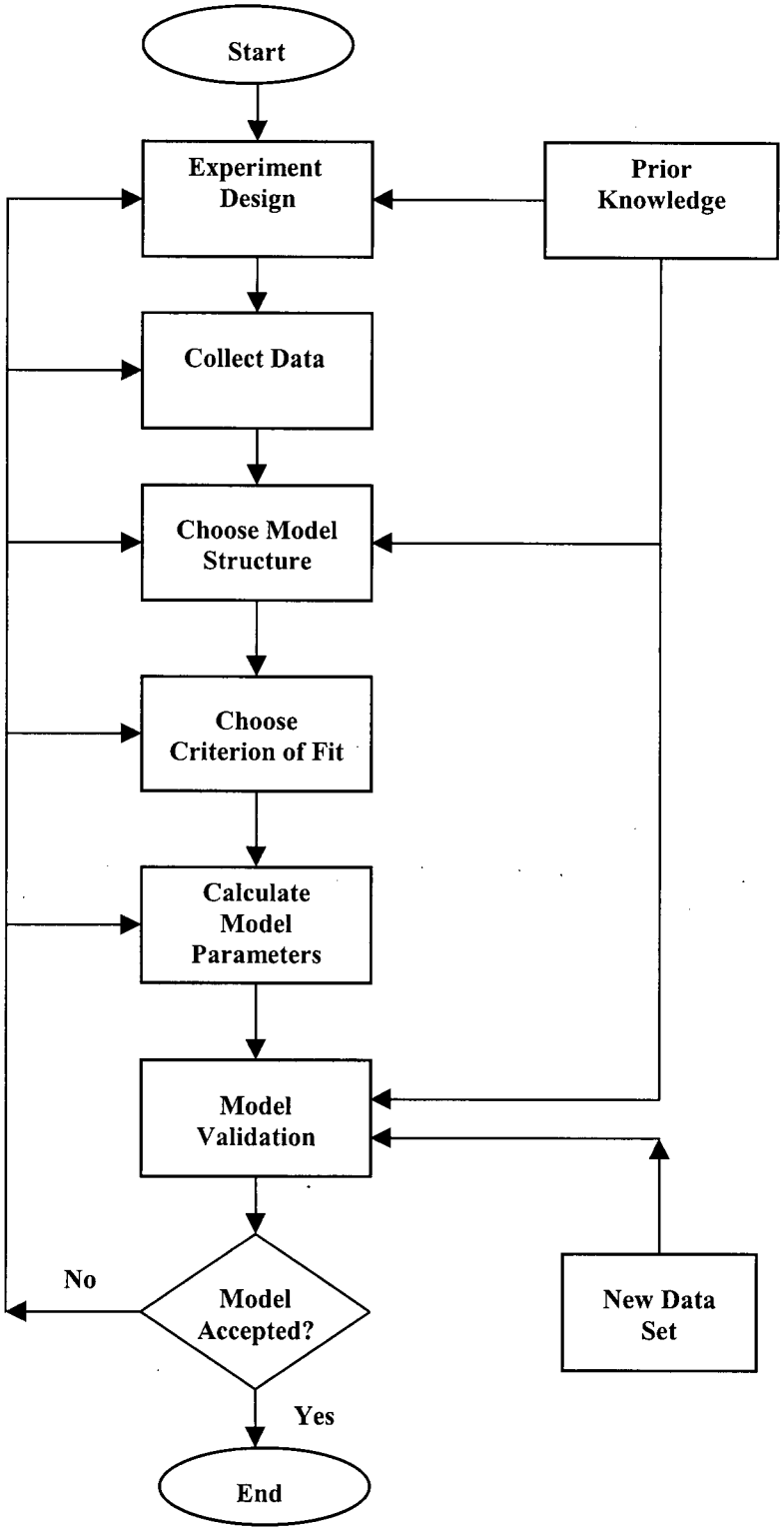

Figure 6.1: System identification loop.

6.2 Excitation procedure

The identification experiment was performed by exciting the system: a saline solution was injected through a computer controlled solenoid valve into the pulp feed stream and the conductivity variations in input and output streams were measured using flow-through conductivity sensors. These signals were recorded in a computer for the estimation of dynamic model parameters.

The choice of sampling time (t_s) is coupled to the time constant of the system. Sampling that is considerably faster than the system dynamics leads to data redundancy and relatively small information value in the new data points. Sampling that is considerably slower than the system dynamics leads to serious difficulties determining the parameters that describe the dynamics. In general it is much worse to sample too slow than too fast. The following rule-of-thumb has been found to provide a good starting choice for sampling time (Ogunnaike and Ray, 1994): "For a process with a dominant time constant τ, it is recommended that the sampling time be chosen as: $t_s \approx 0.2\tau$."

Since the dominant time constant of the agitated pulp stock chest is a function of the suspension volume in the chest and the pulp flow rate through the chest, the sampling time for the dynamic tests made on the scale-model chest was 1-5 s. For instance, the sampling time was one second at Q = 37.1 L/min and it was 5 seconds at Q = 7.9 L/min while the suspension volume in the chest was kept constant.

When the data have been collected from the identification experiment, they are not likely to be suitable for immediate use in identification algorithms. There are several possible deficiencies in the data. It might be that the signal levels drift or that there are high-frequency disturbances above the frequencies of interest to the system dynamics. There also can be obvious outliers, missing data, and non-continuous data records (Ljung and Glad, 1994). These

kinds of deficiencies should be removed from the collected data prior to use. Since these deficiencies were not observed in input-output data recorded during the identification experiments made on the scale-model chest, the signals were not preprocessed and were used directly in the identification algorithm.

The excitation provided in the dynamic experiments was limited to binary sequences as the input signal was controlled by an on-off solenoid valve. The process of model identification required two experiments:

6.2.1 First experiment: system excitation by a rectangular pulse

In the first experiment, the input signal was a rectangular pulse (two step changes) to allow the estimation of an approximate model used to design the excitation for the second experiment. To estimate correctly the unknown parameters in parametric models, it is important that the input signal be persistently exciting (Ljung, 1999). Roughly speaking, this implies that all modes of the system should be exciting during the identification experiment. Therefore, a simple input, such as two step changes, will not provide enough excitation to accurately identify 6 model parameters. However, transient analysis (step response – see chapter 2) is an excellent method to get a quick and easy insight into cause and effect relationships, time delays, time constants, and static gains and it is also a convenient way of deriving crude models.

Figure 6.2 shows the rectangular pulse and the output signal (black line) for a system with these model parameters: $f = 0.15$, $R = 0.44$, $T_1 = 110$ sec, $\tau_1 = 25$ sec, $T_2 = 250$ sec, and $\tau_2 = 40$ sec. The data shown in Figure 6.2 are simulated data. In this figure the effect of initial conditions and measurement noise have been considered. SIMULINK (The MATH WORKS Inc., Natick, MA) was used for this simulation. Figure 6.3 shows our dynamic model (see Figure 5.5) in SIMULINK.

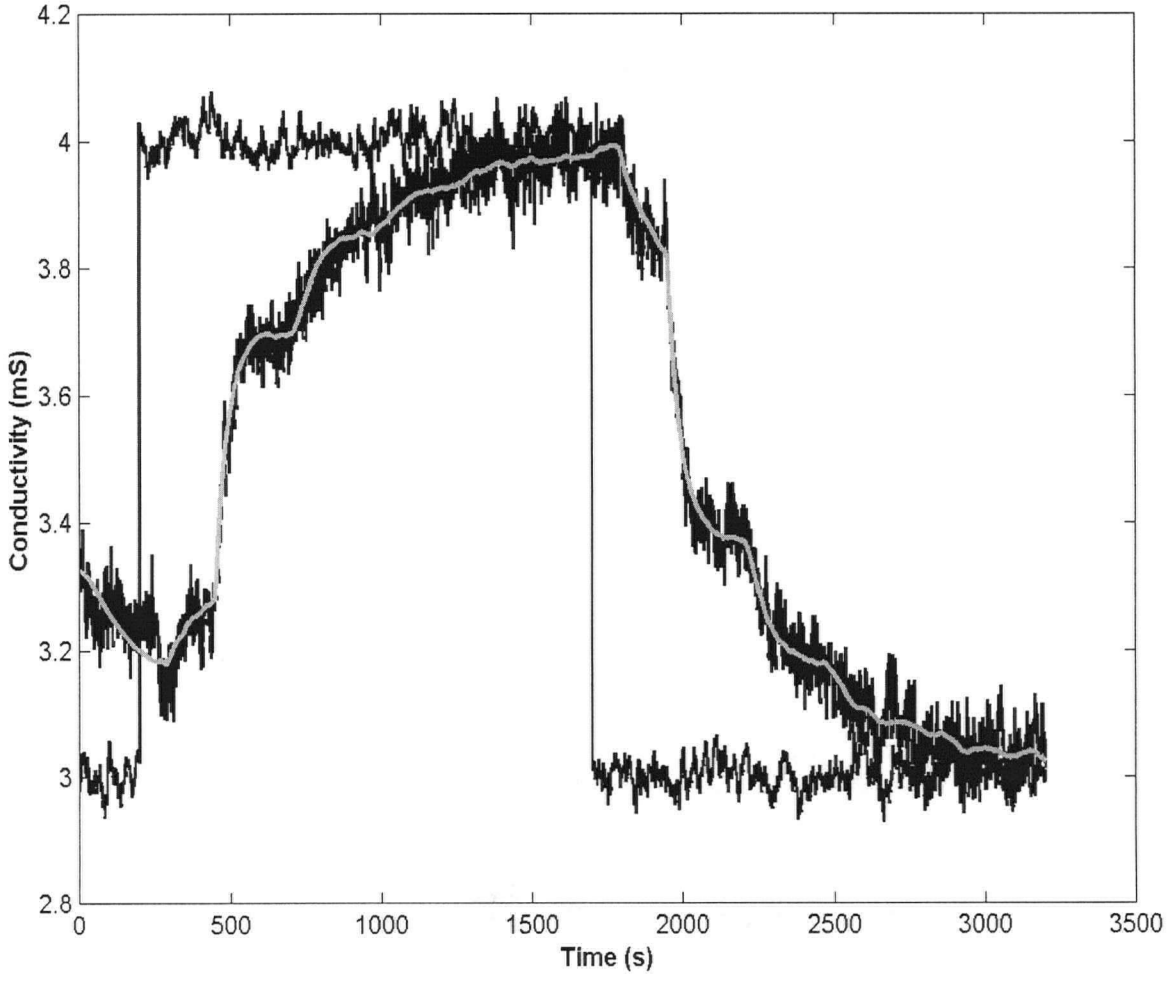

Figure 6.2: Simulated chest input and output signals in black lines and model output in gray line.

The numerical method presented in chapter 5 was used to estimate the dynamic model parameters from input-output data shown in Figure 6.2. Table 6.1 shows both the estimated parameters and the real parameters. It can be seen that the excitation performed by a simple input signal such as a rectangular pulse only provides an approximate model and some of the parameters estimated based on this excitation are not accurate. The gray line in Figure 6.2 contrasts the model output with the measured output. It can be noticed that although some of the estimated parameters are quite distant from their perspective true values, the model provides a good fit.

Table 6.1: Real parameters compared with estimated parameters from the excitation performed by a rectangular pulse.

	f	R	T_1	τ_1	T_2	τ_2
Real parameter	0.15	0.44	110	25	250	40
Estimated parameter	0.23	0.474	91	128	250	39.1

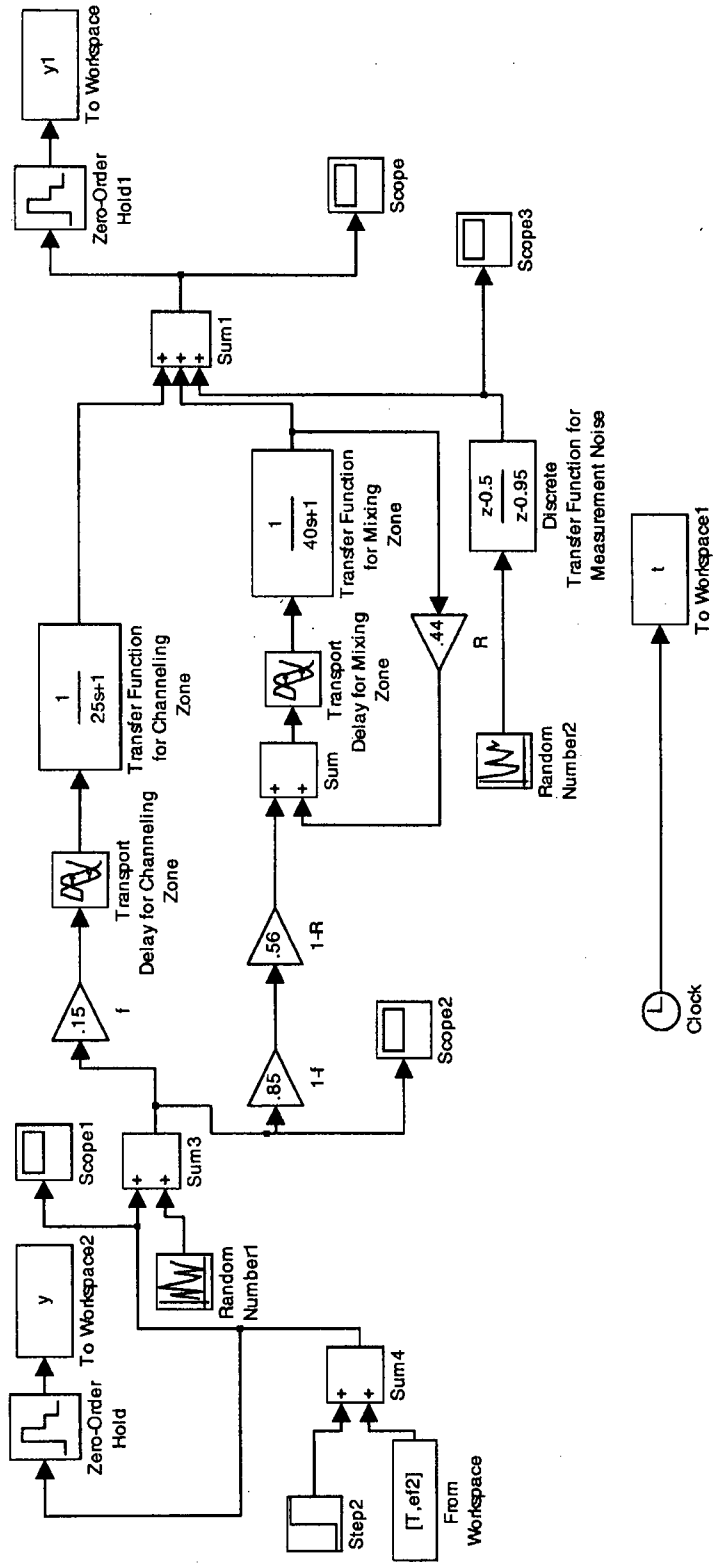

Figure 6.3: Dynamic model of agitated pulp stock chest in SIMULINK.

6.2.2 Second experiment: System excitation by a frequency-modulated random binary signal

In order to improve the quality of the parameter estimation, another experiment was designed. The excitation energy for the second experiment was chosen at frequencies where the magnitude of the Bode plot was sensitive to parameter variations (Ljung, 1999). For this purpose, the magnitude of the Bode plot for the partial derivatives of the approximate model, obtained from the first excitation, with respect to model parameters (f, R, a_1, a_2) are calculated and shown in Figure 6.4. The partial derivatives of the model are calculated by using MATLAB Symbolic Toolbox and "function plder" generates the Bode plot of these partial

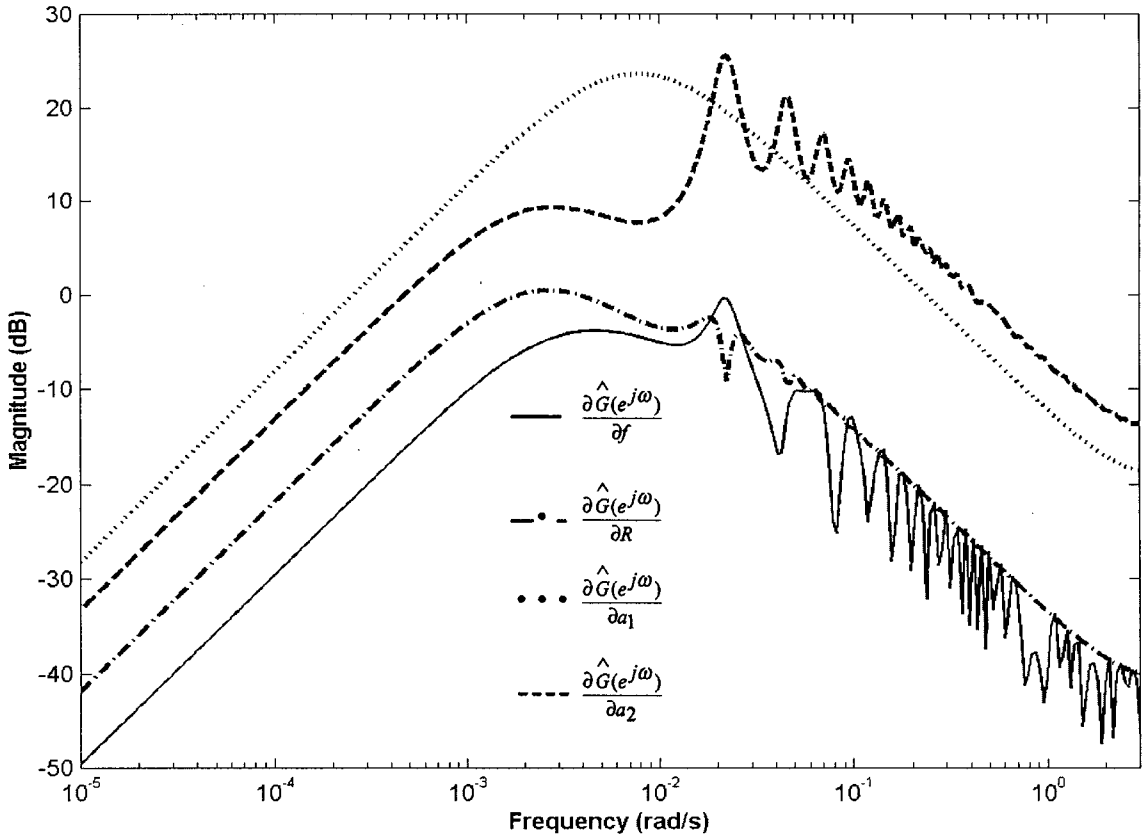

Figure 6.4: Magnitude Bode plot of partial derivatives of the model.

derivatives (see Appendix A). From this figure the frequencies at which the magnitudes are maximum are obtained: ω_f = 0.02 rad/s, ω_R = 0.002 rad/s, ω_{a1} = 0.008 rad/s, ω_{a2} = 0.02 rad/s. Therefore, the excitation energy for the second experiment was concentrated at frequencies from $\min\{\omega_f, \omega_R, \omega_{a1}, \omega_{a2}\}$ = 0.002 rad/s to $\max\{\omega_f, \omega_R, \omega_{a1}, \omega_{a2}\}$ = 0.02 rad/s. By having this information we are able to design a better signal for second excitation. Figure 6.5 shows the procedure for designing a frequency-modulated random binary input signal for the second experiment. First a zero-mean white-noise signal is filtered by a band-pass filter with cut-off frequencies 0.002 rad/s and 0.02 rad/s. Then the filtered signal is converted into a binary sequence by using:

$$u_t^b = \begin{cases} 0 & if \quad e_t^f \le 0 \\ 1 & if \quad e_t^f > 0 \end{cases} \tag{6.1}$$

Such a conversion might change the spectrum of the signal, but it is always possible to check this spectrum before using the signal and see if it is acceptable (Ljung, 1999). The new input and output signals (black line) are shown in Figure 6.6. In this figure the response of the model to the given excitation is in gray line. Table 6.2 shows the real model parameters compared with the estimated parameters from the second excitation performed by a frequency-modulated

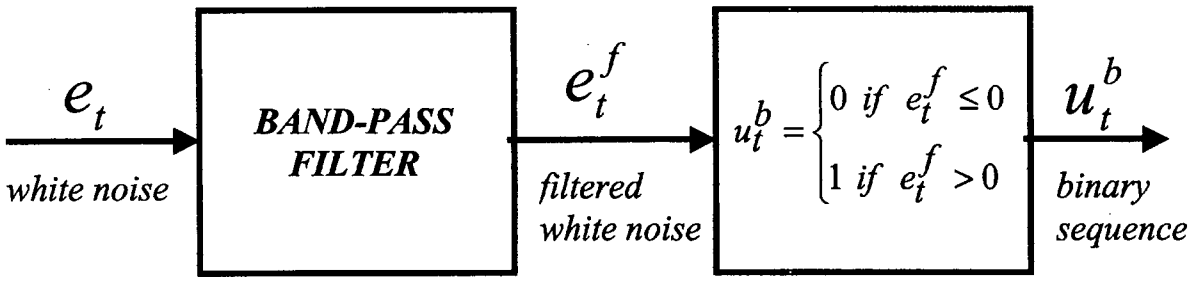

Figure 6.5: Procedure for designing a frequency-modulated random binary input signal.

random binary signal. The improvement in the model quality provided by the new excitation is noticeable and estimated parameters are more accurate due to better excitation in second experiment. Although the discrete-time transfer function (Equation 5.4) is an approximation of the continuous-time model (Figure 5.5), it provides an accurate estimation for all parameters even for R.

Table 6.2: Real parameters compared with the estimated parameters from the excitation performed by a frequency-modulated random binary signal.

	f	R	T_1	τ_1	T_2	τ_2
Real parameter	0.15	0.44	110	25	250	40
Estimated parameter	0.144	0.448	113	22.1	250	39.8

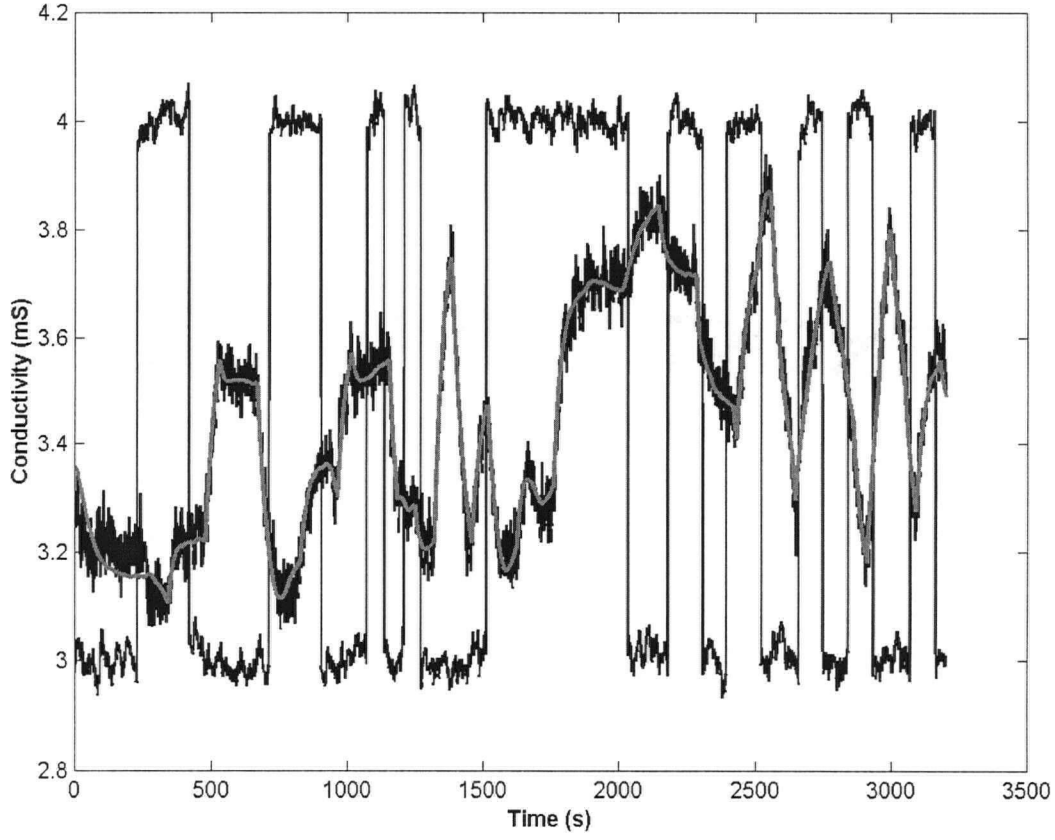

Figure 6.6: Simulated chest input and output signals in black lines and model output in gray line.

6.3 Input signal design for the scale-model chest

The excitation method described in section 6.2 for simulated data was adapted for the excitation of the scale-model chest. In an initial experiment the system was excited by a rectangular pulse (Figure 6.7) which allowed the estimation of an approximate model (gray line in Figure 6.7) used to design the excitation for the second experiment. Figure 6.8 shows the frequency response of the approximate model obtained from the initial experiment. The excitation in the second experiment should concentrate the input energy in those frequencies where the magnitude Bode plots is sensitive to parameter variations. Figure 6.9 shows the Bode plots of the partial derivatives of the approximate model for the scale-model chest with respect

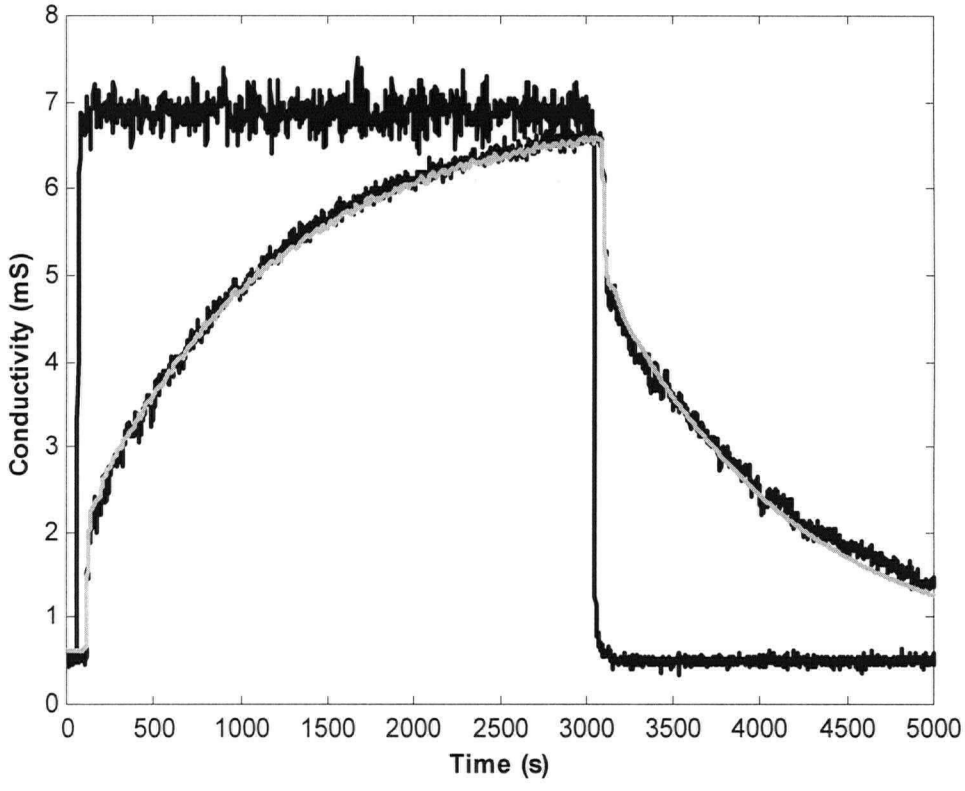

Figure 6.7: Scale-model chest input and output signals in black lines and model output in gray line.

to the parameters f, R, a_1, and a_2. From this figure the frequencies at which the magnitudes are maximum are obtained: ω_f = 0.05 rad/s, ω_R = 0.0009 rad/s, ω_{a1} = 0.15 rad/s, ω_{a2} = 0.001 rad/s. Therefore, we selected the frequency region from 0.0009 rad/s to 0.15 rad/s in order to design a frequency-modulated random binary input signal for the second experiment (see Figure 6.5). The signal designed by this method was then applied to the injection valve. Preliminary dynamic test results showed that the designed signal was too fast for this system. Figure 6.10 shows one of the dynamic tests performed by exciting the system with this input signal. It can be seen that this signal provides a very fast excitation for the scale-model chest, which has a slow dynamics and the parameters estimated from this input-output data are not accurate. The high cut-off frequency (ω_{a1} = 0.15 rad/s) for the band-pass filter was obtained at the maximum value of the partial derivative of the model with respect to a_1 which is correspondent to τ_1 in continuous-time domain. Since a very limited amount of mixing occurs in the channeling zone, the value of τ_1 is very small (a few seconds) for the scale-model chest and should be ignored when designing the input signal. Therefore, the high cut-off frequency for band-pass filter was reduced from ω_{a1} = 0.15 rad/s to ω_f = 0.05 rad/s. Also from Figure 6.8 it can be seen that the degree of upset attenuation is not desirable at frequencies less than 0.05 rad/s compared to that at frequencies greater than 0.05 rad/s. Consequently, the excitation energy for the second experiment was chosen at frequencies less than 0.05 rad/s. Therefore, the high cut-off frequency for band-pass filter was reduced from 0.15 rad/s to 0.05 rad/s. Since the low cut-off frequency for band-pass filter (0.0009 rad/s corresponding to the period $T = 2\pi/\omega$ = 6981 s) was higher than the maximum length of the experimental data (5500 s determined by the feed tank capacity and pulp flow rate through the chest), it was not necessary to consider the low cut-off frequency when designing the input signal (Ein-Mozaffari et al., 2002).

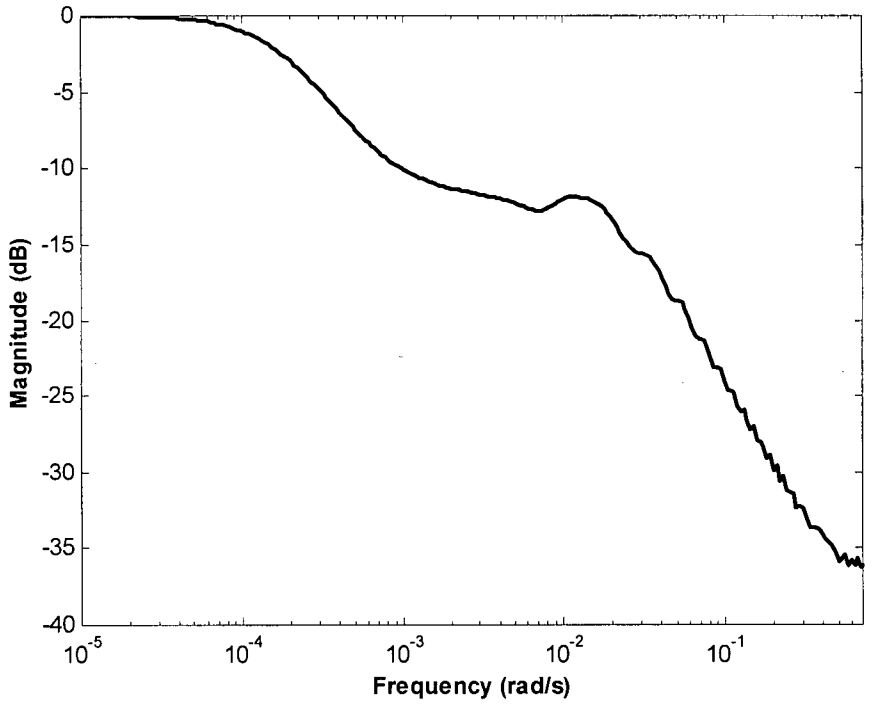

Figure 6.8: Frequency response of the approximate model

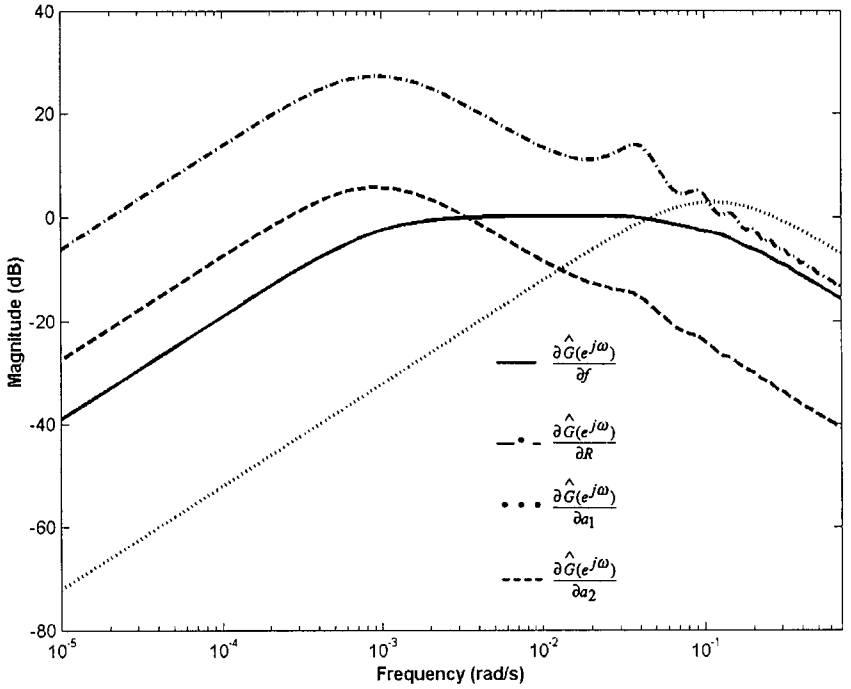

Figure 6.9: Magnitude Bode plot of partial derivatives of the model based on the excitation made on the scale-model chest by a rectangular pulse.

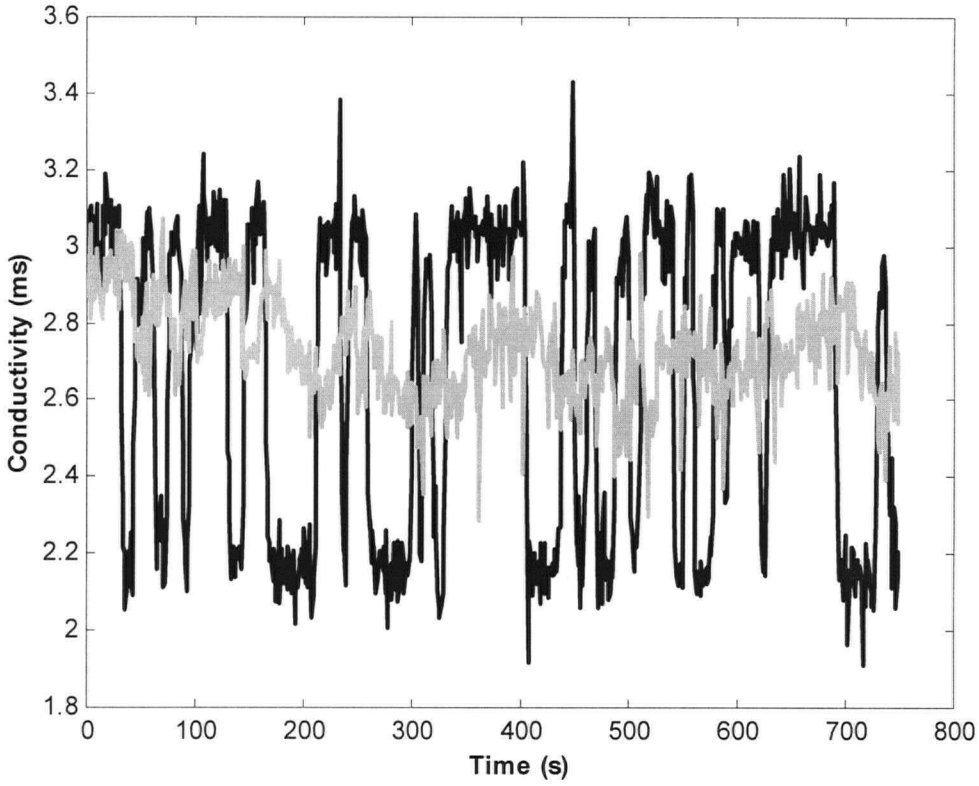

Figure 6.10: Dynamic test made on the scale-model chest by exciting the system with a fast frequency-modulated random binary signal. Input signal is in black line and output signal is in gray line.

Figure 6.11 shows the final frequency-modulated random binary input signal and its spectrum and periodogram. This signal was applied to the injection valve. Figure 6.12 shows the input, measured output and model output signals obtained from one of the dynamic tests made on the scale-model chest.

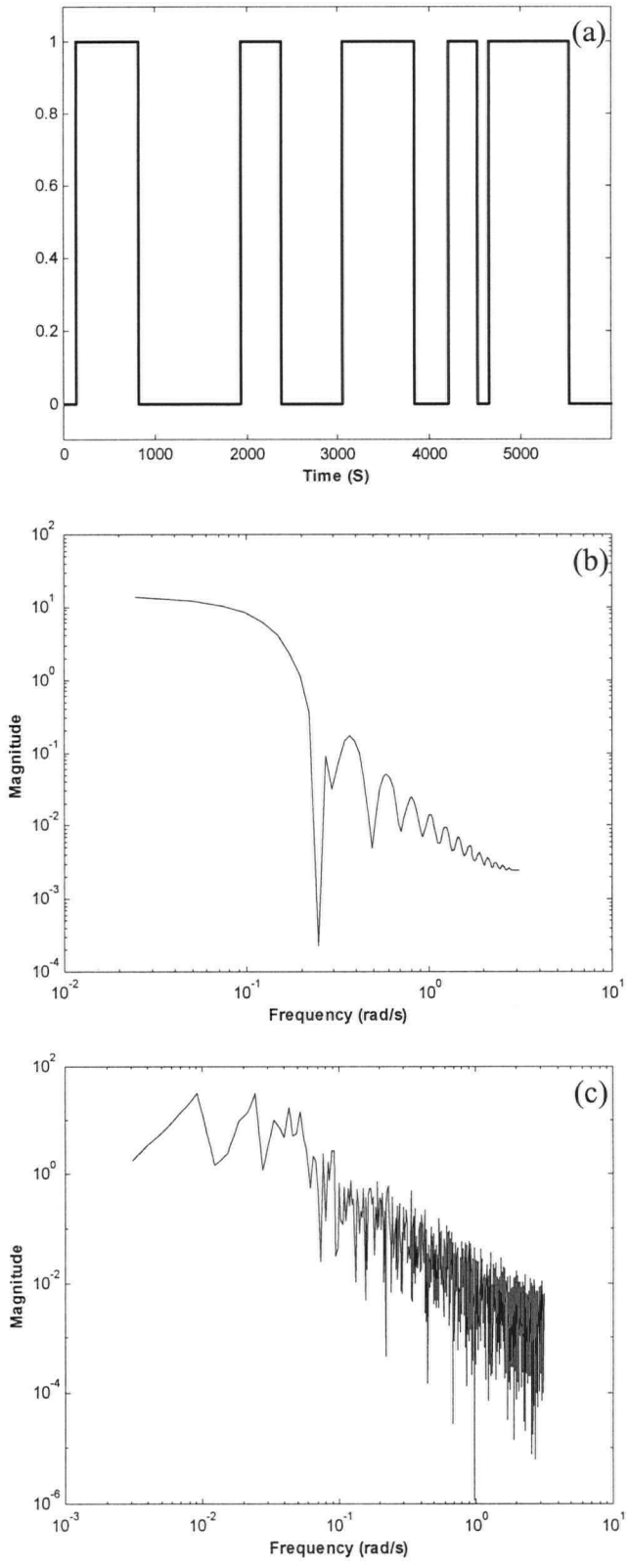

Figure 6.11: Input signal designed for scale-model chest: (a) frequency-modulated random binary signal, (b) its spectrum and (c) its periodogram.

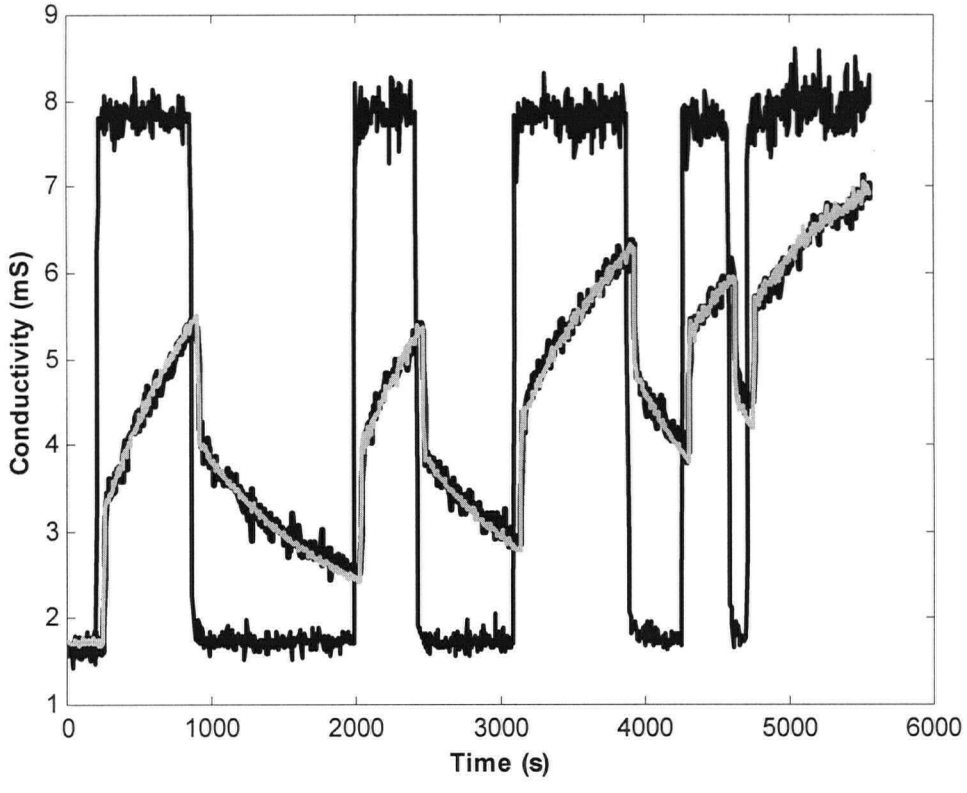

Figure 6.12: Scale-model chest input and output signals in black lines and model output in gray line.

6.4 Model validation

A model is not useful until its validity has been tested and established. A very good way of obtaining insight into the quality of a model is to simulate it with the input from a fresh data set, and compare the simulated output with the measured one (Figure 6.13).

A typical example of data collected from the scale-model chest is shown in Figure 6.14 together with the model output (gray line). The estimated model parameters from this dynamic test (see chapter 5) are summarized in Table 6.3.

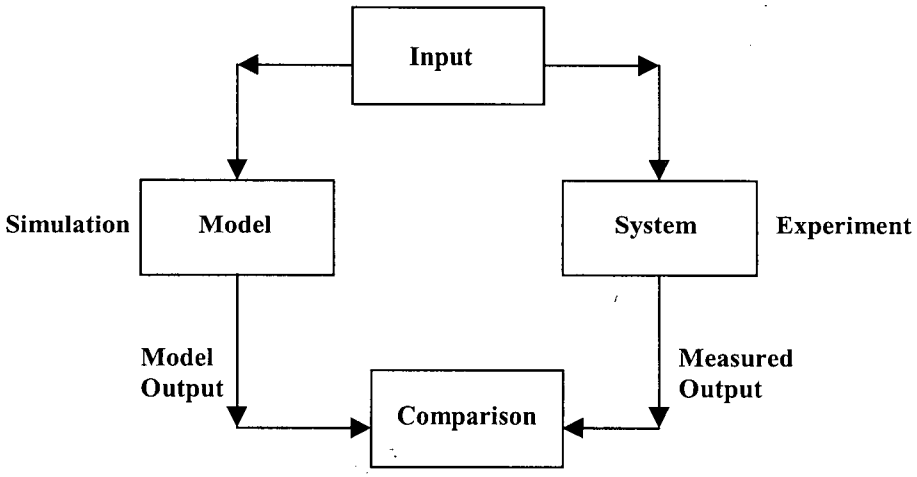

Figure 6.13: Model validation procedure.

To validate the model estimated from the input and output data shown in Figure 6.14, a second experiment was performed under the same operating conditions, except that the pulp was washed to increase the conductivity span. Figure 6.15 shows the validation results obtained from the second set of data. In this figure the measured output is in black line and the simulated data for the model estimated from the first set of data is in gray line. It can be seen that the simulated data and measured output are very close to each other.

Table 6.3: Estimated parameters from the first set of data. These parameters were used for simulation in model validation.

	f	R	T_1	τ_1	T_2	τ_2
Estimated parameter	0.24	0.00	45.0	10.5	100.0	892.2

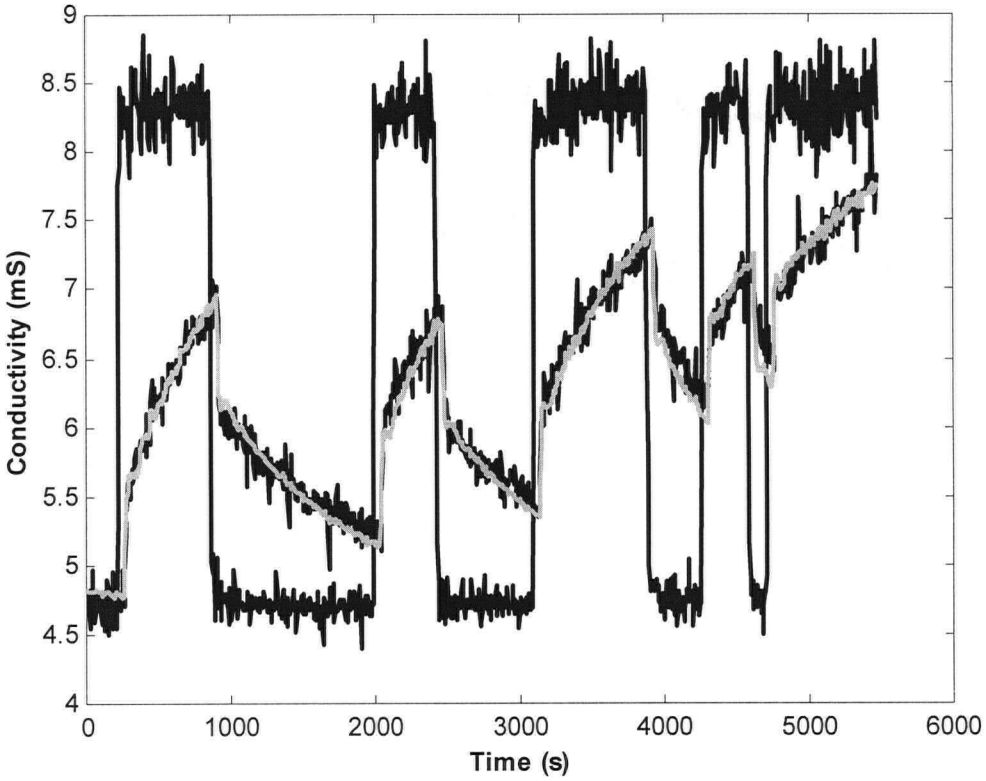

Figure 6.14: Scale-model chest input and output signals (first set of data) in black lines. Model output in gray line.

The validity of the model was checked by residual analysis (Ljung, 1999). First the residuals (e) associated with the data and the model was calculated:

$$e = y - \hat{y} \tag{6.2}$$

where y and $\hat{y}$ are the measured output and model output, respectively. Based on this method, the residuals associated with the validation data and a given model are ideally white and independent of the input (u) for the model to correctly describe the system. The auto-

correlation function of e and the cross-correlation function between e and u for the validation data are shown in Figures 6.16 and 6.17. These two graphs show that e is indeed white and independent of u. Therefore, this model is capable of reproducing new measurements quite well.

In dynamic tests made on the scale-model chest, we did not observe the effect of recirculation as a series of first order exponential responses, each one getting progressively smaller. This causes the step response of the scale-model chest to be smooth, which contrasts with the response collected from the industrial stock chest. This is likely due to the fact that not all process variables can be scaled down in the laboratory apparatus. It is known that often the uncontrolled factor in scale-up and scale-down is the magnitude of the non-ideality of flow, and unfortunately this very often differs widely between large and small units (Levenspiel, 1998).

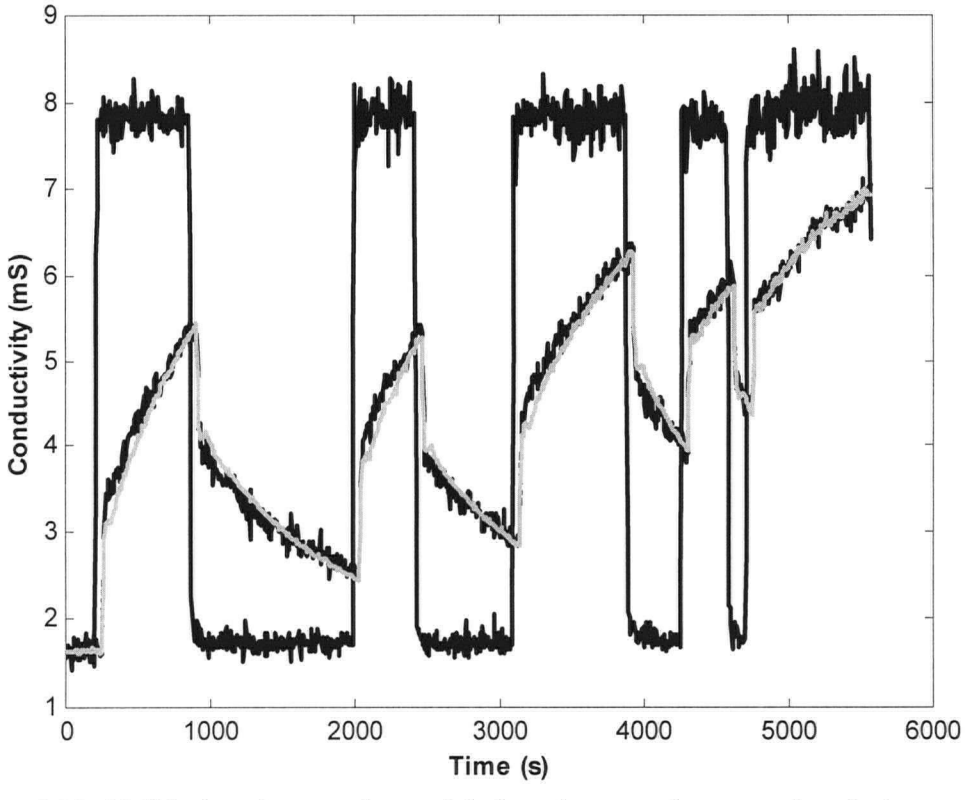

Figure 6.15: Validation data: scale-model chest input and output signals (second set of data) in solid black lines. Estimated model from the first set of data in gray line.

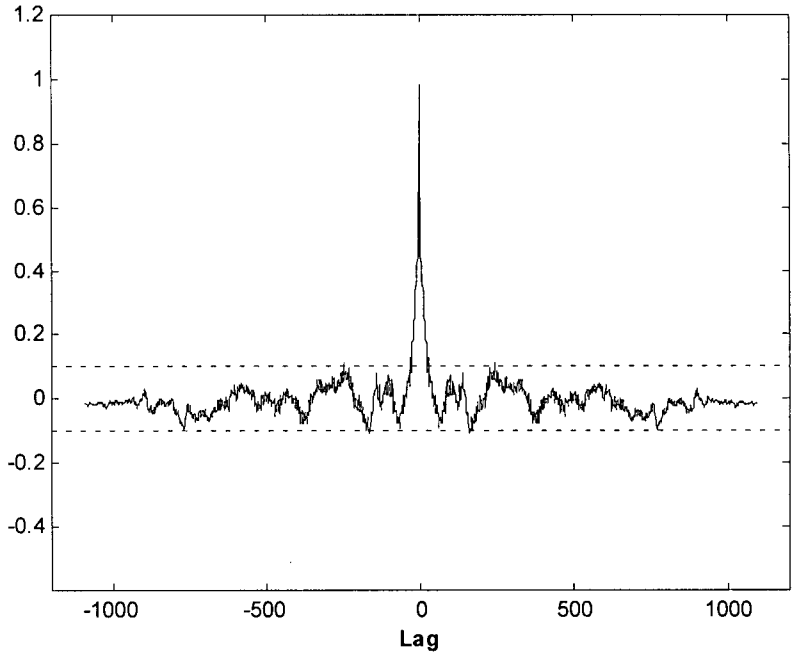

Figure 6.16: Auto-correlation function of the residuals (e) associated with the validation data and the model. Dotted lines denote 99% confidence intervals.

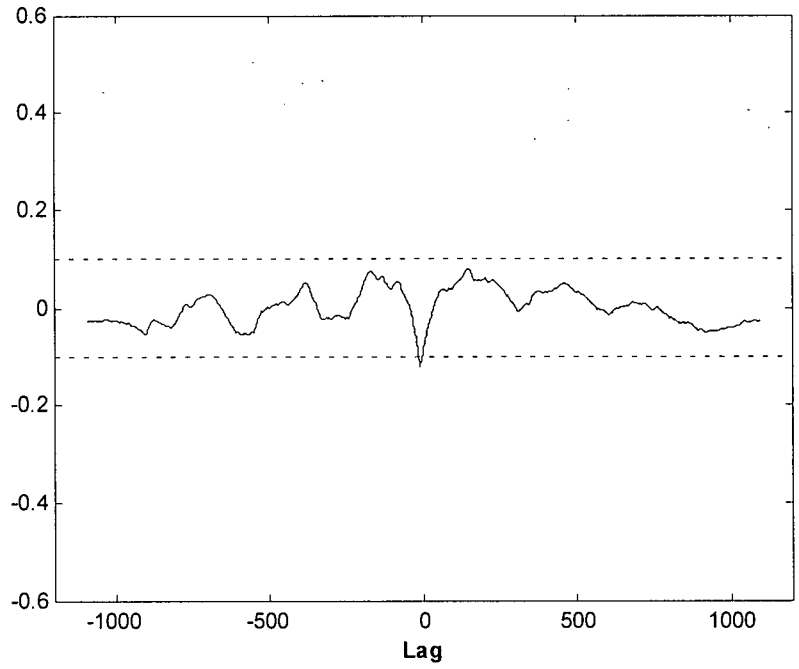

Figure 6.17: Cross-correlation function between the residuals (e) and the input (u) for the validation data. Dotted lines denote 99% confidence intervals.

6.5 Summary

1. The choice of input signals has a very substantial influence on the observed data. To estimate the model parameters, the system must be excited by a proper input signal. In fact all modes of the system should be excited during the identification experiment.
2. The excitation provided in the dynamic tests made on the scale-model chest was limited to binary sequences because the input signal was controlled by an on-off solenoid valve.
3. The whole process of model identification comprises two experiments. In the first experiment the input signal was very simple, like a rectangular pulse, which provided an opportunity to visualize the plant response and also allowed the estimation of an approximate model for designing the excitation for the second experiment.
4. The idea behind the experiment design was to concentrate the excitation energy at frequencies where the Bode plot was sensitive to parameter variations. To achieve this goal, the magnitude of the Bode plot for the partial derivatives of the approximate model, which obtained from the first experiment, with respect to model parameters were calculated. The excitation energy for the second experiment was concentrated at the frequencies where the maximum values for the partial derivatives were found. Since the time constant of the channeling zone for the scale-model chest was very small, the partial derivative of the model with respect to this parameter was ignored when designing the input signal.
5. To design a frequency-modulated random binary signal for the second excitation, first a zero-mean white-noise signal was filtered by a band-pass filter with cut-off frequencies obtained from the magnitude Bode plot of partial derivatives of the approximate model with respect to model parameters. The filtered signal is then converted into a binary sequence by using Equation 6.1.

6. Simulation example showed that the parameters estimated from the second excitation were more accurate due to better excitation provided with the frequency-modulated random binary signal.
7. The validation of the dynamic model estimated from identification experiment was tested. For this purpose, we simulated the model with the input from a fresh data set, and compared the simulated output with the measured one. The validity of the model was checked by residual analysis. The auto-correlation function of residuals (e) and the cross-correlation function between e and the input (u) for the validation data showed that e is indeed white and independent of u. Therefore, our model is capable of reproducing new measurements quite well.

CHAPTER 7

7 RESULTS OF DYNAMIC TESTS MADE ON SCALE-MODEL CHEST

7.1 Introduction

As it was mentioned in chapter 5, the dynamic response of industrial stock chests is not predictable and the upset attenuation in industrial chests is considerably worse than that of a fully mixed chest. To improve the upset attenuation in the chest, the effect of non-ideal flows such as channeling and dead volumes must be reduced. In this chapter we explore the effect of process variables on channeling, fully mixed volume, and disturbance attenuation. Variables examined included impeller speed and diameter, fibre mass concentration, pulp flow rate through the chest, and pulp feed and exit locations for two flow configurations shown in Figure 3.8. Since Config.1 is most widely used in industry, we focused on how the dynamics of this configuration could be improved by changing the chest operating conditions. Table 7.1 summarizes the experimental conditions.

Table 7.1: Experimental conditions.

Impeller speed	700 – 1750 rpm
Fibre mass concentration	2.1% - 3.3%
Pulp flow rate through the chest	7.9 – 37.1 L/min
Impeller diameter	14.0 – 16.5 cm
$L \times W \times Z$	53cm × 40cm × 50cm

7.2 Fully mixed volume calculation

A fully mixed system has a first order transfer function (Ogunnaike and Ray, 1994 and Stephanopoulos, 1984). To calculate the fully mixed volume of the agitated zone, the effect of recirculation is eliminated (R = 0). This is a reasonable assumption, because the effect of recirculation as a series of first order exponential responses was not distinguishable in the dynamic responses of the scale-model chest. Under these circumstances, the time constant for the agitated zone (τ_2) is (see dynamic model of the stock chest shown in Figure 5.5):

$$\tau_2 = \frac{V_{fully\ mixed}}{(1-f)Q} \tag{7.1}$$

where Q is the pulp flow rate through the chest. τ_2 and f can be estimated from input-output data. This allows calculation of fully mixed volume ($V_{fully\ mixed}$) using Equation 7.1. The ideal performance for an agitated pulp stock chest is achieved when $f = 0$ and $V_{fully\ mixed}$ is equal to the total suspension volume inside the chest. Under these circumstances the dynamic behavior of agitated chest is defined only by a first order transfer function.

7.3 Dynamic results and discussion

7.3.1 The effect of impeller speed and pulp flow rate

Figure 7.1 shows the input and output responses for a series of tests where the flow rate into the chest is fixed and the impeller speed (N) changed. At N = 1127 rpm, which is above the criteria of complete surface motion used to size the chest, the output response follows the input signal, indicating complete channeling in the chest. At this impeller speed, the chest does not attenuate the high-frequency variability in input. However disturbance attenuation is progressively improved as the impeller speed is increased to 1732 rpm.

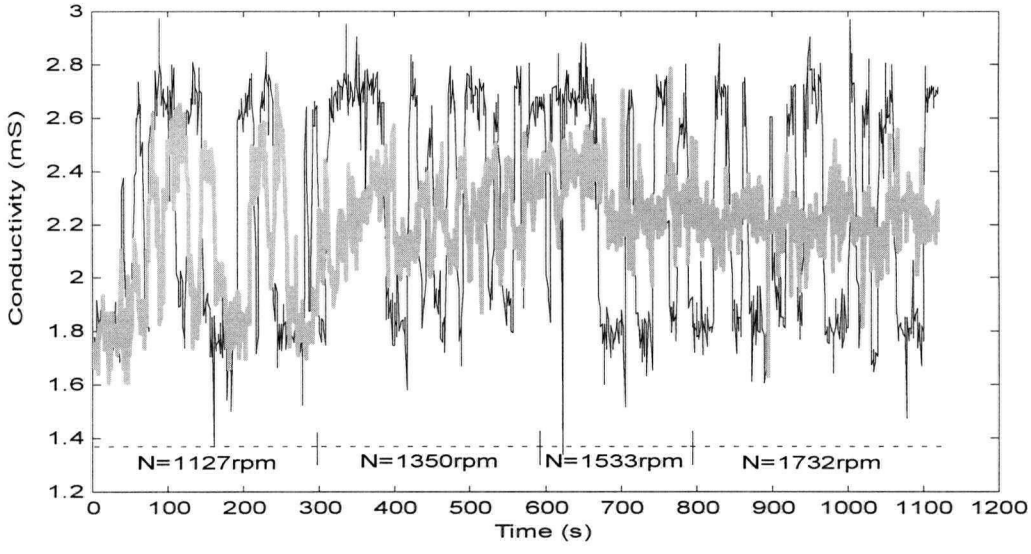

Figure 7.1: The effect of impeller speed on the upset attenuation. Input signal is in black line and output signal is in gray line (Q = 37.1 L/min ; C_m = 3.3% ; Config.1).

Figures 7.2 and 7.3 show the effects of impeller speed and pulp flow rate through the chest on channeling and fully mixed volume, respectively. These data show that channeling decreases and the percentage of the fully mixed volume ($V_{fully\ mixed}/V_{total}$) increases as impeller speed increases. At higher impeller speed the fibre/fibre network is disrupted further from the impeller leading to improved mixing by eliminating non-ideal flows such as channeling and dead zones. Figure 7.4 shows the effect of impeller speed on the frequency response of the stock chest. As it can be seen in this figure, the degree of disturbance attenuation can be improved by increasing the impeller speed. For example, at N = 1724 rpm the dynamic response is very close to an ideal response, which has a simple first order transfer function. It means that increasing the impeller speed eliminates the effect of non-ideal flows such as channeling and dead zones. At N = 1363 rpm and under the circumstances shown in Figure 7.4

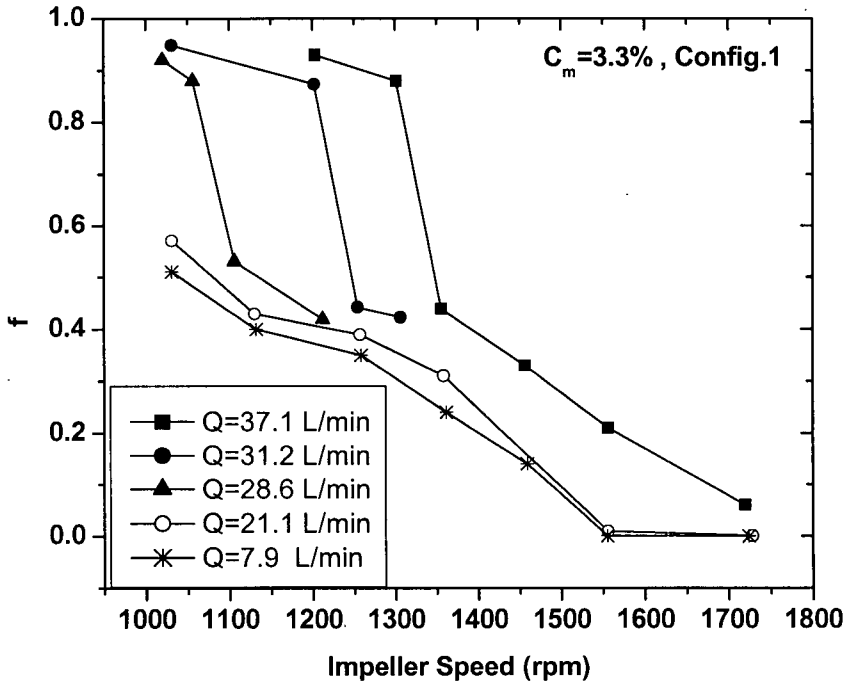

Figure 7.2: The effect of impeller speed and pulp flow rate on channeling.

the whole suspension inside the chest was in motion and no stagnant zones were observed. However, it can be seen that the degree of upset attenuation at this impeller speed is considerably worse than that of perfectly mixed chest due to existence of channeling and dead zones. From Figures 7.2 and 7.3 it can be seen that for these operating conditions the percentage of channeling and dead volumes are 26% and 16%, respectively. Therefore, non-ideal flows could persist in a chest even upon achieving complete motion.

From Figures 7.2 and 7.3 it can be seen that at higher flow rates the system is prone to a higher degree of channeling and a lower percentage of fully mixed volume even at impeller speeds above the criteria of complete motion used to size the chest. Both figures show that the

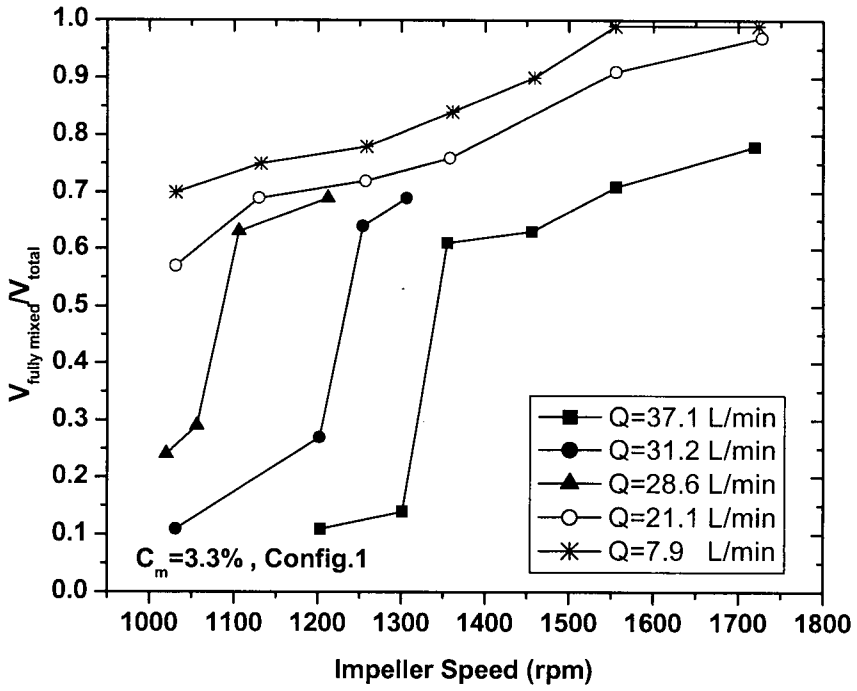

Figure 7.3: The effect of impeller speed and pulp flow rate on fully mixed volume.

onset of significant non-ideal behavior can be quite sudden. Since in Config.1 the pulp exit location is on the impeller wall, one of the possible factors affects the sudden transition to significant non-ideal behavior can be the ratio of the suspension flow induced by the impeller to pulp flow through the chest. Therefore, increasing the impeller speed and decreasing the pulp flow rate should reduce or eliminate the non-ideal flow. Figure 7.5 shows the effect of pulp flow rate through the chest on disturbance attenuation. It can be seen that the degree of upset attenuation is improved by decreasing the pulp flow rate through the chest. A decrease in pulp flow rate decreases the channeling and increases the fully mixed volume leading to improved attenuation by increasing the time constant of the mixing zone.

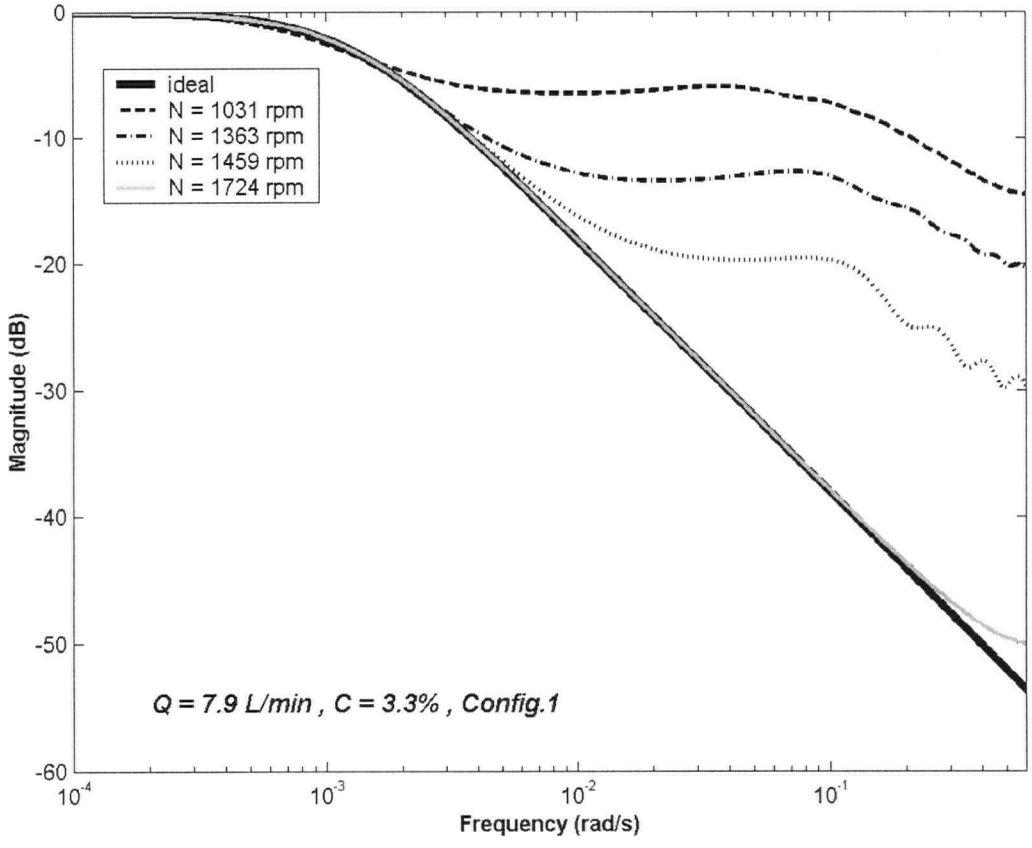

Figure 7.4: The effect of impeller speed on the degree of disturbance attenuation.

7.3.2 The effect of fibre mass concentration

Figures 7.6 and 7.7 show the effect of fibre mass concentration on channeling and fully mixed volume. As the fibre mass concentration increases, the number of fibre/fibre interactions increases which increase network strength (Bennington, 1996). As a result of this behavior, the effect of non-ideal phenomena such as channeling and dead volume increases with increased fibre mass concentration. Figures 7.6 and 7.7 show that at fibre mass concentration greater than 3% a high percentage of channeling and a low percentage of fully mixed volume exist, even at

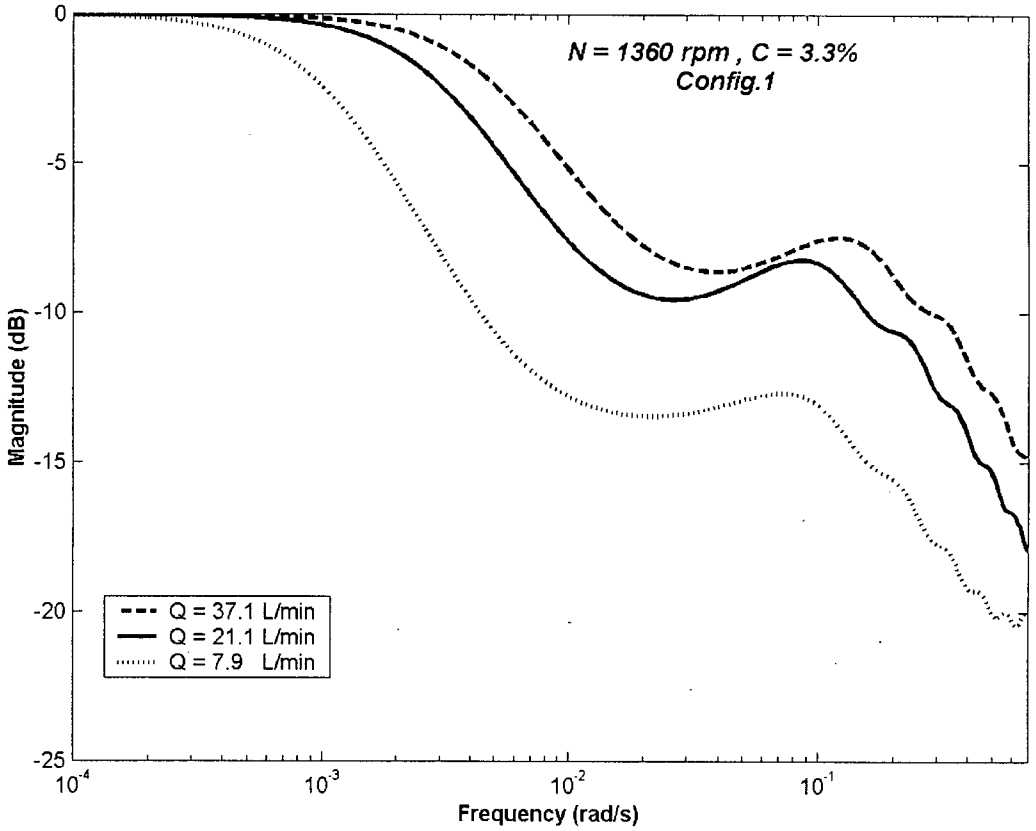

Figure 7.5: The effect of pulp flow rate through the chest on the degree of disturbance attenuation.

impeller speeds greater than that required for complete surface motion. At fibre mass concentration smaller than 3%, full channeling does not occur even at impeller speeds equal to that required for complete surface motion. This phenomenon can cause problems when the fibre mass concentration inside a chest (designed for a lower fibre mass concentration) increases during operation due to disturbances. In this situation the system can shift to full channeling with a low degree of attenuation. In Figure 7.8 the effect of fibre mass concentration on the chest performance has been shown in the frequency domain. In this graph,

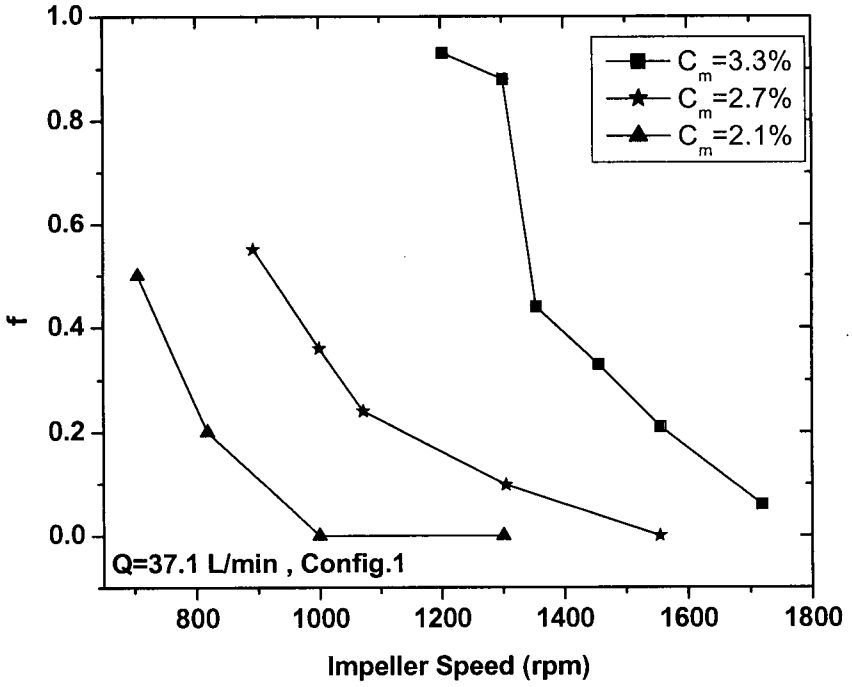

Figure 7.6: The effect of impeller speed and fibre mass concentration on channeling.

the comparison has been done for the beginning of complete motion through the chest at different fibre mass concentration. This data show that the degree of attenuation decreases with an increase in fibre mass concentration. From Figure 7.8 it can be seen that although the whole suspension inside the chest is in motion, no significant attenuation occurs at C_m = 3.3%. However, when the fibre mass concentration decreases to 2.1%, the degree of upset attenuation is significantly improved. Therefore, chests designed using the criterion of the onset of complete motion do not necessarily lead to a fully mixed system especially at fibre mass concentration greater than 2%.

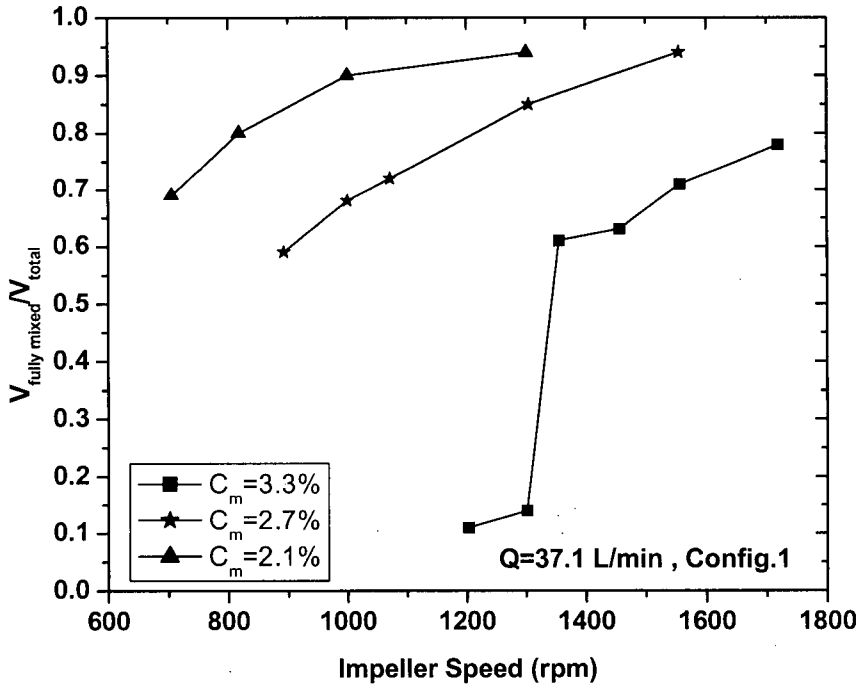

Figure 7.7: The effect of impeller speed and fibre mass concentration on fully mixed volume.

7.3.3 The effect of pulp feed and exit location

Dynamic tests showed that the pulp feed and exit locations significantly affect the degree of upset attenuation and the non-ideal behavior of the mixing chest. Based on results presented previously, non-ideal flow decreases with increasing impeller speed, decreasing pulp flow rate and fibre mass concentration for Config.1. But higher impeller speed requires higher installed power and can cause air to be entrained in the suspension. Decreasing either the pulp flow rate or the fibre mass concentration reduces the production capacity of the chest. The dynamic tests made on the scale-model chest showed that the dynamic performance for Config.1 could be

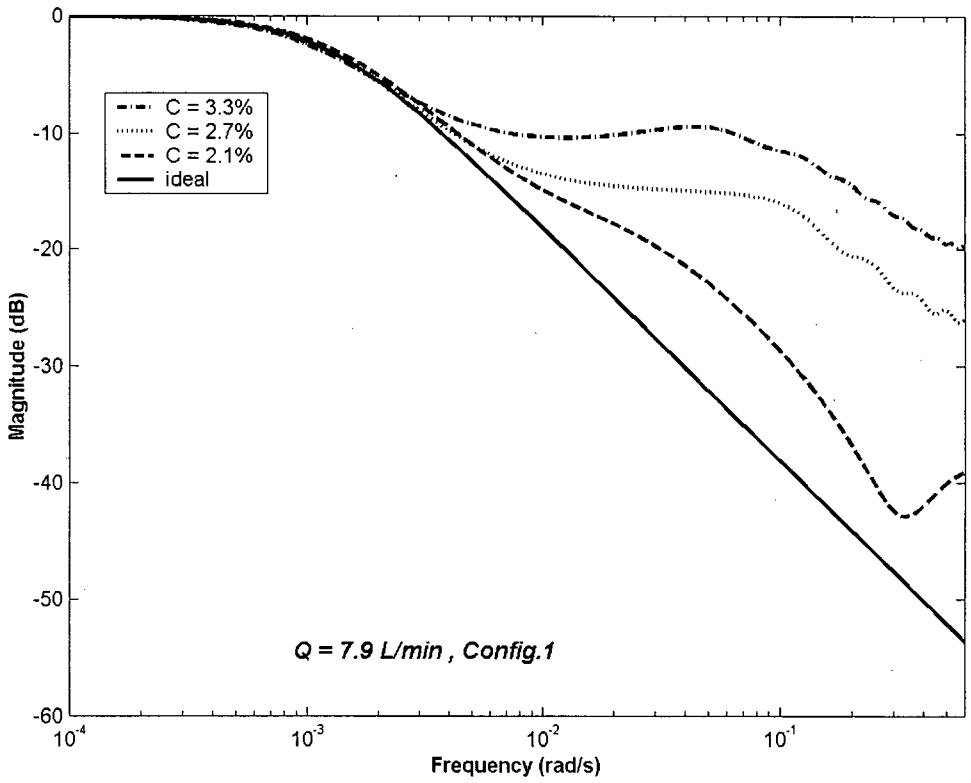

Figure 7.8: The effect of fibre mass concentration on the degree of upset attenuation.

improved by changing the feed and exit locations to that of Config.2 as shown in Figures 7.9 and 7.10. The percentage of channeling and dead volume are much lower for Config.2 at fixed operating conditions. Because from the flow pattern shown in Figure 4.14 it can be seen that in Config.1 a percentage of the pulp feed can easily channel when it moves on the surface toward the exit location at the impeller wall without being forced to the mixing zone by the impeller. However, based on this flow pattern, Config.2 will force flow into the mixing zone before

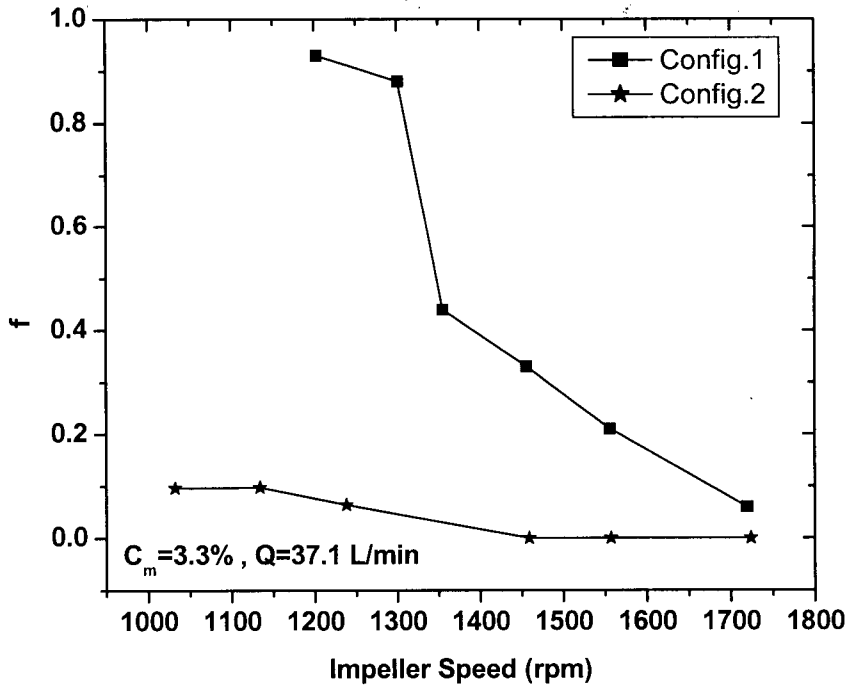

Figure 7.9: The effect of impeller speed and input-output locations on channeling.

leaving the chest. In Figure 7.11 it can be seen that under identical operating conditions, Config.2 can provide greater attenuation and approaches an ideal response.

Dynamic tests made on scale-model chest showed that even the low percentage of channeling for Config.2 shown in Figure 7.9 will be eliminated by reducing the pulp flow rate through the chest. Figures 7.12 and 7.13 show the effect of pulp flow rate through the chest on channeling and fully mixed volume for Config.2, respectively. It can be seen that at Q = 7.9 L/min the effect of channeling has been completely eliminated and the percentage of fully mixed volume has been improved compared to those obtained at Q = 37.1 L/min.

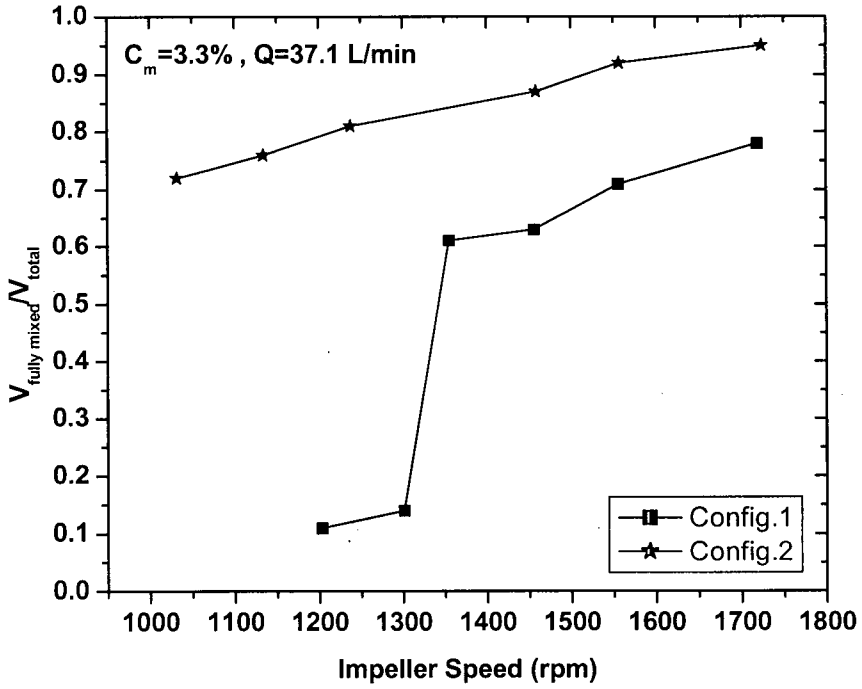

Figure 7.10: The effect of impeller speed and input-output locations on fully mixed volume.

Also channeling was not observed at fibre mass concentration lower than 3% for Config.2. Figures 7.14 and 7.15 show the effect of fibre mass concentration on channeling and fully mixed volume for Config.2. These data show that at $C_m = 2.7\%$ and $C_m = 2.1\%$ channeling does not exist and fully mixed volume significantly increases and rapidly approaches to the total chest volume at fibre mass concentration lower than 3%.

Sufficient motion must be provided at the pulp exit location to prevent dewatering of stock before it enters the discharge pump. Therefore, the exit port can not be located at the impeller opposite wall where insufficient motion is induced by the impeller. In both Config.1

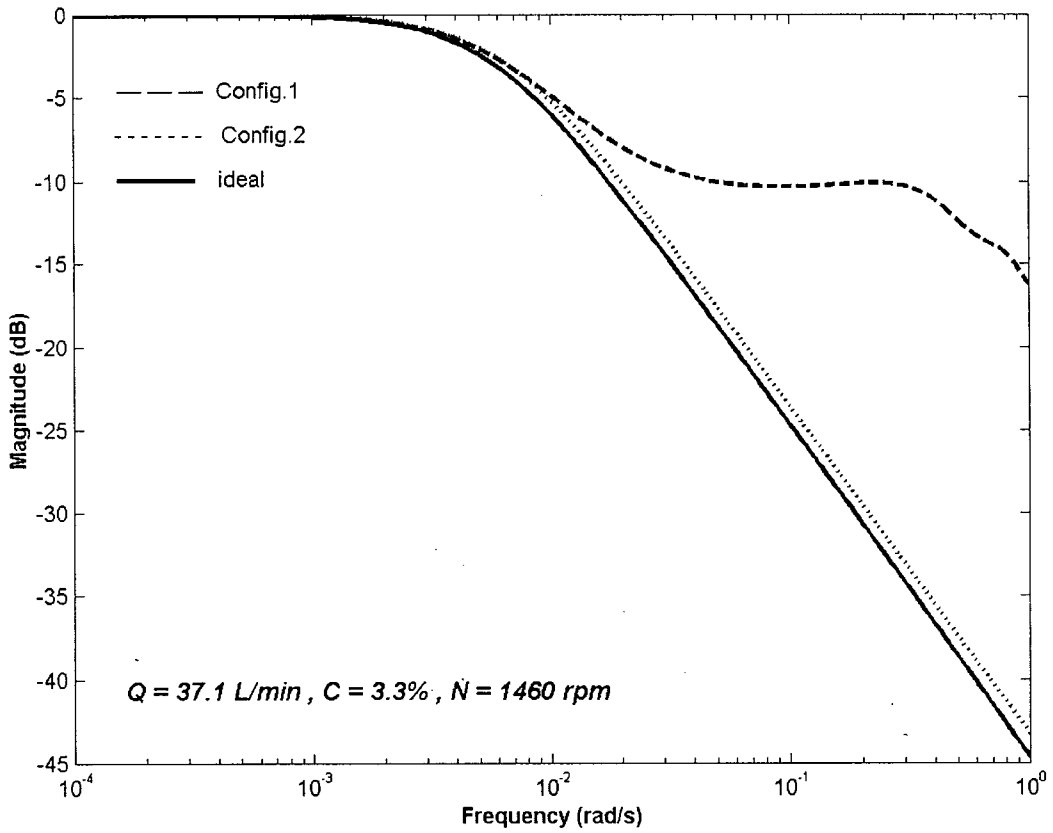

Figure 7.11: The effect of input-output locations on the degree of disturbance attenuation.

and Config.2 sufficient motion exists at the pulp exit locations. However, Config.1 is widely used in industry due to the ease of mechanical installation and maintenance.

7.3.4 Impeller momentum flux and dynamic response

Based on batch test results presented in chapter 4, the mixing time in agitated pulp stock chests is a function of fibre mass concentration and N^2D^4, which is proportional to the impeller momentum flux. This means that for given fibre mass concentration the same mixing results could be achieved for different impeller diameters providing equal momentum fluxes. It can be concluded that for a given fibre mass concentration, the degree of upset attenuation is equal for

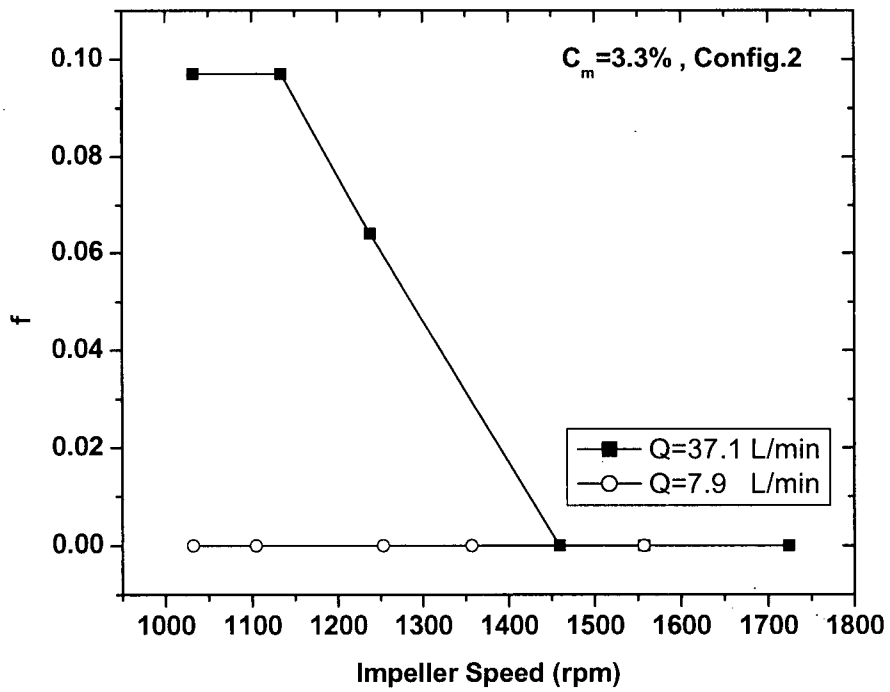

Figure 7.12: The effect of impeller speed and pulp flow rate through the chest on channeling for Config.2.

different impeller diameters as long as the momentum flux is the same. Dynamic responses of the scale-model chest in frequency domain shown in Figure 7.16 (a case where no channeling exists) and Figure 7.17 (a case where channeling exists) support this conclusion. From Figures 7.16 and 7.17 it can be seen that the degree of upset attenuation for different impeller diameters (16.5 cm and 14 cm) are very close to each other when the impeller momentum flux is constant. In fact, the same dynamic result in a given mixing operation could be achieved with various power inputs by changing the diameter and speed of the impeller. A large, low speed impeller could produce an equivalent mixing results with less power than a smaller, high-speed impeller (see Table 7.2). It must be mentioned that the impeller diameter to chest width ratio is

an important factor in the design of agitated pulp chests and Yackel (1990) recommends that it should be in the range 0.20 – 0.45. This ratio for the scale-model chest is 0.41 (see chapter 4).

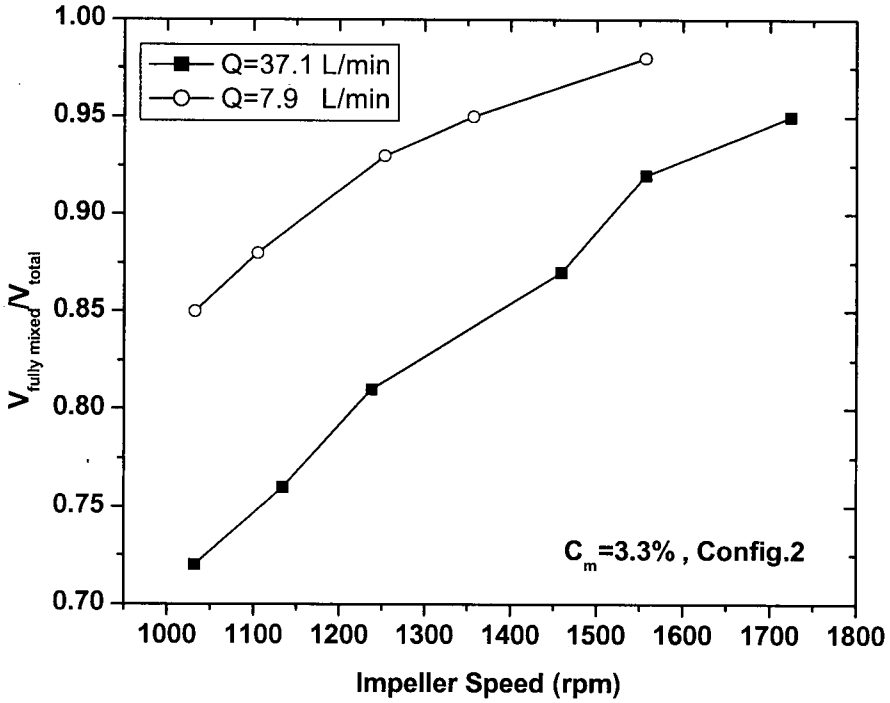

Figure 7.13: The effect of impeller speed and pulp flow rate through the chest on fully mixed volume for Config.2.

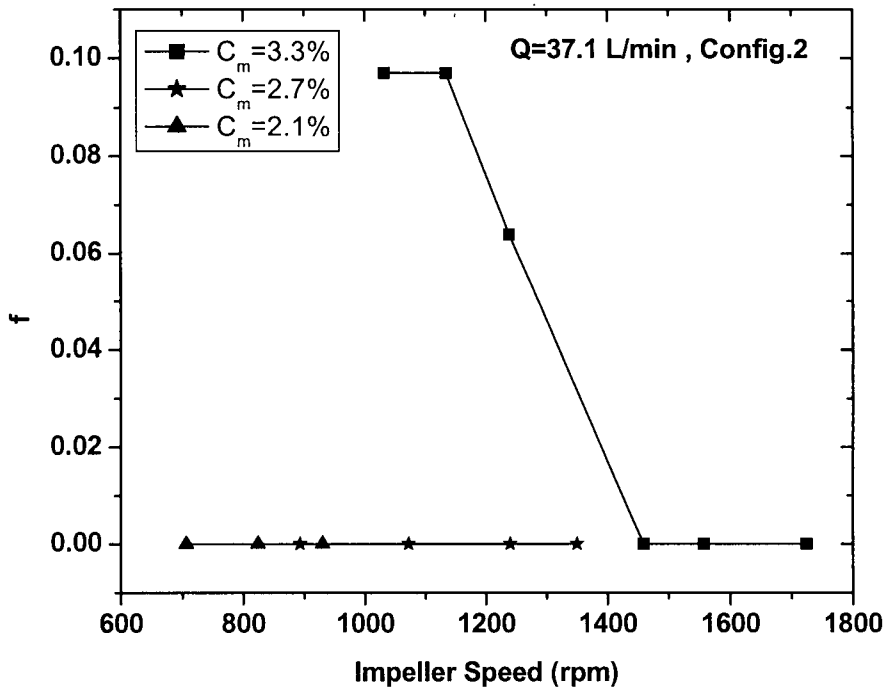

Figure 7.14: The effect of impeller speed and fibre mass concentration on channeling for Config.2.

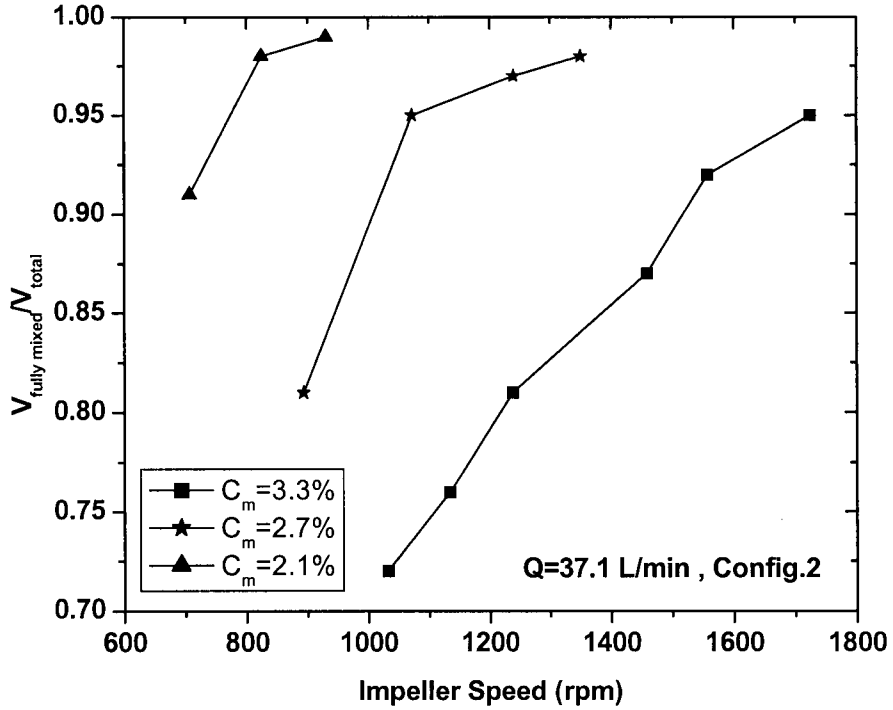

Figure 7.15: The effect of impeller speed and fibre mass concentration on fully mixed volume for Config.2.

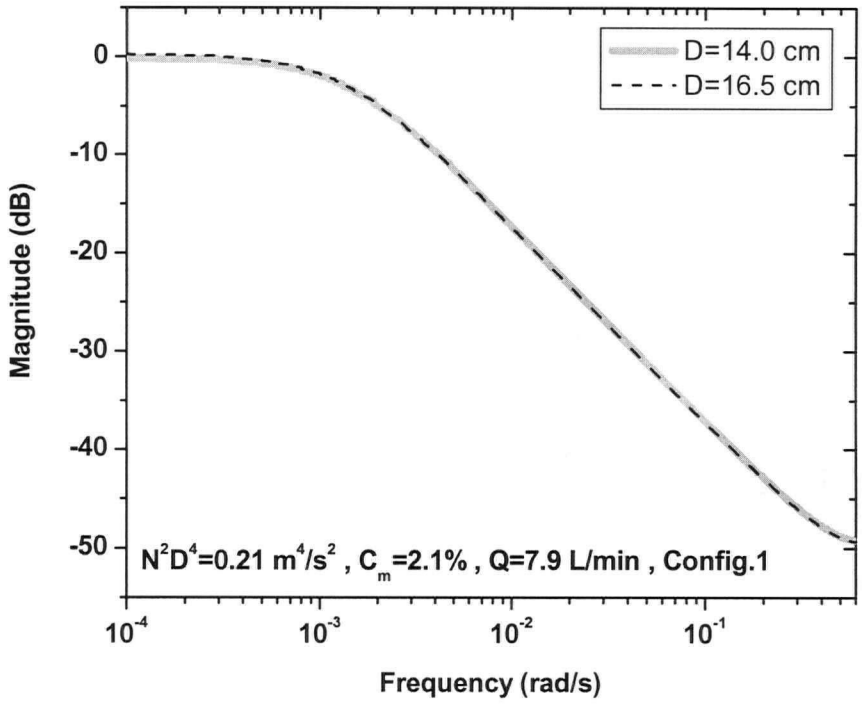

Figure 7.16: Frequency response measured for two impellers having different diameters but providing same momentum flux (a case where no channeling exists).

Table 7.2: Power consumption for two impellers having different diameters but providing same momentum flux.

Operating Conditions	Power Consumption (W)	
	D = 16.5 cm	D = 14.0 cm
Shown in Figure 7.16	164	200
Shown in Figure 7.17	167	186

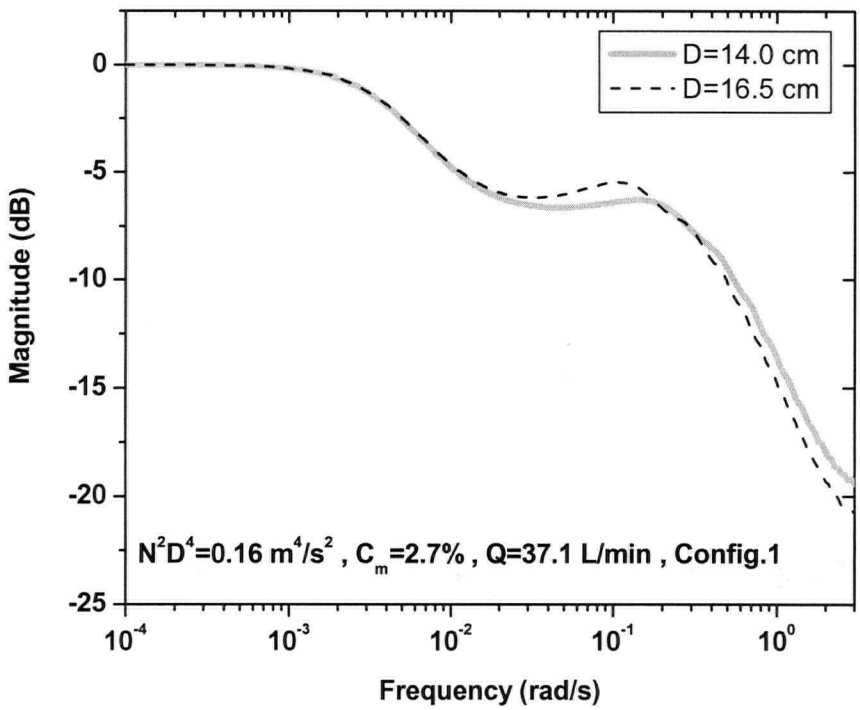

Figure 7.17: Frequency response measured for two impellers having different diameters but providing same momentum flux (a case where channeling exists).

7.3.5 Design criteria and dynamic response

Oldshue and Gretton (1956) assumed that "complete motion" in a chest was achieved when complete stock movement occurred across the surface of the chest. Industrial design is based on achieving this state. As we explained in chapter 4, stagnation zones could persist in the chest corners even when complete surface motion was achieved. In this study, "complete motion" is defined to exist when there are no stagnant zones in the chest.

One method used for designing agitated pulp stock chests is Yackel's method (Yackel, 1990) based on the momentum flux generated by the impeller (see chapter 2). In Figure 7.18 the power calculated using Yackel's method is compared with that required for complete motion. It can be seen that Yackel's method underpredicts the power required. The most likely reason for this is that Yackel based his method on the power required to achieve surface motion in the chest. Since we define "complete motion" as occurring when no stagnant zones exist in the chest, additional power was required. From Figure 7.18 it can be seen that even with the power required for complete motion, the effect of non-ideal flows such as channeling and dead volume is not eliminated. To achieve an ideal dynamic response (without channeling and dead zones) additional power above that required for complete motion is needed.

Figure 7.18 shows that the ratio of required power for ideal response to that for

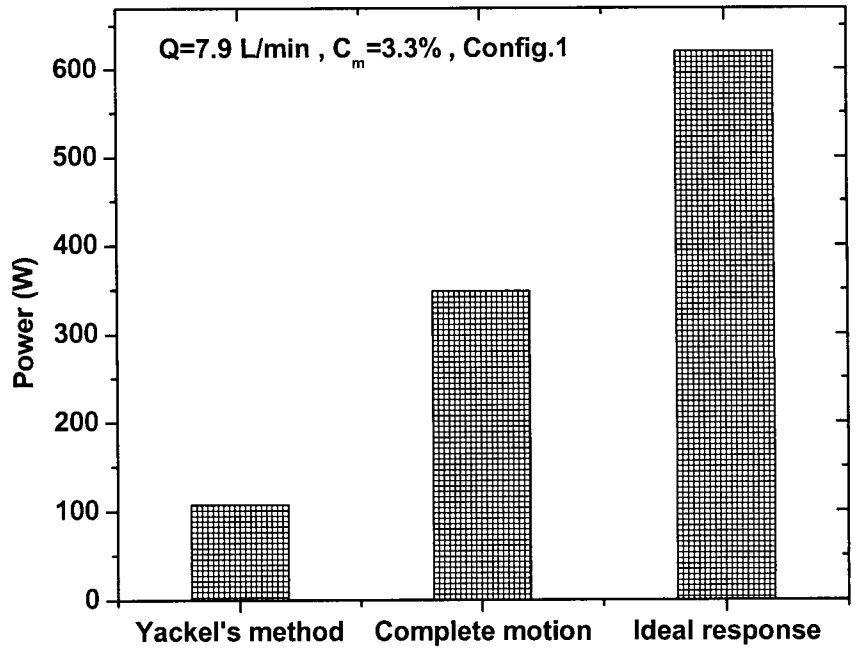

Figure 7.18: The effect of chest performance on power consumption (Q = 7.9 L/min , C_m = 3.3% , Config.1).

complete motion is $P_{ideal\ response} / P_{complete\ motion} = 1.8$. Dynamic tests showed that this ratio is dependent on fibre mass concentration, pulp flow rate through the chest, and pulp feed and exit locations. In Figure 7.19 the power calculated using Yackel's method is compared with those required for complete motion and an ideal response at $C_m = 2.7\%$. But the other operating conditions are the same with those shown in Figure 7.18. At $C_m = 2.7\%$, $P_{ideal\ response} / P_{complete\ motion}$ is equal to 1.3 which is lower than that calculated at $C_m = 3.3\%$. As it was shown in section 7.3.2, at fibre mass concentration greater than 3% the system is susceptible to high percentage of channeling and dead volume, while at fibre mass concentration lower than 3% the effect of non-ideal flow significantly decreases. Therefore, at higher fibre mass concentration $P_{ideal\ response} / P_{complete\ motion}$ is greater than that at lower fibre mass concentration.

In Figure 7.20 the power calculated using Yackel's method is compared with those

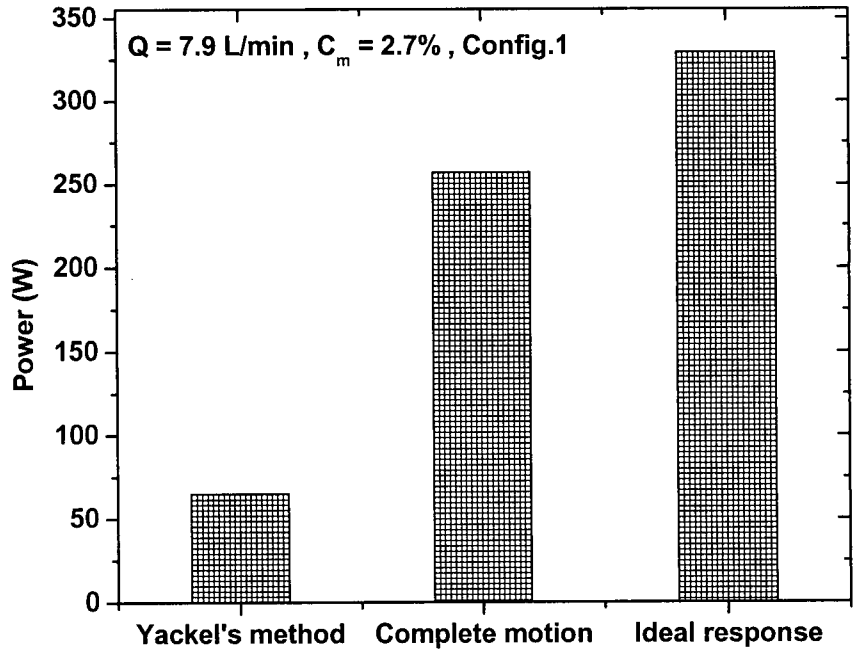

Figure 7.19: The effect of chest performance on power consumption (Q = 7.9 L/min , C_m = 2.7% , Config.1).

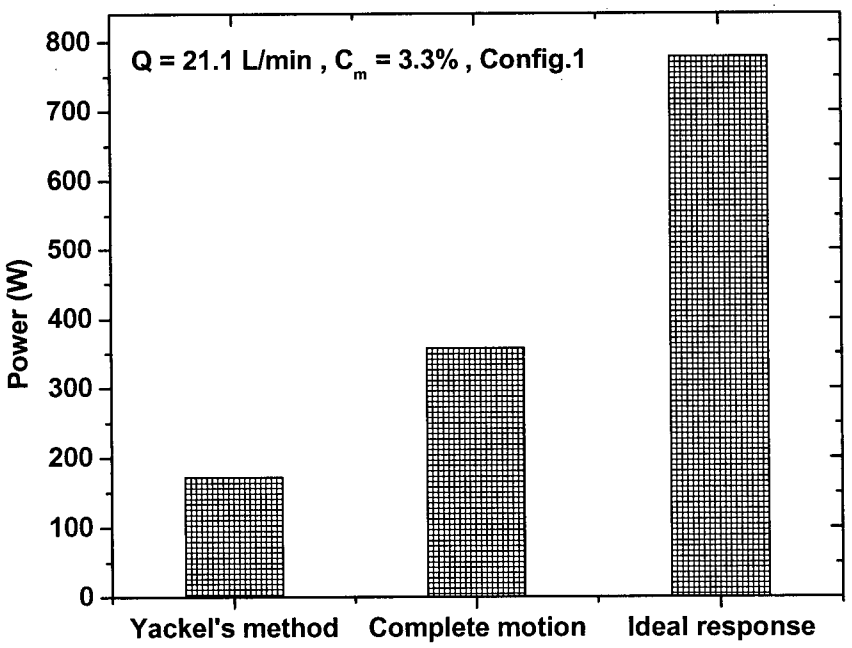

Figure 7.20: The effect of chest performance on power consumption (Q = 21.1 L/min , C_m = 3.3% , Config.1).

required for complete motion and an ideal response at Q = 21.1 L/min. But the other operating conditions are the same with those shown in Figure 7.18. At Q = 21.1 L/min, $P_{ideal\ response}$ / $P_{complete\ motion}$ is equal to 2.2 which is higher than that calculated at Q = 7.9 L/min. Based on results presented in section 7.3.1, at higher flow rates the system is prone to a higher degree of channeling and dead volume. Therefore, at higher pulp flow rate through the chest $P_{ideal\ response}$/ $P_{complete\ motion}$ is greater than that at lower flow rate.

Pulp feed and exit location has significant effect on the ratio of required power for ideal response to that for complete motion. In Figure 7.21 the power calculated using Yackel's method is compared with those required for complete motion and an ideal response for

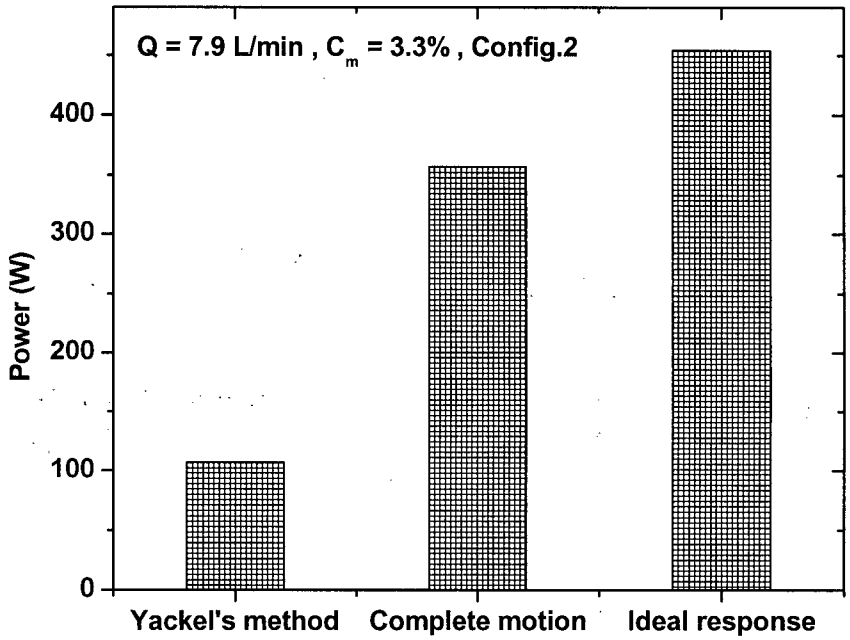

Figure 7.21: The effect of chest performance on power consumption (Q = 7.9 L/min , C_m = 3.3% , Config.2).

Config.2. The operating conditions are the same with those shown in Figure 7.18. For Config.2, $P_{ideal\ response} / P_{complete\ motion}$ is equal to 1.2 which is much lower than that calculated for Config.1. As it was shown in section 7.3.3, the percentage of channeling and dead volume is much lower for Config.2 at fixed operating conditions. Therefore, $P_{ideal\ response} / P_{complete\ motion}$ for Config.2 is lower than that for Config.1.

Therefore, if the purpose of using a stock chest is to keep the suspension moving to prevent dewatering of stock throughout the chest (as a storage tank), smooth surface motion can still lead to stagnant zones within the chest. To eliminate these stagnant zones, the installed power must be at least equal to the power required for the onset of "complete motion". If the

purpose of the stock chest is to attenuate high-frequency variations in fibre mass concentration (as a low-pass filter), the required installed power can be considerably greater than that by Yackel (1990) or required for "complete motion".

7.4 Summary

1. Dynamic tests made on scale-model chest confirm the existence of non-ideal flow such as channeling and dead zones. These non-ideal flows affect the performance of the chest as a low-pass filter and reduce the degree of upset attenuation. The effect of impeller speed and diameter, fibre mass concentration, pulp flow rate through the chest, and pulp feed and exit location on channeling, fully mixed volume, and disturbance attenuation was investigated.
2. Since at higher impeller speeds the fibre/fibre network is disrupted further from the impeller, channeling and dead zones are progressively decreased as impeller speed is increased.
3. At higher flow rates the system is prone to a higher degree of channeling, a lower percentage of fully mixed volume, and a lower degree of upset attenuation even at impeller speeds above the criteria of complete motion used to size the chest. The onset of significant non-ideal behavior can be quite sudden. Under these circumstances, the degree of disturbance attenuation could be improved by reducing the pulp flow rate through the chest.
4. Pulp feed and exit locations have significant effect on channeling, dead volume, and disturbance attenuation. To prevent dewatering of stock before it enters the discharge pump, sufficient motion must be provided at the pulp exit location.

5. At suspension mass concentrations greater than 3%, the system is susceptible to a high percentage of channeling and dead volume, and a low degree of attenuation.
6. It was found that the degree of upset attenuation is a function of the impeller momentum flux, rather than the power input.
7. Dynamic tests made on scale-model chest show that the power calculated based on smooth surface motion and even the onset of complete motion inside the chest does not completely eliminate dead volume and channeling. Additional power is required to have a desired dynamic response from the chest.

CHAPTER 8

8 RESULTS OF DYNAMIC TESTS MADE ON INDUSTRIAL STOCK CHESTS

8.1 Introduction

Dynamic tests made on industrial stock chests show that non-ideal flows such as channeling, recirculation, and stagnant zones exist in agitated pulp stock chests. Due to existence of these non-ideal flows, the dynamic response of industrial stock chests is not predictable and the upset attenuation in industrial chests is considerably worse than that of a fully mixed chest. In this chapter we evaluate the performance of some of the industrial stock chests based on dynamic tests made on these chests.

8.2 Performance of industrial blend chest #1

Figure 8.1 shows the configuration of blend chest #1 and Table 8.1 summarizes the operating conditions and design parameters for this chest. To study the performance of this chest, both the hardwood and softwood fibre mass concentrations were bumped together from 3.7% to 4.2% at t = 200s. Figure 8.2 shows the dynamic results. The upper curve is the input signal and the lower curve is the output response. At about t = 300s the output shows an initial bump which is due to hardwood short circuiting within the chest. From Figure 8.1 it can be seen that a portion of hardwood feed can be easily channeled from input location to the suction of the discharge pump. To eliminate or reduce the percentage of short circuiting, the stock chest piping into the blend chest should be redesigned to allow softwood and hardwood streams to enter together through a common pipe at the same location where the softwood presently

enters. Based on configuration shown in Figure 8.1 it appears to be little possibility for the softwood to short circuit. The response also shows a series of first order exponential responses, each one getting progressively smaller. From this it can be concluded that a portion of stock is recirculated within the chest. The theoretical time constant for this blend chest is 14 minutes. However, the real time constant calculated from the dynamic test shown in Figure 8.2 is 5.8 minutes. It can be concluded that only (5.8 / 14) × 100 = 41% of the chest volume is fully mixed and 59% of the chest volume is dead (stagnant and/or very slowly moving). The installed power for the blend chest is 40 hp, while the required power recommended by Yackel (1990) is 60 hp. From dynamic tests made on scale-model chest, we found that even the power calculated using Yackel's method does not completely eliminate dead volume and channeling. Therefore, the installed power for this blend chest is not sufficient to achieve a fully mixed system.

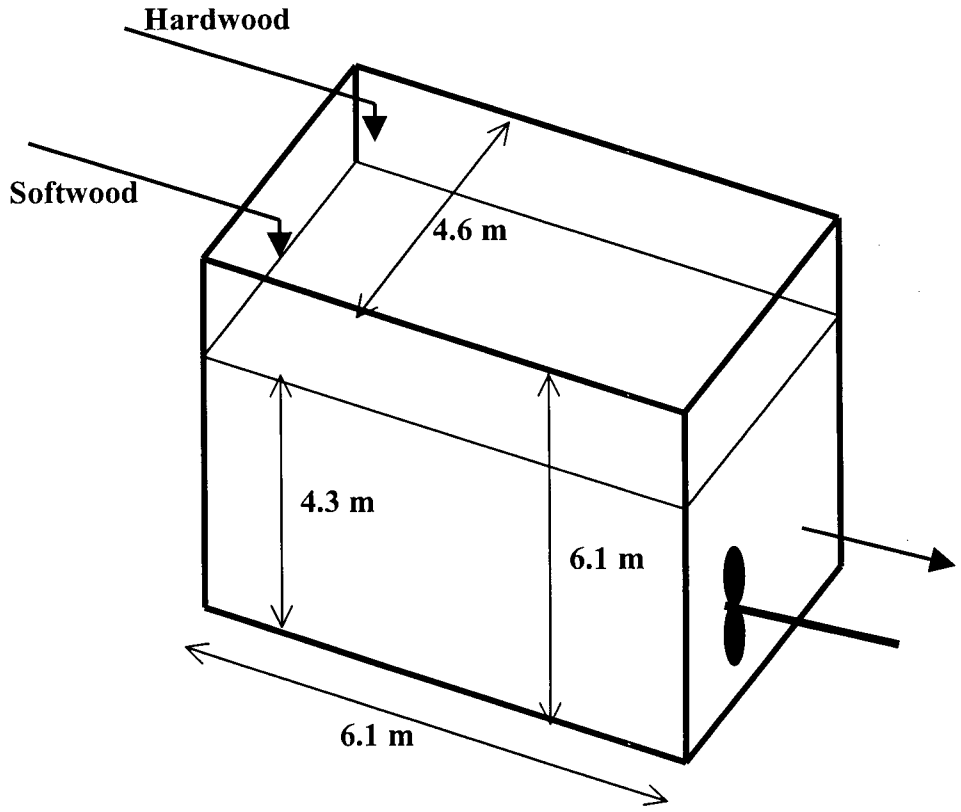

Figure 8.1: Configuration of the blend chest #1.

Table 8.1: Specifications of blend chest #1.

Chest length	6.1 m
Chest width	4.6 m
Chest height	6.1 m
Stock height	4.3 m
Hardwood flow rate	6056 L/min
Softwood flow rate	2460 L/min
Fibre mass concentration	3.7%
Theoretical time constant	14 min
Installed power	40 hp

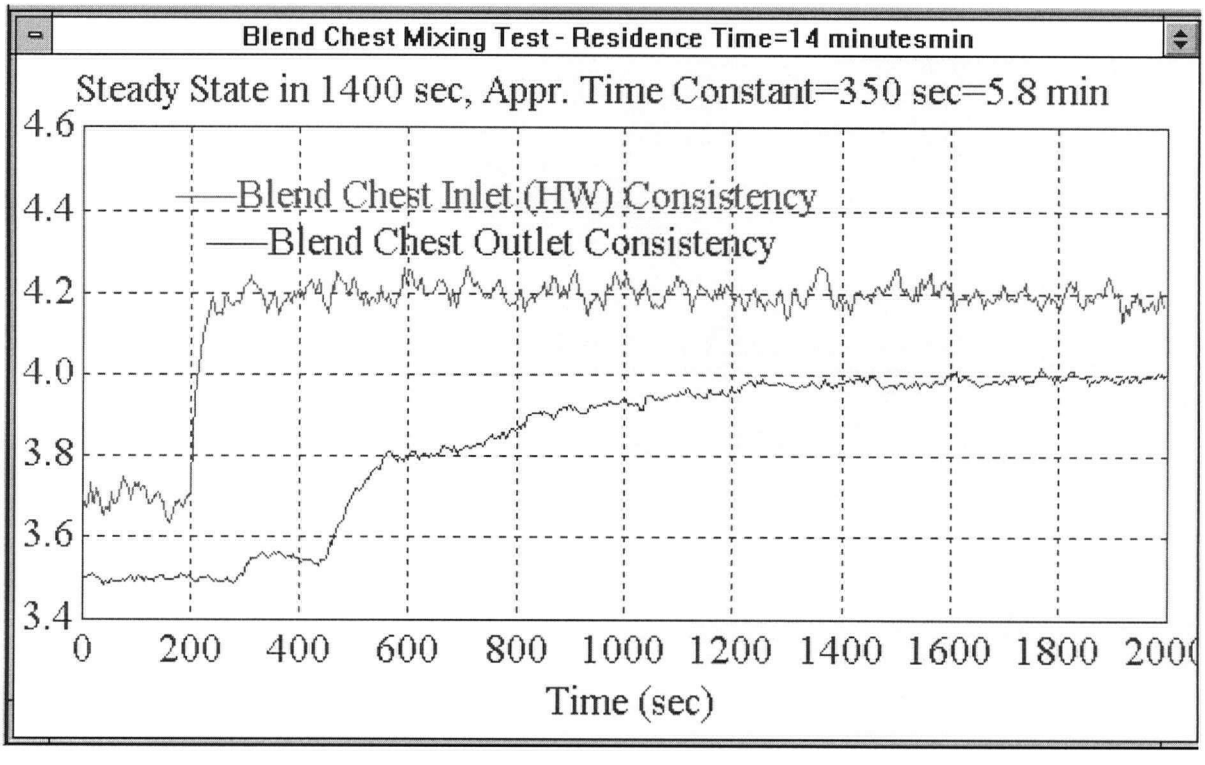

Figure 8.2: Step response of the industrial blend chest #1. The output signal has been shifted by –0.2 so as not to overlap with the input signal.

8.3 Performance of industrial machine chest #2

Figure 8.3 shows the configuration of machine chest #2 and Table 8.2 summarizes the operating conditions and design parameters for this chest. To evaluate the performance of the chest, a step change from 3.55% to 3.8% was applied in fibre mass concentration of pulp feed stream. The result is presented in Figure 8.4. There was no evidence of short-circuiting in the chest. For input-output location shown in Figure 8.3, it seems there is no chance for the pulp feed to short circuit. The theoretical time constant for this chest is 12.9 minutes. The measured response curve, shown in Figure 8.4, shows a fully mixed zone of approximately 7.5 minutes time constant. These numbers show that about (7.5 / 12.9) × 100 = 58% of the chest volume is

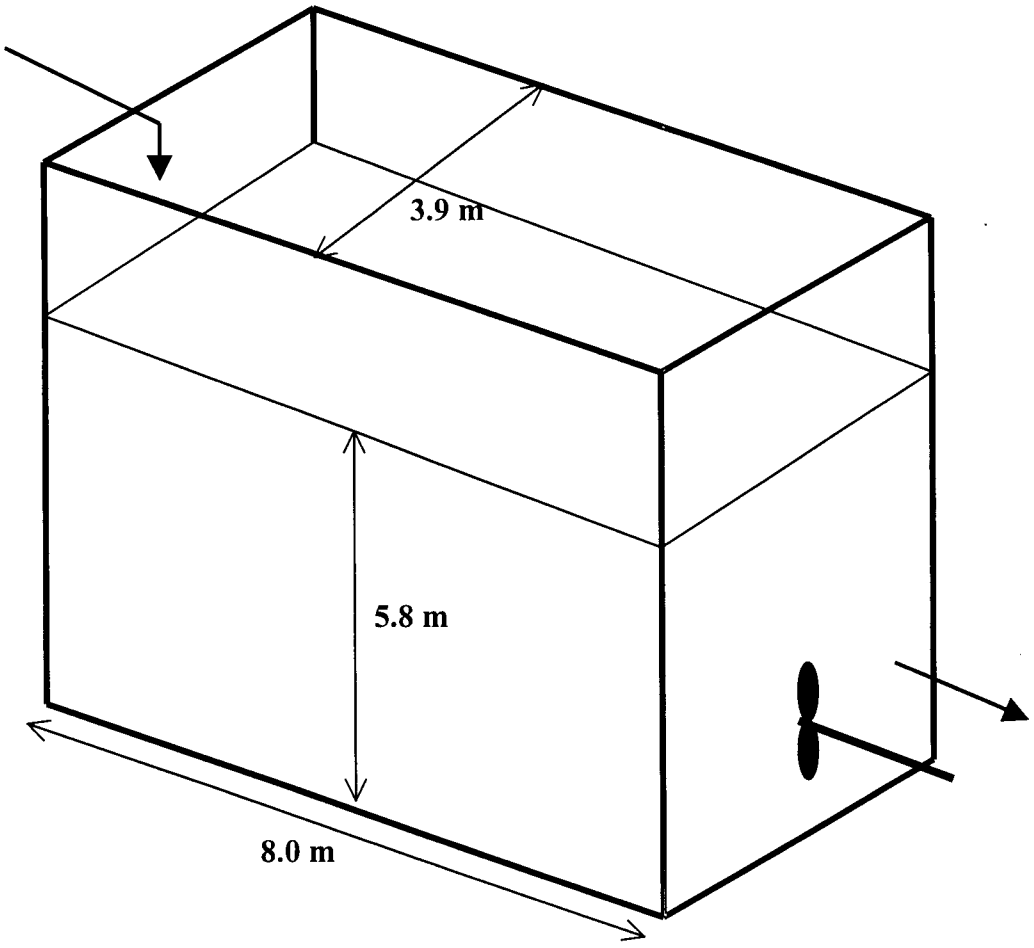

Figure 8.3: Configuration of the machine chest #2.

fully mixed and the percentage of dead volume is 42%. The installed power for this chest is 35 hp which is even less than that recommended by Yackel (50 hp). Therefore, the existence of stagnant and poor-mixing zones in this chest is inevitable. Figure 8.3 shows that this chest has not been properly designed. As it was mentioned in chapters two and four, a general rule of thumb is that the chest length to chest width ratio (L/W) should not exceed 1.5. If it is necessary to have a chest in which the L/W ratio exceeds 1.5 to 2.0, then two agitators will be required. But the L/W for this chest equipped with one impeller is 2.0. Also the suspension height to chest width ratio (Z/W) for this chest is 1.5 which is much greater than the optimum ratio of $Z/W = 1$.

Table 8.2: Specifications of machine chest #2

Chest length	8.0 m
Chest width	3.9 m
Stock height	5.8 m
Stock type	kraft pulp
Pulp flow rate	14000 L/min
Fibre mass concentration	3.4%
Theoretical time constant	12.9 min
Installed power	35 hp

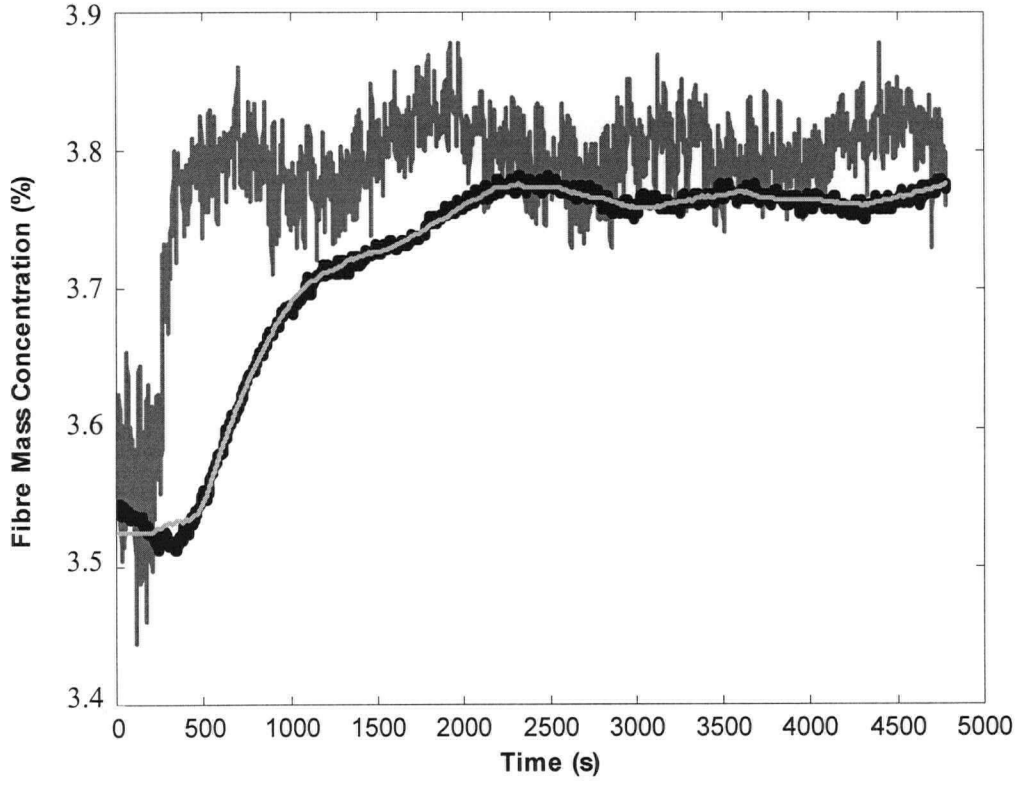

Figure 8.4: Step response of the industrial machine chest #2 (model output in gray line).

8.4 Performance of industrial chest #3

Figure 8.5 shows the configuration of industrial stock chest #3 and table 8.3 summarizes the operating conditions and design parameters for this chest. To study the performance of this chest, the fibre mass concentration of pulp feed was bumped from 4.3% to 3.3%. Figure 8.6 shows the measured input, measured output, and model output. It seems that for input-output location, shown in Figure 8.5, pulp feed is forced into the mixing zone before leaving the chest. Therefore, short-circuiting was not observed in output signal.

The theoretical time constant for this chest is 8.4 minutes. But based on bump test shown in Figure 8.6, the measured time constant is 5.7 minutes. Therefore, it can be concluded that (5.7 / 8.4) × 100 = 68% of the chest volume is fully mixed and 32% of the chest volume is dead. The installed power for this chest is 200hp, which is equal to the power recommended by Yackel. This confirms the dynamic result obtained from scale-model chest (see chapter 7) that the power calculated based on Yackel's method does not completely eliminate dead volume.

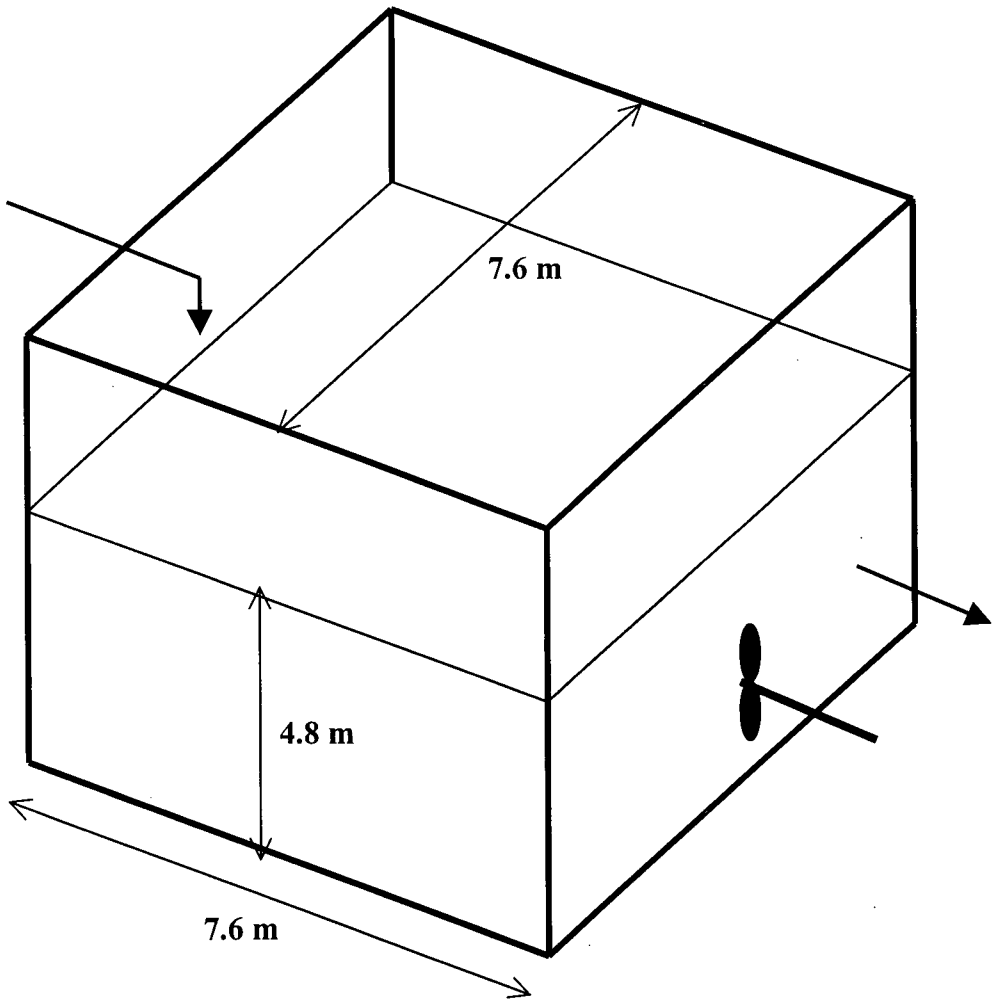

Figure 8.5: Configuration of the industrial chest #3.

Table 8.3: Specifications of industrial chest #3

Chest length	7.6 m
Chest width	7.6 m
Stock height	4.8 m
Pulp flow rate	32930 L/min
Stock type	kraft pulp
Fibre mass Concentration	4%
Theoretical time constant	8.4 min
Installed power	200 hp

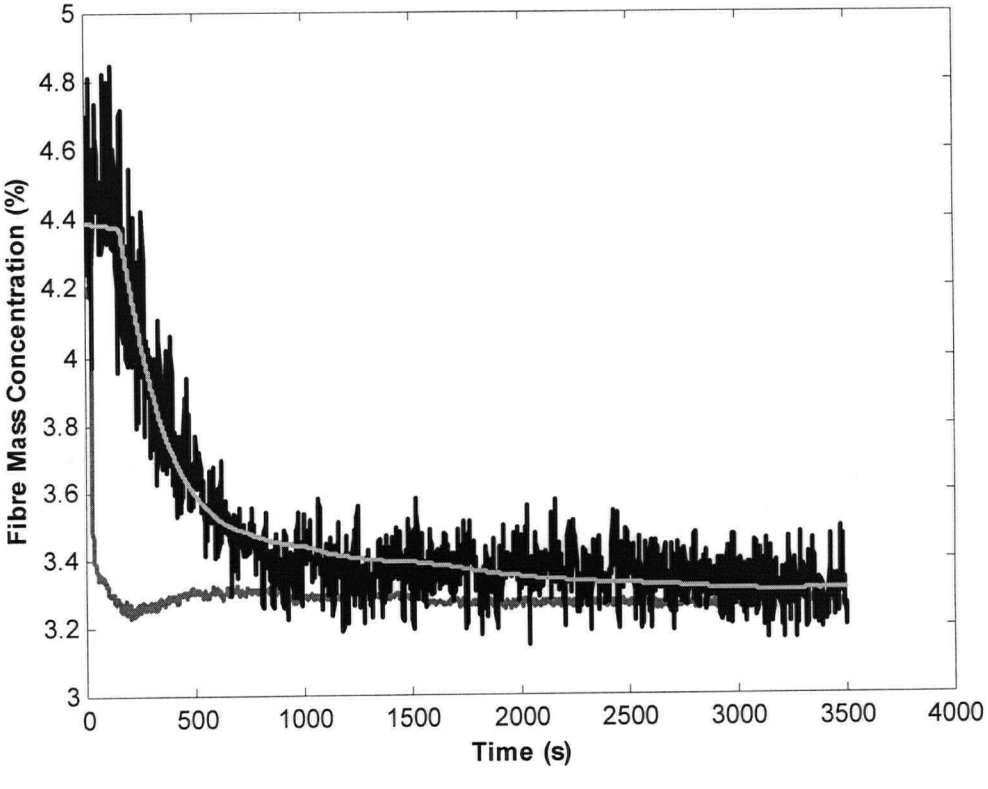

Figure 8.6: Step response of the industrial stock chest #3 (model output in gray line).

8.5 Performance of industrial blend chest #4

Figure 8.7 shows the configuration of blend chest #4 and Table 8.4 summarizes the operating conditions and design parameters for this chest. Since the chest length to chest width ratio for this chest is $L/W = 2$ and is greater than 1.5, the chest has been equipped with two impellers. As it was mentioned in Chapter two, the L/W ratio should not exceed 1.5. Also the suspension height to chest width ratio (Z/W) for this chest is 0.58 which is much lower than the optimum ratio of $Z/W = 1$. Therefore, this chest has a long and shallow shape, which limits the effectiveness of fluid momentum transfer.

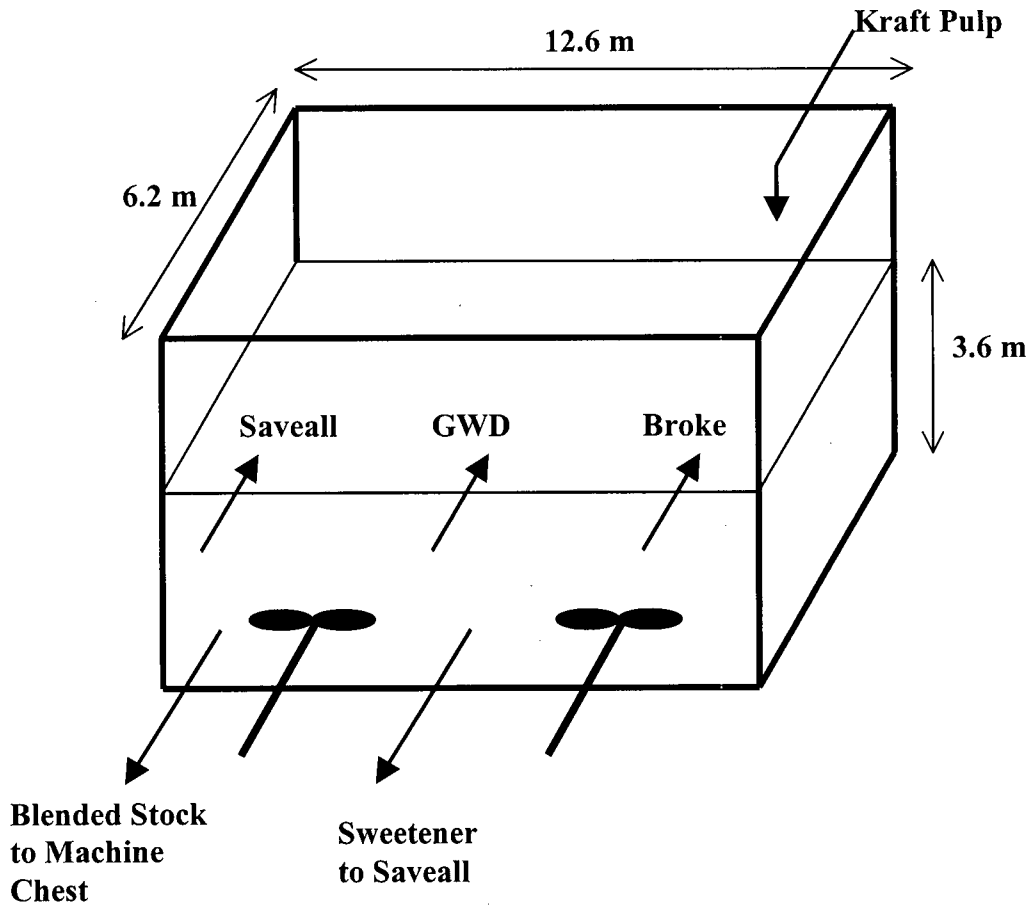

Figure 8.7: Configuration of the industrial blend chest #4.

From Figure 8.7 it can be seen that the feed streams have not been properly located. There is strong possibility of short-circuiting of ground wood stock (GWD) to the saveall sweetener pump suction and also strong possibility of short-circuiting of saveall stream to the suction of the blend chest stock pump. To eliminate or reduce the percentage of short-circuiting, and to increase the percentage of fully mixed volume, the stock chest piping into the blend chest should be redesigned to allow the kraft, GWD, broke and saveall streams to enter together through a common pipe at the same location where the kraft stream presently enters.

Table 8.4: Specifications of industrial blend chest #4.

Chest length	12.6 m
Chest width	6.2 m
Stock height	3.6 m
Fibre mass concentration	3.8%
Theoretical time constant	16 min
Total installed power (for both impellers)	300 hp

To evaluate the performance of this blend chest, a series of bump tests were carried out by bumping both kraft and GWD inlet fibre mass concentrations, sometimes together and sometimes individually (Figure 8.8). Bump #1 occurred at about minute 80. It consisted of simultaneous down bumps of 0.1% on both GWD and kraft. Bump #2 occurred at minute 112 as an up bump of about 0.15% in kraft stock only and a second bump of 0.09% was made at minute 125. Bump #3 occurred at minute 146 and consisted of a GWD up bump of about 0.1%. Bump #4 was initiated at minute 185 and consisted of simultaneous down bump on both GWD and kraft. At minute 90 and minute 137 two major upsets caused by upsets in saveall stream

occurred in output signal. This shows that saveall stock was not being entered to the mixing zone, but directly short-circuited to the suction of the blend chest stock pump.

The theoretical time constant for this blend chest is 16 minutes, but the real time constant calculated from the bump tests shown in Figure 8.8 is 10.1 minutes. This result indicates that only about (10.1 /16) × 100 = 63% of the chest volume is fully mixed and 37% is not effectively agitated. This is despite the fact that the total installed power for this chest is 300 hp, which is 2.5 times greater than that recommended by Yackel (120 hp). Again this confirms the dynamic results obtained from scale-model chest that the power calculated using Yackel's method does not eliminate the non-ideal flows. Additional power is required to have a desired dynamic response from the chest.

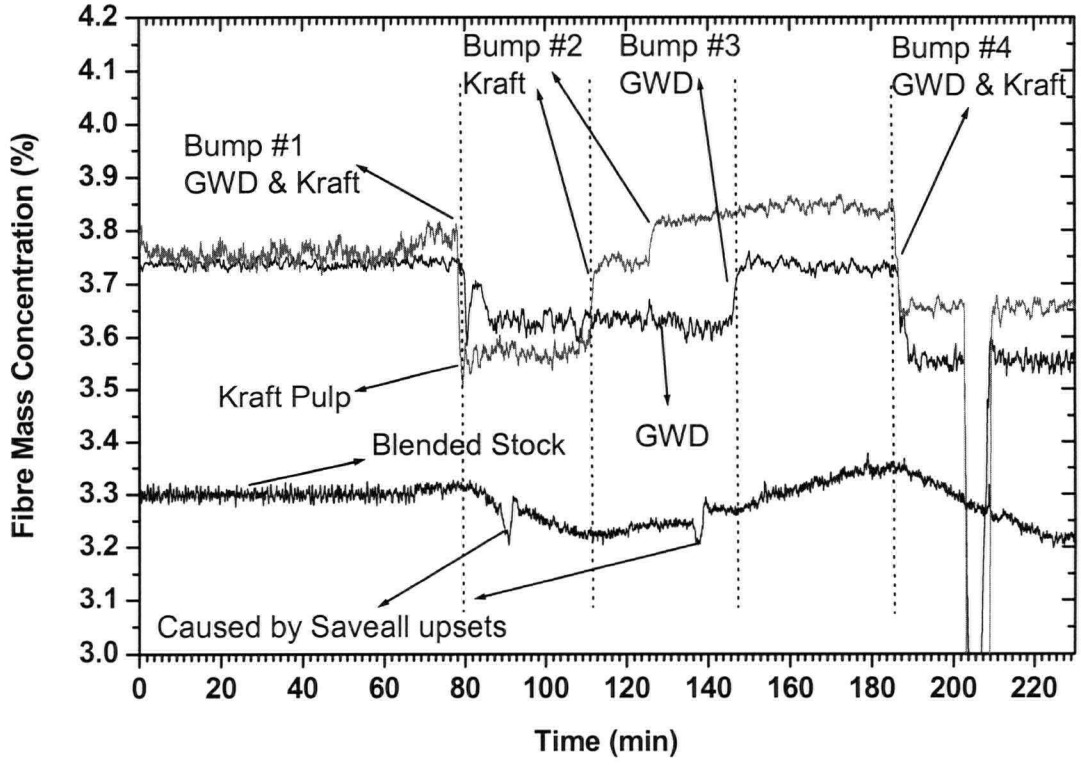

Figure 8.8: Step response of the industrial blend chest #4.

8.6 Performance of industrial machine chest #5

Figure 8.9 shows the configuration of industrial machine chest #5 and Table 8.5 summarizes the operating conditions and design parameters for this chest. The chest length to chest width ratio is $L/W = 1.5$. Therefore, two impellers have been considered for this chest. Since the L/W ratio for this chest is less than that for the blend chest #4 ($L/W = 2$), the chest #5 may produce a process result, which is better than that achieved by the chest #4. Figure 8.9 shows that the feed and exit streams have been properly located and it appears to be little possibility for the pulp feed to short circuit.

The performance of machine chest #5 was tested by bumping the fibre mass

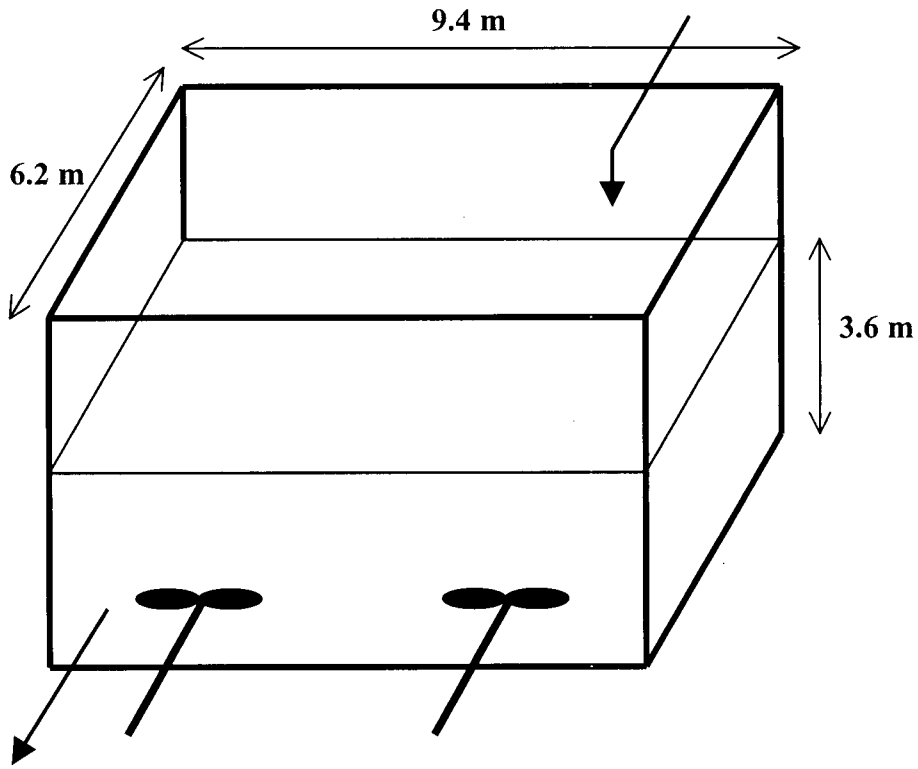

Figure 8.9: Configuration of the industrial machine chest #5.

concentration of pulp feed from 3.3% to 3.4% (Figure 8.10). There was no evidence of short-circuiting in the chest. The theoretical time constant for this chest is 12.5 minutes. However, the real time constant measured from the dynamic test shown in Figure 8.10 is 10.9 minutes. It can be concluded that about (10.9 / 12.5) × 100 = 87% of the chest volume is fully mixed and the percentage of dead volume is only 13% of the chest volume. This mixing result has been achieved by 300 hp (for both impellers) which is three times greater than that calculated using Yackel's method (100 hp for both impellers). Again this result confirms the dynamic results obtained from scale-model chest that the existing design criterion underpredicts the power requirement needs for a fully mixed stock chest.

Table 8.5: Specifications of industrial machine chest #5.

Chest length	9.4 m
Chest width	6.2 m
Stock height	3.6 m
Stock type	bleached – refined kraft pulp
Fibre mass concentration	3.8%
Theoretical time constant	12.5 min
Total installed power (for both impellers)	300 hp

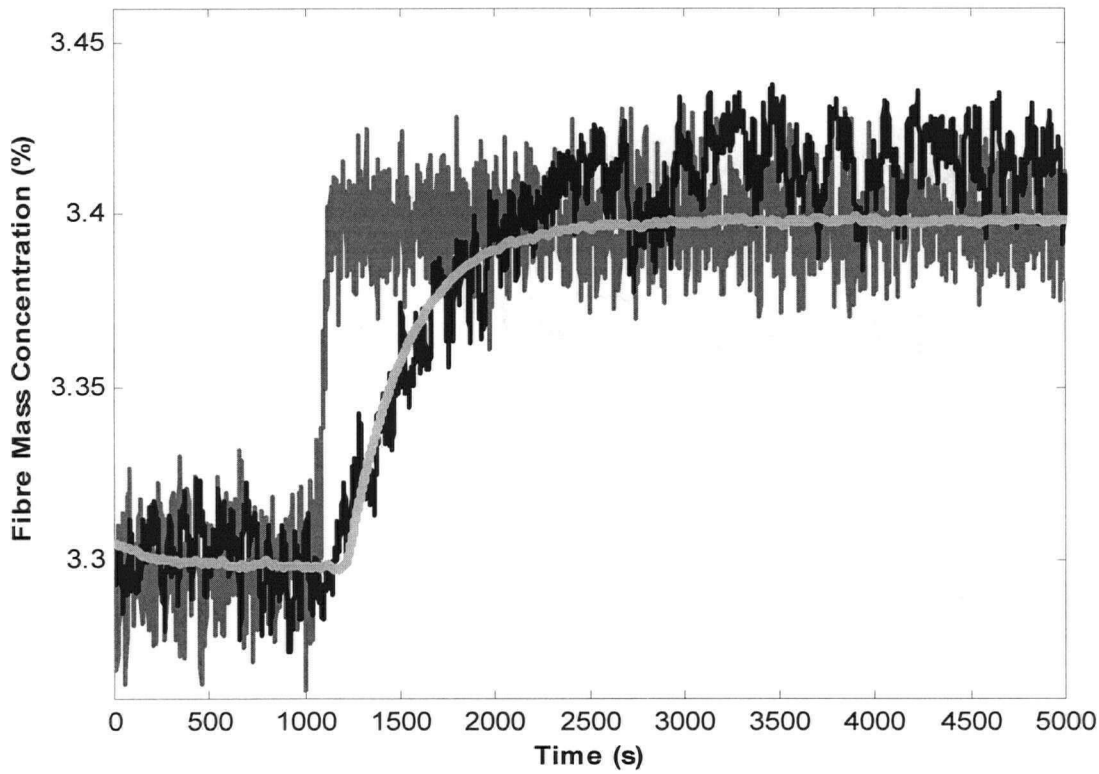

Figure 8.10: Step response of the industrial machine chest #5 (model output is in gray line).

8.7 Performance of latency removal chest #6

Figure 8.11 shows the configuration of industrial latency removal chest #6 equipped with four impellers and midfeather wall at the centre of the chest and Table 8.6 summarizes the operating conditions and design parameters for this chest. To evaluate the mixing performance, the fibre mass concentration of pulp feed was dropped from 4.26% to 4.09%. Figure 8.12 shows the measured input, measured output, and model output. There was no evidence of short-circuiting in the chest. For chest configuration shown in Figure 8.11, it seems the pulp feed is forced to

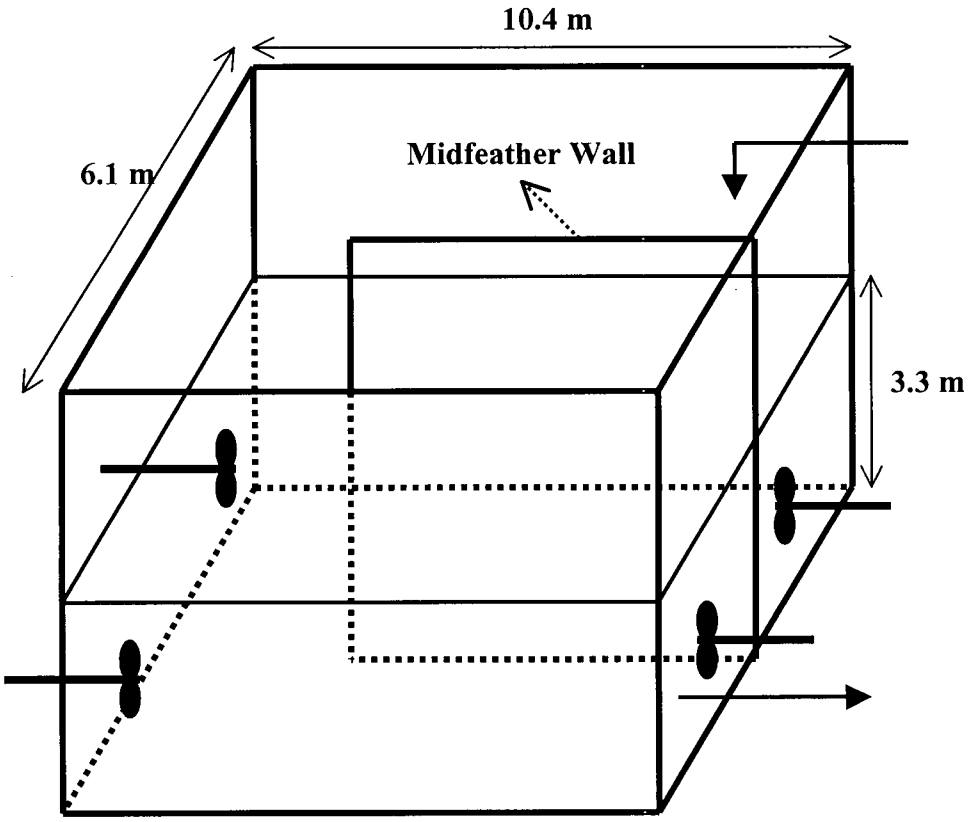

Figure 8.11: Configuration of the industrial latency removal chest #6.

pass through the four mixing zones generated by four impellers before leaving the chest because of midfeather wall.

Based on the chest dimensions and operating conditions on the day of the test, the theoretical time constant is 37 minutes. However, the measured response curve shows a fully mixed zone of approximately 10 minutes time constant. It can be concluded that only (10 /37) × 100 = 27% of the chest volume is involved in active mixing.

While the piping approach to the stock chest added only 0.5% to the system volume and was ignored in the calculations, the measured response curve shows a delay of 13.5 minutes (plug flow). The plug flow regions likely occur between the mixed zones of the impellers and

midfeather wall helps the formation of plug flow inside the chest. We estimate that 37% of the chest volume is dead (very slowly moving / little or no mixing), 36% is involved in plug flow, leaving only 27% involved in active mixing. Therefore, for latency removal the pulp would spent 23.5 minutes at temperature 80 ^{0}C, but only 10 minutes of this would it be when subjected to mechanical action (shear) by the impellers. The total installed power (for four impellers) is 120 hp, which is even less than that recommended by Yackel (160 hp). Hence, the existence of stagnant and poor-mixing zones and plug flow regions in this chest is inevitable.

Table 8.6: Specifications of industrial latency removal chest #6.

Chest length	10.4 m
Chest width	6.1 m
Stock height	3.28 m
Stock type	unbleached thermomechanical pulp(TMP)
Fibre mass concentration	4.5%
Temperature	80 ^{0}C
Theoretical time constant	37 min
Total installed power (for four impellers)	120 hp

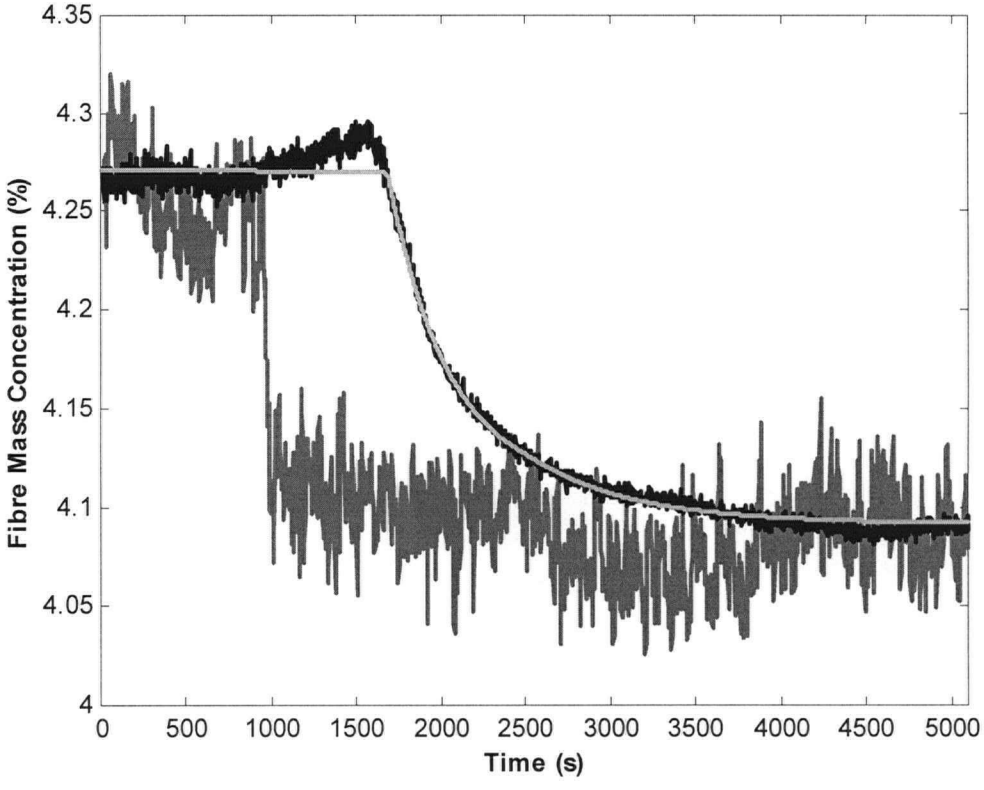

Figure 8.12: Step response of the industrial latency removal chest #6 (model output is in gray line).

8.8 Summary

Table 8.7 summarizes the results of dynamic tests made for six industrial stock chests. In three cases (#1, #2, #6) the installed power is less than that recommended by Yackel (1990) and the fully mixed volumes are less than 60% of total chest volume. However, for all chests, the fully mixed volume is less than the theoretical value (100%), despite installations where the power input is three times greater than that calculated using Yackel's method. This confirms the dynamic results obtained from scale-model chest (see chapter 7). Therefore, chests designed using the criterion of complete surface motion, or even the onset of complete chest motion, do

not necessarily lead to a 100% fully mixed volume. If the purpose of using a stock chest is to keep the suspension moving to prevent dewatering of stock throughout the chest (as a storage tank), smooth surface motion can still lead to dead zones within the chest. To eliminate these dead zones, the installed power must be at least equal to the power required for the onset of "complete motion". If the purpose of the stock chest is to attenuate high frequency variations in fibre mass concentration (as a low-pass filter), the required installed power can be considerably greater than that recommended by Yackel or required for "complete motion".

Table 8.7: Industrial results.

Chest No.	$L \times W \times Z$ (m×m×m)	Installed power (hp)	Calculated power using Yackel's method (hp)	Sampling time (s)	f (%)	Theoretical time constant (min)	Real time constant (min)	Mixed volume (%)
1	6.1×4.6×4.3	40	60	1	10	14	5.8	41
2	8.0×3.9×5.8	35	50	1	0	12.9	7.5	58
3	7.6×7.6×4.8	200	200	1	0	8.4	5.7	68
4	12.6×6.2×3.6	300	120	1	0	16	10.1	63
5	9.4×6.2×3.6	300	100	10	0	12.5	10.9	87
6	10.4×6.1×3.3	120	160	4	0	37	10	27

CHAPTER 9

9 OVERALL CONCLUSIONS AND RECOMMENDATIONS FOR FUTURE WORK

9.1 Overall conclusions

Dynamic tests made on industrial and scale-model chests show that non-ideal flow such as channeling, recirculation, and stagnant zones exist in agitated pulp stock chests. These non-ideal flows reduce the degree of upset attenuation from the chest, especially at frequencies higher than the cut-off frequencies of paper machine control loops. Therefore, disturbances at these frequencies would not be attenuated and would affect paper quality and machine run-ability. A dynamic model of agitated pulp stock chests, incorporating these non-ideal flows was developed.

Fully bleached kraft pulp (FBK) was used for preparation of the pulp suspensions. Batch results showed that required power for complete motion varying as the square of fibre mass concentration over the range of 1.1 – 4.7%. The optimum *Z/W*, *L/W*, and *D/W* ratios for the scale-model chest are in the range suggested in literature. However, existing design criteria underpredict the power and momentum flux requirements need for agitation at the laboratory scale. The experimental data obtained with the scale-model chest showed that the power number is not only a function of *ND/m* but also of the fibre mass concentration. Therefore, the rheology of a pulp suspension can not be solely described by the $m = (\tau_y/\rho)^{1/2}$ and Bingham fluid did not fully described the rheology of the pulp suspension. Dynamic response of liquid and solid phase tracers showed that at fibre mass concentrations >2%, the mixing responses of solid and liquid phases are very similar. Hence, a liquid phase tracer can be used to study the

dynamic response of stock chests. The batch mixing time was found to be given by an empirical equation: $\theta_m = A(Mo)^n$, where A and n are functions of the suspension mass concentration and Mo is the impeller momentum flux.

Our visual observation with the aid of a digital video camera showed that even when the whole suspension is in motion, poor mixing regions still exist at the bottom of the chest along the impeller opposite wall and on the surface of the chest along the impeller wall and impeller opposite wall where pulp flows significantly slower than in the bulk motion zone. In these regions pulp remains for a longer time, which decreases the percentage of fully mixed volume within the chest.

To estimate dynamic model parameters, the system was excited by a frequency-modulated random binary input signal. A new identification method was developed for estimation of dynamic model parameters from input-output data. The excitation energy was chosen at frequencies where the magnitude of the Bode plot is sensitive to parameter variations. In this study the effect of impeller speed and diameter, fibre mass concentration, pulp flow rate through the chest, and pulp feed and exit location on channeling, fully mixed volume, and disturbance attenuation was investigated.

Since at higher impeller speed the fibre/fibre network is disrupted further from the impeller, channeling and dead volume are progressively decreased as impeller speed is increased. But higher impeller speed can cause air to be entrained in the suspension. At higher pulp flow rates through the chest and fibre mass concentration greater than 3%, the system is susceptible to a high percentage of channeling and dead volume, and a low degree of disturbance attenuation even at impeller speeds greater than that required for complete motion. While the dynamic response can be improved by reducing pulp flow rate through the chest, this effectively reduces the operating capacity of the system. It was found that the pulp feed and

exit locations have significant effect on channeling, dead zone, and disturbance attenuation. To prevent dewatering of stock before it enters the discharge pump, sufficient motion must be provided at the pulp exit location.

It was found that a large, low speed impeller can produce equivalent dynamic response with less power than is required with a smaller, higher speed impeller. It means that the degree of upset attenuation is a function of the impeller momentum flux, rather than the power input. Dynamic tests made on scale-model and industrial chests showed that chests designed using the criterion of complete surface motion, or even the onset of complete chest motion, do not necessarily lead to a 100% fully mixed volume. If the purpose of using a stock chest is to keep the suspension moving to prevent dewatering of stock throughout the chest (as a storage tank), smooth surface motion can still lead to dead zones within the chest. To eliminate these dead zones, the installed power must be at least equal to the power required for the onset of "complete motion". If the purpose of the stock chest is to attenuate high frequency variations in fibre mass concentration (as a low-pass filter), the required installed power can be considerably greater than that recommended by Yackel or required for "complete motion".

This study reports various important features of macroscale mixing and dynamic behavior of agitated pulp chests, that hopefully will contribute to the better understanding of the principles and operation of the agitated pulp chest as a low pass filter. Applying the finding of this study will reduce the effects of non-ideal flow, improve fibre mass concentration control in stock chests, and increase paper quality and machine run-ability.

9.2 Recommendations for future work

The findings of this study highlighted the areas for future consideration as follows:

- To investigate the effect of chest shape on dynamic behavior of the system, the tests made on rectangular chest in this study should be repeated for a cylindrical chest.
- Higher impeller speeds lead to improved mixing by eliminating non-ideal flows such as channeling and dead zones. But at higher impeller speed more air is entrained in the suspension. Therefore, the effect of impeller speed on the entrained air in the suspension should be studied.
- Further work should be made to examine the effect of stock type, impeller type, impeller location, fillets, and midfeather wall on the disturbance attenuation in agitated pulp stock chests.
- The performance of a chest equipped with two impellers should be compared to the performance of two chests in series.

NOMENCLATURE

A	fibre aspect ratio, dimensionless
c	clearance of impeller off vessel bottom, m
C	impeller C factor, dimensionless
C_m	fibre mass concentration, %
d_1, d_2	dynamic model parameters in discrete-time domain
D	impeller diameter, m
D_T	housing diameter, m
e	residuals associated with the validation data and the model
e_t	white noise signal
e_t^f	filtered white noise
f	percentage of channeling, fraction
g	gravitational acceleration, m/s^2
G_1	transfer function for channeling zone
G_2	transfer function for mixing zone
$\hat{G}(q)$	Discrete-time transfer function of the system
J_N	cost function
l	blade length, m
L	chest length, m
L_l	fibre length weighted average length, m
L_w	fibre weighted average length, m
LMo	level momentum, m^2/s^2
m	suspension property (Eqn. 2.12), m/s

M	torque, N.m
Mo	impeller momentum number, m^4/s^2
n	number of blades
N	impeller rotational speed, s^{-1}
N_{Fr}	Froude number, dimensionless
N_P	power number, dimensionless
$N_{P,turb}$	power number for fully turbulent flow (dimensionless)
N_Q	impeller flow number, dimensionless
N_{Re}	Reynolds number, dimensionless
p	pitch of blades, m
P	power, W
q^{-1}	backward shift operator
Q	pulp flow rate through the chest, m^3/s
$Q_{impeller}$	impeller pumping rate, m^3/s
R	percentage of recirculation, fraction
t	time, s
t_s	sampling time, s
T	tank diameter, m
T_1	time delay for the channeling zone, s
T_2	time delay for the mixing zone, s
T_c	period at cut-off frequency, s
u	input signal
u_t^b	frequency-modulated random binary input signal
v	fluid velocity leaving the impeller, m/s

v_{bulk}	bulk velocity, m/s
V	suspension volume inside the chest, m^3
$V_{fully\ mixed}$	fully mixed volume, m^3
w	blade width, m
W	chest width, m
X_g	gas content of the suspension, fraction
y	output signal
Z	suspension height, m

Greek letters

γ	shear rate, s^{-1}
γ_{avg}	average shear rate in the mixing vessel, s^{-1}
ε_{avg}	power consumption per unit mass, W/kg
ε_f	power dissipation at point of fluidization, W/m^3
η_p	plastic viscosity, $N.s/m^2$
θ_m	mixing time, s
λ	closed loop time constant, s
μ	fluid viscosity, $N.s/m^2$
μ_a	apparent viscosity, $N.s/m^2$
ρ	fluid density, kg/m^3
$\rho_1, \rho_2, \ldots, \rho_9$	dynamic model parameters in discrete-time domain
τ	shear stress, N/m^2
τ_1	time constant for the channeling zone, s

τ_2	time constant for the mixing zone, s
τ_y	yield stress, N/m^2
ω	frequency, rad/s
ω_{a1}	frequency at which the magnitude Bode plot of the partial derivative of the dynamic model with respect to a_1 is maximum, rad/s
ω_{a2}	frequency at which the magnitude Bode plot of the partial derivative of the dynamic model with respect to a_2 is maximum, rad/s
ω_f	frequency at which the magnitude Bode plot of the partial derivative of the dynamic model with respect to f is maximum, rad/s
ω_R	frequency at which the magnitude Bode plot of the partial derivative of the dynamic model with respect to R is maximum, rad/s

Abbreviations

ARMAX	autoregressive moving average with external input
ARX	autoregressive with external input
BJ	Box-Jenkins model structure
CFD	computational fluid dynamics
FBK	fully bleached kraft
OE	output error model structure
RTD	residence time distribution
TMP	thermomechanical pulp
ZOH	zero order hold

BIBLIOGRAPHY

Attwood, D. and J.D. Gibbon, "The Agitation of Paper stock", Paper Technology, 4(1):54-62 (1963).

Bakker, A. and B. Fasano, "A Computational Study of the Flow Pattern in an Industrial Paper Pulp Stock Chest With a Side-Entering Impeller", AIChE Symposium Series, 89(293):118-124 (1993).

Bennington, C.P.J., "Mixing Pulp Suspensions", PhD Thesis, University of British Columbia (1988).

Bennington, C.P.J., "Mixers and Mixing" in "Pulp Bleaching: Principles and Practice", C.W. Dence and R.W. Reeve (eds), TAPPI Press, Atlanta, GA (1996).

Bennington, C.P.J., G. Azevedo, D.A. John, S.M. Birt and B.H. Wolgast, "The Yield Stress of Medium and High Consistency Mechanical Pulp Suspensions at High Gas Contents", J. Pulp and Paper Sci., 21(4):J111-J118 (1995).

Bennington, C.P.J., R.J. Kerekes and J.R. Grace, "The Yield Stress of Fibre Suspensions", The Canadian Journal of Chemical Engineering, 68:748-757 (1990).

Bennington, C.P.J., R.J. Kerekes and J.R. Grace, "Motion of Pulp Fibre Suspensions in Rotary Devices", The Canadian Journal of Chemical Engineering, 69:251-258 (1991).

Bennington, C.P.J. and R.J. Kerekes, "Power Requirements for Pulp Suspension Fluidization", TAPPI Journal, 79(2):253-258 (1996).

Bialkowski, W.L., "Process Control Related Variability and the Link to End-Use Performance", Control Systems Conference, Helsinki, Finland, 220-248 (1990).

Bialkowski, W.L., "Newsprint Variability and Its Impact on Competitive Position", Pulp and Paper Canada, 93(11):T299-T306 (1992).

Blasinski, H. and E. Rzyski, "Mixing of Non-Newtonian Liquids. Power Consumption for Fibrous Suspensions", Inz. Chem., 2(1):169-182 (1972).

Brodkey, R.S., "Turbulance in Mixing Operations: Theory and Application to Mixing and Reaction", Academic Press, New York (1975).

Brown, J.R., "The Dynamic Behavior of Paper Mill Stock Chests", Southern Pulp and Paper Manufacturer, 31(6):103-112 (1968).

Bubbico, R., D. Cave and B. Mazzarotta, "Influence of Solid Concentration and Type of Impeller on the Agitation of Large PVC Particles in Water", Recents Progres en Genie des Procedes, 11(52):81-88 (1997).

Calderbank, P.H. and M.B. Moo-Young, "The Prediction of Power Consumption in The Agitation of Non-Newtonian Fluids", Trans. Instn. Chem. Engrs., 37:26-33 (1959).

Dickey, D.S., "AIChE Equipment Testing Procedures: Mixing Equipment (Impeller Type)", AIChE, New York, 3rd edition (2001).

Edgar, T.F., D.M. Himmelblau and L.S. Lasdon, "Optimization of Chemical Processes", McGraw-Hill, New York, 2nd edition (2001).

Ein-Mozaffari, F., G.A. Dumont and C.P.J. Bennington, "Performance and Design of Agitated Pulp Stock Chests", PACWEST Conference, Whistler, B.C., Paper No. 3B6, 1-8 (2001).

Ein-Mozaffari, F., L.C. Kammer, G.A. Dumont and C.P.J. Bennington, "Dynamic Modeling of Agitated Pulp Stock Chests", Control Systems Conference, Stockholm, Sweden, 194-199 (2002).

Ein-Mozaffari, F., L.C. Kammer, G.A. Dumont and C.P.J. Bennington, "Design Criteria for Dynamic Behavior of Agitated Pulp Stock Chests", PACWEST Conference, Jasper, AB, Paper No. 2B2, 1-9 (2002).

Fletcher, R., "Practical Methods of Optimization", John Wiley and Sons, Chichester, U.K., 2nd edition (1987).

Fox, E.A. and V.E. Gex, "Single-phase Blending of Liquids", AIChE Journal, 2(4):539-544 (1956).

Gibbon, J.D. and D. Attwood, "Prediction of Power Requirements in The Agitation of Fibre Suspensions", Trans. Inst. Chem. Engrs., 40:75-82 (1962).

Gullichsen, J., E. Harkonen, "Medium Consistency Technology", TAPPI Journal, 64(6):69-72 (1981).

Harnby, N., M.F. Edwards and A.W. Nienow, "Mixing in the Process Industries", Butterworths, London (1985).

Head, V.P. and R.E. Durst, "Stock slurry Hydraulics", TAPPI Journal, 40(12):931-936 (1957).

Herrald, L., "An Introduction to Process Variability and Control in Paper Machine Stock Preparation", In TAPPI Stock Preparation Short Course Proceedings, Atlanta, GA, 267-294 (1998).

Holland, F.A., F.S. Chapman, "Liquid Mixing and Processing in Stirred Tanks", Chapman and Hall Ltd., London (1966).

Johansson, R., "Identification of Continuous-Time Models", IEEE Transactions on Signal Processing, 42(4):887-897 (1994).

Johansson, R., M. Verhaegen and C.T. Chou, "Stochastic Theory of Continuous-Time State-space Identification", IEEE Transactions on Signal Processing, 47(1):41-51 (1999).

Kammer, L.C., F. Ein-Mozaffari, G.A. Dumont and C.P.J. Bennington, "Identification of Channeling and Recirculation Parameters of Agitated Pulp Stock Chests", AIChE Conference, Reno, Nevada, Paper No. 328g, 1-12 (2001).

Kerekes, R.J., "Pulp Flocculation in Decaying Turbulence: A Literature Review" J. Pulp and Paper Sci., 19(3):TR86-TR91 (1983).

Levenspiel, O., "Chemical Reaction Engineering", John Wiley and Sons, 3rd edition (1998).

Ljung, L., "System Identification Toolbox, User's Guide", The Math. Works Inc. (1992).

Ljung, L., "System Identification: Theory for the user", 3rd edition, PTR Prentice Hall, USA (1999).

Ljung, L. and T. Glad, "Modeling of Dynamic Systems", Prentice Hall, Englewood Cliffs, NJ (1994).

McDonough, R.J., "Mixing for the Process Industries", Van Nostrand Reinhold, New York (1992).

Metzner, A.B. and R.E. Otto, "Agitation of Non-Newtonian Fluids", AIChE Journal, 3(1):3-10 (1957).

Mmbaga, J.P. and C.P.J. Bennington, "Energy Dissipation Rates in Medium Intensity Mixing of Solid-Liquid and Gas-Solid-Liquid Systems", AIChE Conference, Los Angeles, Paper No. 114f (1997).

Nagata, S., "Mixing, Principles and applications", John Wiley, Toronto (1975).

Nauman, E.B., B.A. Buffman, "Mixing in Continuous Flow Systems", John Wiley, Toronto (1983).

Nienow, A.W., "On Impeller Circulation and Mixing Effectiveness in The Turbulent Flow Regime", Chem. Eng. Sci., 52(15):2557-2565 (1997).

Ogunnaike, B.A. and W.H. Ray, "Process Dynamics, Modeling, and Control", Oxford University Press, New York (1994).

Oldshue, J.Y., "Agitation in Groundwood Blending", Pulp and Paper Magazine of Canada, 72(12):T375-T380 (1971).

Oldshue, J.Y., "Fluid Mixing Technology", McGraw-Hill, New York (1983).

Oldshue, J.Y. and T.C. Devries, "Fluid Mixing Principles in Paper Pulp Slurries", TAPPI Medium Consistency Mixing Seminar, Hollywood, FL, 1-8 (1985).

Oldshue, J.Y., A.T. Gretton, "Performance and Design of Paper Stock Mixers", TAPPI Journal, 39(6):378-390 (1956).

Oldshue, J.Y., A.T. Gretton, "Side-Entering Propeller Mixers in Vertical Cylindrical Stock Chests", Pulp and Paper Magazine of Canada, 118-122 (1958).

Reed, C.S., "Agitation and Blending", TAPPI Stock Preparation Short Course, San Francisco, CA, 75-96 (1994).

Reed, C.S., "Selecting The Right Equipment for Agitation and Blending, Part 1", TAPPI Journal, 78(6):252-254 (1995).

Reed, C.S., "Selecting The Right Equipment for Agitation and Blending, Part 2", TAPPI Journal, 78(7):241-244 (1995).

Reed, C.S., "Selecting The Right Equipment for Agitation and Blending, Part 3", TAPPI Journal, 78(8):248-250 (1995).

Reynolds, E., J.D. Gibbon and D. Attwood, "Smoothing Quality Variations in Storage Chests Holding Paper Stock", Trans. Instn. Chem. Engrs., 42:T13-T21 (1964).

Rushton, J.H., E.W. Costich and H.J. Everett, "Power Characteristics of Mixing Impellers", Chem. Eng. Progress, Part I: 46(8):395-404 (1950), Part II: 46(9):467-476 (1950).

Ruszkowski, S., "A Rational Method for Measuring Blending Performance and Comparison of Different Impeller Types", In Proc. 8th Europ. Mixing Conference, Inst. Chem. Engrs. Rugby, U.K., 283-291 (1994).

Seborg, D.E., T.F. Edgar and D.A. Mellichamp, "Process Dynamics and Control", John Wiley and Sons (1989).

Sell, N.J., "Process Control Fundementals For The Pulp and Paper Industry", TAPPI Press, Atlanta, GA (1995).

Silvester, R.S., "Mixing of Non-Newtonian Media: A Technical Review", BHRA Fluid Engineering, England (1985).

Soderstrom, T., H. Fan, B. Carlsson and S. Bigi, "Least Squares Parameter Estimation of Continuous-Time ARX Models from Discrete-Time Data", IEEE Transactions on Automatic Control, 42(5):659-673 (1997).

Soderstrom, T. and P. Stoica, "System Identification", Prentice Hall (1989).

Stephanopoulos, G., "Chemical Process Control: An Introduction to Theory and Practice", Prentice-Hall Inc., New Jersey (1984).

Sung, S.W. and I.B. Lee, "Prediction Error Identification Method for Continuous-Time Processes With Time-Delay", Industrial Engineering Chemical Research, 40:5743-5751 (2001).

Uhl, V.W. and J.B. Gray, "Mixing, Theory and Practice", Academic Press, New York (1966).

Ulbrecht, J.J., G.K. Patterson, "Mixing of Liquids by Mechanical Agitation", Gordon and Breach Science Publishers, New York (1985).

Wahren, D., "Fibre Network Structures in Paper Making Operations", Conference Paper Science and Technology, The Cutting Edge, Institute of Paper Chemistry, Appleton, WI, 112-132 (1980).

Walker, O.J. and A. Cholette, "Determination of the Optimum Size and Efficiency of Stock Chests. Part I: The Ideal Chest", Pulp and Paper Magazine of Canada, 59:113-117 (1958).

Wang, Q.G., X. Guo and Y. Zhang, "Direct Identification of Continuous Time Delay Systems from Step Responses", Journal of Process Control, 11:531-542 (2001).

Wesselingh, J.A., "Mixing of Liquids in Cylindrical Storage Tanks With Side-Entering Propellers", Chem. Eng. Sci., 30:973-981 (1975).

Whitfield, A.H. and N. Messali, "Integral-Equation Approach to System Identification", International Journal of Control, 45(4):1431-1445 (1987).

Wickstrom, T. and A. Rasmuson, "The Agitation of Pulp Suspension With a Jet Nozzle Agitator", Nordic Pulp and Paper Research Journal, 13(2):88-94 (1998).

Yackel, D.C., "Agitation: Theory, Mechanics and Application", in "Pulp and Paper Manufacture", Vol. 6: "Stock Preparation", R.W. Hagemeyer and D.W. Manson, TAPPI Press, Atlanta, GA (1983).

Yackel, D.C., "Pulp and Paper Agitation: The History, Mechanics and Process" TAPPI Press, Atlanta, GA (1990).

Yackel, D.C. and L.H. Mahony, "Agitation and Mixing in the Pulp and Paper Industry", TAPPI Engineering Conference, Houston, Texas, 207-216 (1976).

Zlokarnik, M., "Stirring, Theory and Practice", Wiley-VCH, Germany (2001).

APPENDIX A

A. COMPUTER PROGRAM

A computer program written in MATLAB to estimate the dynamic model parameters from input-output data based on numerical method described in chapter 5 is listed here:

```
% This program computes the dynamic model parameters in discrete-time
% domain and continuous-time domain from input-output signals measured
% during the identification experiment.

fign = 1;

% ts: sampling time
ts = 1;

% Loading input-output signals from file (i.e. mixdata10512.mat).
ndata =10512;
ndchar = int2str(ndata);
filename = ['mixdata' ndchar];
eval(['load ' filename]);
eval(['u = ' filename '(:,1);']);
eval(['y = ' filename '(:,2);']);
eval(['clear ' filename]);

% Removing the initial condition
u0 = u(1);
y = y-u0;
u = u-u0;

% Limits for dynamic model parameters (f, R, a1 and a2), as well as the
% initial condition (y0): rho [f R a1 a2 y0].
rmin = [0 0 0 0 -1];
rmax = [1-eps 1-eps 1-eps 1-eps 1];

% Initializing auxiliary variables
n = length(y);
t = ts*(0:n-1)';

figure(fign),fign=fign+1;
clf
subplot(2,1,1);

% Plot measured input and measured output.
plot(t, u+u0, t, y+u0);

findpar = 1;
if findpar
   clf
   hold on;
```

```
% Creating a 5 by 5 grid linearly spaced by a power of 2 and computing
% the cost function associated with each of the 25 points {d1,d2} in the
% grid.
r1 = max(1,2^(floor(log2(n/8)-1)));

d1o = 5+2*r1;
d2o = 5+2*r1;
VnM = zeros(5,5);
row = 1;
col = 1;
while r1~=0
   while ((row~=3) | (col~=3))
      for ld1=1:5
         for ld2=1:5
            if VnM(ld1,ld2)==0

               % Estimation of the model parameters in discrete-time
               % domain via least square method and the cost function
               % associated with it.
               VnM(ld1,ld2) = phi4(y,u,d1o+(ld1-3)*r1,d2o+(ld2-3)*r1);
               plot(d1o+(ld1-3)*r1, d2o+(ld2-3)*r1, '.');
               drawnow;
            end
         end
      end

      % Finding the minimum cost function for the 5 by 5 grid.
      [val,row] = min(VnM);
      [val,col] = min(val);
      row = row(col);

      plot(d1o+(row-3)*r1, d2o+(col-3)*r1, 'r.');
      drawnow;
      if row<3
         VnM = [0 0 0 0 0; VnM(1:4,:)];
         d1o = d1o-r1;
      elseif row>3
         VnM = [VnM(2:5,:); 0 0 0 0 0];
         d1o = d1o+r1;
      end
      if col<3
         VnM = [zeros(5,1) VnM(:,1:4)];
         d2o = d2o-r1;
      elseif col>3
         VnM = [VnM(:,2:5) zeros(5,1)];
         d2o = d2o+r1;
      end
   end
   disp(['[d1,d2]: ' num2str([d1o d2o])]);


   % Forming a new 5 by 5 grid with the half of the previous spacing (if
   % the grid spacing is larger than one) and computing the cost
   % functions for the new points.
   if r1>1
      r1 = r1/2;
      VnM = [VnM(2,2) 0 VnM(2,3) 0 VnM(2,4); zeros(1,5); ...
```

```
            VnM(3,2) 0 VnM(3,3) 0 VnM(3,4); zeros(1,5); ...
            VnM(4,2) 0 VnM(4,3) 0 VnM(4,4)];
        for ld1=1:5
           for ld2=1:5
              if VnM(ld1,ld2)==0

                 % Estimation of the model parameters in discrete-time
                 % domain via least square method and the cost function
                 % associated with it for the new 5 by 5 grid.
                 VnM(ld1,ld2) = phi4(y,u,d1o+(ld1-3)*r1,d2o+(ld2-3)*r1);
                 plot(d1o+(ld1-3)*r1,d2o+(ld2-3)*r1,'.');
                 drawnow;
              end
           end
        end

        % Finding the minimum cost function for the new 5 by 5 grid.
        [val,row] = min(VnM);
        [val,col] = min(val);
        row = row(col);

        plot(d1o+(row-3)*r1,d2o+(col-3)*r1,'ro');

            else
        r1 = 0;
     end
  end
  disp(['1st stage [d1,d2]: ' num2str([d1o d2o])]);
  plot(d1o,d2o,'gx','Linewidth',2);
  xlabel('d_1');
  ylabel('d_2');
  hold off;

  % Initial conditions
  d1 = d1o;
  d2 = d2o;
  a2 = 0.8;
  a1 = 0.8;
  f = 0.5;
  R = 0.5;
end

rho = [f R a1 a2 y(1)];
if ~all(isfinite(rho))
  f = 0.1;
  R = 0.5;
  a1 = 0.9;
  a2 = 0.9;
  rho = [f R a1 a2 y(1)];
end

% Estimation of the model parameters f, R, a1 and a2, as well as the initial
% condition y0 via a Sequential Quadratic Programming (SQP) for a given pair
% of d1 and d2.
options = optimset('GradObj','off','Hessian','off','LargeScale','off');
options = optimset(options,'Display','off');
```

```
[rho,Vn,exitflag] = fmincon('ctfun2', rho, [], [], ...
   [], [], rmin, rmax, [], options, ...
   d1, d2, y, u);
figure(fign), fign=fign+1;
clf;
subplot(2,1,1)
plfun2(rho,d1,d2,y,u,ts,u0);

[rho1,Vn1,exitflag1] = fmincon('ctfun2', rho, [], [], ...
   [], [], rmin, rmax, [], options, ...
   d2, d1, y, u);
subplot(2,1,2)
plfun2(rho1,d2,d1,y,u,ts,u0);
drawnow;
clf;

if Vn1<Vn | (exitflag==0 & exitflag1==1)
   aux = d1;
   d1 = d2;
   d2 = aux;
   rho = rho1;
end

% Creating a 3 by 3 grid of unitary spacing and performing a line search in
% the direction of the minimum cost function.
d10 = d1;
d20 = d2;
VnM = zeros(3,3);
rhoM = zeros(3,3,5);
row = 1;
col = 1;
while((row~=2) | (col~=2))
   for d1=d10-1:d10+1
      for d2=d20-1:d20+1
         if VnM(d1+2-d10,d2+2-d20)==0
            [rho,Vn,exitflag] = fmincon('ctfun2', rho, [], [], ...
               [], [], rmin, rmax, [], options, ...
               d1, d2, y, u);

            disp(['Initial parameters [f R a1 a2 y0]: ', num2str(rho)]);
            disp(['Cost function - Vn (flag): ', num2str(Vn) ' (' ...
                  int2str(exitflag) ')']);

            VnM(d1+2-d10,d2+2-d20) = Vn;
            rhoM(d1+2-d10,d2+2-d20,:) = rho;

            subplot(2,1,2);
            hold on
            plot(d1, d2, 'o', 'LineWidth', 1.5);
            hold off
            drawnow;
         end
      end
   end

   [val,row] = min(VnM);
   [val,col] = min(val);
```

```
row = row(col);

subplot(2,1,2);
hold on
plot(d10+row-2, d20+col-2, 'xr', 'LineWidth', 2);
hold off
drawnow;

if row==1
   VnM = [0 0 0; VnM(1:2,:)];
   rhoM = [zeros(1,3,5); rhoM(1:2,:,:)];
elseif row==3
   VnM = [VnM(2:3,:); 0 0 0];
   rhoM = [rhoM(2:3,:,:); zeros(1,3,5)];
end
dd10 = row-2;
d10 = d10+dd10;

if col==1
   VnM = [zeros(3,1) VnM(:,1:2)];
   rhoM = [zeros(3,1,5) rhoM(:,1:2,:)];
elseif col==3
   VnM = [VnM(:,2:3) zeros(3,1)];
   rhoM = [rhoM(:,2:3,:) zeros(3,1,5)];
end
dd20 = col-2;
d20 = d20+dd20;
disp(['Current delays [d1 d2]: ' num2str([d10 d20])]);

disp(['Initial parameters [f R a1 a2 y0]: ', num2str(rho)]);
disp(['Cost function - Vn (flag): ', num2str(Vn) ' (' ...
      int2str(exitflag) ')']);

subplot(2,1,1)
plfun2(rho,d10,d20,y,u,ts,u0);
drawnow;

if any([row col] ~= 2)
   [rho,VnM(2+dd10,2+dd20),exitflag] = ...
      fmincon('ctfun2', rho, [], [], ...
      [], [], rmin, rmax, [], options, ...
      d10+dd10, d20+dd20, y, u);
   rhoM(2+dd10,2+dd20,:) = rho;

   while VnM(2+dd10,2+dd20) < VnM(2,2)
      subplot(2,1,2);
      hold on
      plot(d10+dd10, d20+dd20, 'xr', 'LineWidth', 2);
      hold off
      drawnow;

      if dd10==-1
         VnM = [0 0 0; VnM(1:2,:)];
         rhoM = [zeros(1,3,5); rhoM(1:2,:,:)];
      elseif dd10==1
         VnM = [VnM(2:3,:); 0 0 0];
         rhoM = [rhoM(2:3,:,:); zeros(1,3,5)];
```

```
            end
            d10 = d10+dd10;

            if dd20==-1
               VnM = [zeros(3,1) VnM(:,1:2)];
               rhoM = [zeros(3,1,5) rhoM(:,1:2,:)];
            elseif dd20==1
               VnM = [VnM(:,2:3) zeros(3,1)];
               rhoM = [rhoM(:,2:3,:) zeros(3,1,5)];
            end
            d20 = d20+dd20;

            [rho,VnM(2+dd10,2+dd20),exitflag] = ...
               fmincon('ctfun2', rho, [], [], [], [], ...
               rmin, rmax, [], options, d10+dd10, d20+dd20, y, u);
            rhoM(2+dd10,2+dd20,:) = rho;
         end
         subplot(2,1,2);
         hold on
         plot(d10+dd10, d20+dd20, 'o', 'LineWidth', 1.5);
         hold off
         drawnow;
      end
   end
   subplot(2,1,2);
   xlabel('d_1');
   ylabel('d_2');

   [rho,Vn,exitflag] = fmincon('ctfun2', rho, [], [], ...
      [], [], rmin, rmax, [], options, ...
      d1, d2, y, u);
   [rho1,Vn1,exitflag1] = fmincon('ctfun2', rho, [], [], ...
      [], [], rmin, rmax, [], options, ...
      d2, d1, y, u);

   if Vn1<Vn | (exitflag==0 & exitflag1==1)
      disp('Warning: it is very likely that d1 and d2 should be swaped');
   end

   % Computing the dynamic model parameters (f, R, tau1, tau2, T1 and T2)in
   % continuous-time domain using the dynamic model parameters in discrete-time
   % domain.
   d1 = d10;
   T1 = ts*(d1-1);
   d2 = d20;
   T2 = ts*(d2-1);
   f = rhoM(2,2,1);
   R = rhoM(2,2,2);
   a1 = rhoM(2,2,3);
   tau1 = -ts/log(a1);
   a2 = rhoM(2,2,4);
   tau2 = -ts/log(a2);

   disp('Final parameters:');
   disp(['  f = ' num2str(f)]);
   disp(['  R = ' num2str(R)]);
   disp(['  T1 = ' num2str(T1) ' seconds']);
```

```
disp(['  tau1 = ' num2str(tau1) ' seconds']);
disp(['  T2 = ' num2str(T2) ' seconds']);
disp(['  tau2 = ' num2str(tau2) ' seconds']);
```

```
% This function computes model output and plots measured input, measured
% output, and model output.

function plfun2(rho,d1,d2,y,u,ts,u0)

f = rho(1);
R = rho(2);
a1 = rho(3);
a2 = rho(4);
y0 = rho(5);

num = zeros(1,d1+d2+1);
den = num;

num(1,[d1+1 d1+2 d2+1 d2+2 d1+d2+1]) = ...
   [f*(1-a1) -a2*f*(1-a1) (1-f)*(1-R)*(1-a2) ...
      -a1*(1-f)*(1-R)*(1-a2) -f*R*(1-a2)*(1-a1)];
den(1,[1 2 3 d2+1 d2+2]) = [1 -a1-a2 a1*a2 -R*(1-a2) a1*R*(1-a2)];
ic = filtic(num,den,y0*ones(d1+d2,1));
yh = filter(num,den,u,ic);

t = ts*(1:length(y));
plot(t, u+u0, t, y+u0);
hold on
plot(t, yh+u0, 'm', 'LineWidth', 1.5)
hold off
```

```
% This function computes the cost function associated with the model
% parameters estimated using Sequential Quadratic programming.

function V = ctfun2(rho,d1,d2,y,u)

if d1>d2
   V = inf;
   return
end

f = rho(1);
R = rho(2);
a1 = rho(3);
a2 = rho(4);
y0 = rho(5);

num = zeros(1,d1+d2+1);
den = num;

num(1,[d1+1 d1+2 d2+1 d2+2 d1+d2+1]) = ...
   [f*(1-a1) -a2*f*(1-a1) (1-f)*(1-R)*(1-a2) ...
      -a1*(1-f)*(1-R)*(1-a2) -f*R*(1-a2)*(1-a1)];
den(1,[1 2 3 d2+1 d2+2]) = [1 -a1-a2 a1*a2 -R*(1-a2) a1*R*(1-a2)];
ic = filtic(num,den,y0*ones(d1+d2,1));
eh = y - filter(num,den,u,ic);

% Cost function
V = sum(eh.^2);
```

```
% This function computes the dynamic model parameters in discrete-time
% domain for each pair of time delays via least squares method and
% calculates the cost function associated with each d1 and d2.

function l = phi4(y,u,d1,d2)

if (d1<2) | (d2<3) | d2<d1
   l = inf;
   return
end

yy = y;
uu = u;

y = [y(1)*ones(d1+d2,1); y];
u = [zeros(d1+d2,1); u];
n = length(y);

% Preparation for Least Squares
np = 6 + (d1~=d2) + (abs(d1-d2)>1);
R = zeros(n-d1-d2,np);

% u associated with the parameter rho_9 (eliminated)
u9 = u(1:n-d1-d2);

R(:,1:4) = [u9-y(d1+d2:n-1) u9-y(d1+d2-1:n-2) u9-y(d1+1:n-d2) ...
            u9-y(d1:n-d2-1)];
R(:,5:6) = [u(d2+1:n-d1)-u9 u(d2:n-d1-1)-u9];
if d2==d1+1
   R(:,7) = u(d1:n-d2-1)-u9;
elseif d2==d1-1
   R(:,7) = u(d1+1:n-d2)-u9;
elseif d2~=d1
   R(:,7:8) = [u(d1+1:n-d2)-u9 u(d1:n-d2-1)-u9];
end
Y = y(d1+d2+1:n)-u9;
th = R \ Y;

den = zeros(1,d1+d2+1);
num = den;
den([1:3 d2+1 d2+2]) = [1 th(1) th(2) th(3) th(4)];
num(d1+1:d1+2) = [th(5) th(6)];
if d2==d1+1
   num(d2+2) = th(7);
elseif d2==d1-1
   num(d2+1) = th(7);
elseif d2~=d1
   num(d2+1:d2+2) = [th(7) th(8)];
end
num(d1+d2+1) = 1+sum(th(1:4))-sum(th(5:np));

y = yy;
u = uu;

ic = filtic(num,den,y(1)*ones(d1+d2,1));
yh = filter(num,den,u,ic);
l = sum((y-yh).^2);
```

```
% This function generates the Bode plot of the partial derivatives of the
% model with respect to f, R, a1, and a2.

function plder(rho,d1,d2)

f = rho(1);
R = rho(2);
a1 = rho(3);
a2 = rho(4);

num = zeros(1,d1+d2+1);
den = num;

num(1,[d1+1 d1+2 d2+1 d2+2 d1+d2+1]) = ...
   [f*(1-a1) -a2*f*(1-a1) (1-f)*(1-R)*(1-a2) ...
      -a1*(1-f)*(1-R)*(1-a2) -f*R*(1-a2)*(1-a1)];
den(1,[1 2 3 d2+1 d2+2]) = [1 -a1-a2 a1*a2 -R*(1-a2) a1*R*(1-a2)];


den1(1,[1 2 3 d1+2]) = [1 -2*a1 a1^2 0];
G3 = tf([zeros(1,d1) -f f], den1, -1);


num1(1,[1 2 d2+1]) = [-1 1 0];
den2(1,[1 2 d2+1]) = [1 -a2 -R*(1-a2)];
den22 = conv(den2,den2);
G4 = tf([zeros(1,d2) (1-f)*(1-R)*num1], den22, -1);


num2(1,[d1+1 d1+2 d2+1 d2+2 d1+d2+1]) = ...
   [1-a1 -(1-a1)*a2 -(1-R)*(1-a2) (1-R)*a1*(1-a2) -R*(1-a1)*(1-a2)];
den3(1,[1 2 d1+1]) = [1 -a1 0];
G1 = tf(num2, conv(den2,den3), -1);


num3(1,[1 2 d2+1]) = [-1 a2 1-a2];
G2 = tf([zeros(1,d2) (1-a2)*(1-f)*num3], den22, -1);

bode(G1,G2,G3,G4);
```

APPENDIX B

B. DYNAMIC DATA ANALYSIS

To estimate dynamic model parameters, the system was excited by a frequency-modulated random binary input signal (see chapter 6). A saline solution was injected through a computer controlled solenoid valve into the pulp feed stream. Conductivity variations in the input and output streams were measured using flow-through conductivity sensors. These signals were recorded in an Excel worksheet. Figure B.1 shows the input-output data obtained from one of the dynamic tests made on scale-model chest. Then these signals were saved as a ".mat" file in MATLAB (i.e. mixdata10512.mat). When the computer program listed in appendix A is run, it

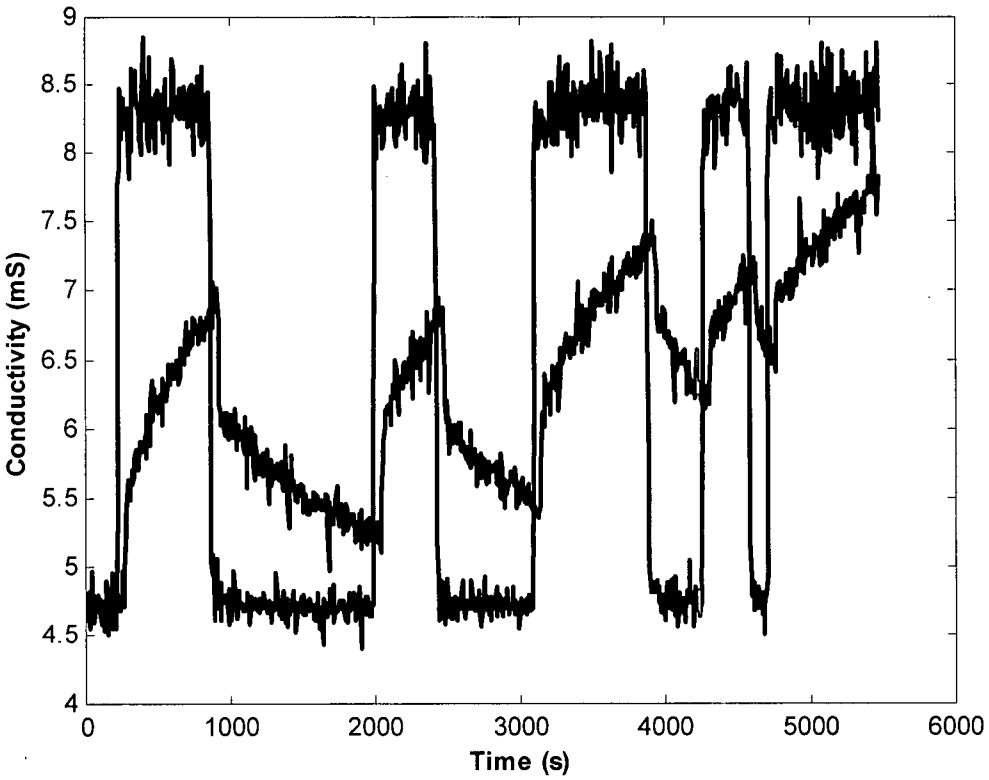

Figure B.1: Scale-model chest input and output signals (Q = 7.9 L/min , C_m = 3.3% , N = 1363 rpm , Config.1).

reads the input-output data from this file and calculates the dynamic model parameters and the model output response. Figure B.2 shows these results. The estimated dynamic model parameters in continuous-time domain from these data are:

$$f = 0.24 \ , \ R = 0.00 \ , \ T_1 = 45.0\,s \ , \ \tau_1 = 10.5\,s \ , \ T_2 = 100.0\,s \ , \ \tau_2 = 892.2\,s \tag{B.1}$$

The frequency response of the system was calculated by using the discrete-time transfer function. The estimated model parameters in discrete-time domain are (see chapter 5):

$$\begin{aligned}
&t_s = 5\,s \ , \ a_1 = e^{-t_s/\tau_1} = 0.6211 \ , \ a_2 = e^{-t_s/\tau_2} = 0.9944 \\
&d_1 = 1 + \frac{T_1}{t_s} = 10 \ , \ d_2 = 1 + \frac{T_2}{t_s} = 21 \\
&\rho_1 = f(1-a_1) = 0.0909 \ , \ \rho_2 = -f(1-a_1)a_2 = -0.0904 \\
&\rho_3 = (1-f)(1-R)(1-a_2) = 4.26\times10^{-3} \\
&\rho_4 = -(1-f)(1-R)a_1(1-a_2) = -2.64\times10^{-3} \\
&\rho_5 = -fR(1-a_1)(1-a_2) = 0 \\
&\rho_6 = -a_1 - a_2 = -1.6155 \ , \ \rho_7 = a_1 a_2 = 0.6176 \\
&\rho_8 = -R(1-a_2) = 0 \ , \ \rho_9 = Ra_1(1-a_2) = 0
\end{aligned} \tag{B.2}$$

Then the discrete-time transfer function of the system becomes:

$$\begin{aligned}
\hat{G}(q) &= \frac{\rho_1 q^{-d_1} + \rho_2 q^{-(d_1+1)} + \rho_3 q^{-d_2} + \rho_4 q^{-(d_2+1)} + \rho_5 q^{-(d_1+d_2)}}{1 + \rho_6 q^{-1} + \rho_7 q^{-2} + \rho_8 q^{-d_2} + \rho_9 q^{-(d_2+1)}} \\
&= \frac{0.0909 q^{-10} - 0.0904 q^{-11} + 4.26\times10^{-3} q^{-21} - 2.64\times10^{-3} q^{-22}}{1 - 1.6155 q^{-1} + 0.6176 q^{-2}}
\end{aligned} \tag{B.3}$$

By using MATLAB, the Bode plot of this discrete-time transfer function can be easily generated:

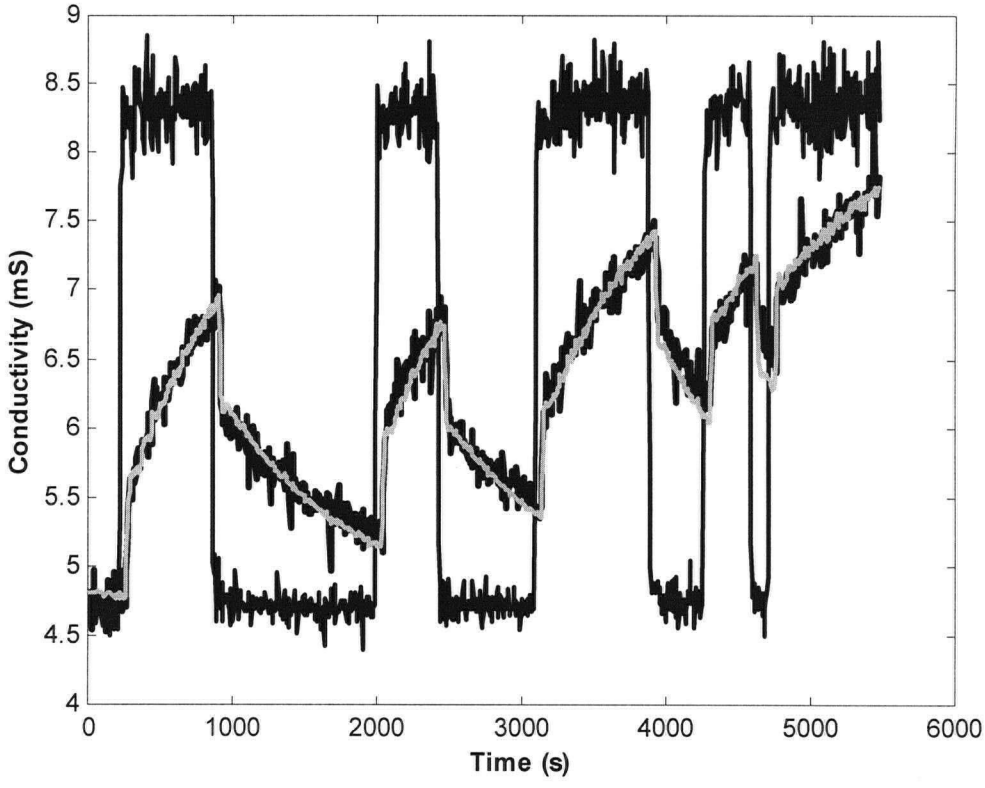

Figure B.2: Scale-model chest input and output signals in black lines and model output in gray line (Q = 7.9 L/min , C_m = 3.3% , N = 1363 rpm , Config.1).

```
ts = 5;
d1 = 10;
d2 = 21;
f = 0.24;
R = 0.00;
a1 = 0.6211;
a2 = 0.9944;

num = zeros(1,d1+d2+1);
den = num;

num(1,[d1+1 d1+2 d2+1 d2+2 d1+d2+1]) = ...
   [f*(1-a1) -a2*f*(1-a1) (1-f)*(1-R)*(1-a2) ...
      -a1*(1-f)*(1-R)*(1-a2) -f*R*(1-a2)*(1-a1)];
den(1,[1 2 3 d2+1 d2+2]) = [1 -a1-a2 a1*a2 -R*(1-a2) a1*R*(1-a2)];
bode(tf(num,den,ts))
```

Figure B.3 shows the magnitude Bode plot for the discrete-time transfer function (Equation B.3) estimated from input-output data shown in Figure B.1.

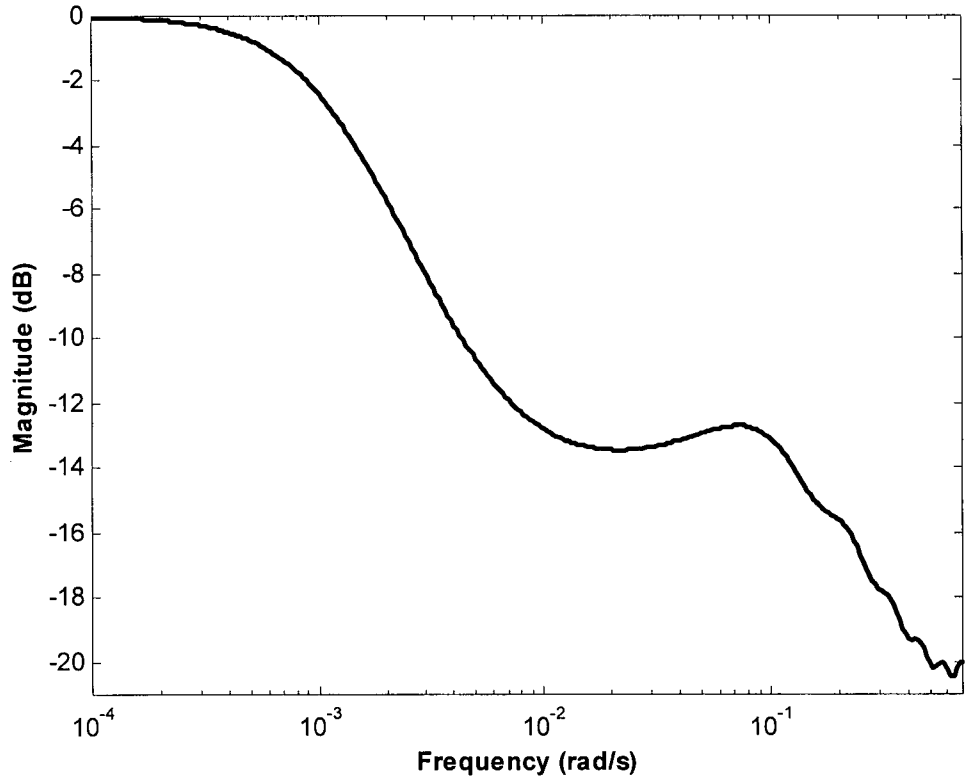

Figure B.3: Frequency response of the scale-model chest (Q = 7.9 L/min , C_m = 3.3% , N = 1363 rpm , Config.1).

APPENDIX C

C. DATA TABLES

Table C.1: Dynamic data (Q = 37.1 L/min , C_m = 3.3% , Config.1).

N (rpm)	P (W)	Mo (m^4/s^2)	f	R	τ_2 (s)	$V_{fully\ mixed}$ (L)	$V_{fully\ mixed}$ (%)
1203	329.9	0.122	0.93	0.00	269.4	11.66	11
1301	400.3	0.143	0.88	0.00	200.0	14.84	14
1355	441.1	0.155	0.44	0.00	186.7	64.66	61
1456	519.7	0.179	0.33	0.00	161.2	66.78	63
1556	630.3	0.204	0.21	0.00	154.1	75.26	71
1719	797.1	0.249	0.06	0.00	142.2	82.68	78

Table C.2: Dynamic data (Q = 31.2 L/min , C_m = 3.3% , Config.1)

N (rpm)	P (W)	Mo (m^4/s^2)	f	R	τ_2 (s)	$V_{fully\ mixed}$ (L)	$V_{fully\ mixed}$ (%)
1031	230.9	0.090	0.95	0.00	436.2	11.66	11
1202	330.0	0.122	0.87	0.00	435.2	28.62	27
1254	367.5	0.133	0.44	0.00	234.2	67.84	64
1306	405.1	0.144	0.42	0.00	244.1	73.14	69

Table C.3: Dynamic data (Q = 28.6 L/min , C_m = 3.3% , Config.1)

N (rpm)	P (W)	Mo (m^4/s^2)	f	R	τ_2 (s)	$V_{fully\ mixed}$ (L)	$V_{fully\ mixed}$ (%)
1020	224.5	0.088	0.92	0.00	667.1	25.44	24
1056	248.1	0.094	0.88	0.00	537.4	30.74	29
1106	275.4	0.103	0.53	0.00	298.1	66.78	63
1212	339.3	0.124	0.42	0.00	264.6	73.14	69

Table C.4: Dynamic data (Q = 21.1 L/min , C_m = 3.3% , Config.1).

N (rpm)	P (W)	Mo (m^4/s^2)	f	R	τ_2 (s)	$V_{fully\ mixed}$ (L)	$V_{fully\ mixed}$ (%)
1031	231.6	0.090	0.57	0.00	399.6	60.42	57
1130	288.3	0.108	0.43	0.00	364.9	73.14	69
1257	368.4	0.133	0.39	0.00	355.8	76.32	72
1358	442.0	0.155	0.31	0.00	332.0	80.56	76
1556	629.8	0.204	0.01	0.00	277.1	96.46	91
1728	805.3	0.252	0.00	0.00	292.4	102.82	97

Table C.5: Dynamic data (Q = 7.9 L/min , C_m = 3.3% , Config.1).

N (rpm)	P (W)	Mo (m^4/s^2)	f	R	τ_2 (s)	$V_{fully\ mixed}$ (L)	$V_{fully\ mixed}$ (%)
1031	233.0	0.090	0.51	0.00	1150.1	74.20	70
1132	290.1	0.108	0.40	0.00	1006.3	79.50	75
1258	372.2	0.133	0.35	0.00	966.1	82.68	78
1363	447.3	0.157	0.24	0.00	892.2	89.28	84
1459	521.7	0.179	0.14	0.00	842.5	95.40	90
1555	630.0	0.204	0.00	0.00	797.0	104.94	99
1724	803.9	0.250	0.00	0.00	797.0	104.94	99

Table C.6: Dynamic data (Q = 37.1 L/min , C_m = 3.3% , Config.2).

N (rpm)	P (W)	Mo (m^4/s^2)	f	R	τ_2 (s)	$V_{fully\ mixed}$ (L)	$V_{fully\ mixed}$ (%)
1032	232.0	0.090	0.09	0.00	135.9	76.32	72
1134	290.8	0.108	0.09	0.00	143.2	80.56	76
1238	353.7	0.129	0.06	0.00	148.4	85.86	81
1459	521.1	0.179	0.00	0.00	149.1	92.22	87
1557	631.3	0.204	0.00	0.00	157.7	97.52	92
1724	804.4	0.250	0.00	0.00	162.9	100.70	95

Table C.7: Dynamic data (Q = 7.9 L/min , C_m = 3.3% , Config.2).

N (rpm)	P (W)	Mo (m^4/s^2)	f	R	τ_2 (s)	$V_{fully\ mixed}$ (L)	$V_{fully\ mixed}$ (%)
1032	234.4	0.090	0.00	0.00	684.3	90.10	85
1105	273.9	0.103	0.00	0.00	708.5	93.28	88
1253	369.1	0.132	0.00	0.00	748.7	98.58	93
1357	440.9	0.155	0.00	0.00	764.8	100.70	95
1557	632.0	0.204	0.00	0.00	789.0	103.88	98

Table C.8: Dynamic data (Q = 37.1 L/min , C_m = 2.7% , Config.1).

N (rpm)	P (W)	Mo (m^4/s^2)	f	R	τ_2 (s)	$V_{fully\ mixed}$ (L)	$V_{fully\ mixed}$ (%)
893	167.3	0.067	0.55	0.00	224.8	62.54	59
1000	216.7	0.084	0.36	0.00	182.1	72.08	68
1072	254.7	0.097	0.24	0.00	162.4	76.32	72
1305	386.5	0.144	0.10	0.00	161.5	90.10	85
1555	590.8	0.204	0.00	0.00	161.1	99.64	94

Table C.9: Dynamic Data (Q = 37.1 L/min , C_m = 2.7% , Config.2).

N (rpm)	P (W)	Mo (m^4/s^2)	f	R	τ_2 (s)	$V_{fully\ mixed}$ (L)	$V_{fully\ mixed}$ (%)
893	165.0	0.067	0.00	0.00	138.8	85.86	81
1072	254.2	0.097	0.00	0.00	162.8	100.70	95
1240	347.7	0.130	0.00	0.00	166.3	102.82	97
1350	420.7	0.154	0.00	0.00	168.0	103.88	98

Table C.10: Dynamic Data (Q = 37.1 L/min , C_m = 2.1% , Config.1).

N (rpm)	P (W)	Mo (m^4/s^2)	f	R	τ_2 (s)	$V_{fully\ mixed}$ (L)	$V_{fully\ mixed}$ (%)
706	72.4	0.042	0.50	0.00	236.6	73.14	69
818	104.5	0.056	0.20	0.00	171.4	84.80	80
1000	165.4	0.084	0.00	0.00	154.3	95.40	90
1301	337.7	0.143	0.00	0.00	161.1	99.64	94

Table C.11: Dynamic data (Q = 37.1 L/min , C_m = 2.1% , Config.2).

N (rpm)	P (w)	Mo (m^4/s^2)	f	R	τ_2 (s)	$V_{fully\ mixed}$ (L)	$V_{fully\ mixed}$ (%)
707	72.9	0.042	0.00	0.00	156.0	96.46	91
824	107.5	0.057	0.00	0.00	168.0	103.88	98
930	142.0	0.073	0.00	0.00	169.7	104.94	99